Development of DNA Aptamers Targeting Breast Cancer Derived Extracellular Vesicles for Biomarker Discovery

Vanessa Susevski

Thesis submitted to the University of Ottawa
in partial Fulfillment of the requirements for the degree of

Master of Science

Department of Chemistry and Biomolecular Science
Faculty of Science
University of Ottawa

ABSTRACT

Detection of cancer at the early stages greatly increases the chance for successful treatment and favourable prognosis for patients. However, a liquid-based biopsy has yet to be developed for most cancers. Extracellular vesicles (EVs) are an attractive candidate for early cancer detection since their surface proteome mirrors the cell of origin. Thus, there is a need for the development of reliable probes that can detect cancer derived EVs. In this thesis, the VBS-1 aptamer was developed to selectively bind to triple-negative breast cancer cell line derived EVs. Initially, several EV isolation methods were compared and isolated EVs were validated and characterized. Aptamer clones were developed by Systematic Evolution of Ligands by Exponential Enrichment to EVs isolated by differential ultracentrifugation and their binding was validated by flow cytometry. The binding partner of the selected VBS-1 aptamer was identified by LC-MS/MS to be the transmembrane protein ATP1A1. The presence of an ATP1A1-positive EV population was validated by flow cytometry. The selected aptamer may find further application in biosensors for the detection of EVs as cancer biomarkers in biological fluids.

Keywords: Extracellular vesicles, aptamers, biomarker discovery, cancer, extracellular vesicle-based diagnostic

LIST OF CONTRIBUTIONS

Presentations (O = Oral, P = Poster)

P1 Chemical and Synthetic Biology Symposium, University of Ottawa, ON, October 26th, 2018

O2 "Aptamer Assisted Analysis of Exosomes", 9th Annual NanoOntario conference, Carleton University, ON

O3 "Development of DNA Aptamers to Salivary Exosomes for Oral Cancer Diagnostics and Applications", 13th Annual Chemical Biophysics, University of Toronto, ON

O4 "Development of DNA Aptamers to Cancer-Derived EVs for Biomarker Discovery", Chemical and Synthetic Biology Symposium, University of Ottawa, ON, 2019

O5 "Aptamer-Facilitated Biomarker Discovery of Extracellular Vesicles", e-Extracellular Vesicle Symposium, 2020

O6 "Aptamer-Facilitated Biomarker Discovery of Extracellular Vesicles", Canadian Chemistry Conference and Exhibition (CCCE), TBD

Dedication

I dedicate this work to my mother Guiselle Susevski, my father Eli Susevski, my brother Anthony Susevski and my best friend Loïc Muhirwa.

ACKNOWLEDGEMENTS

Perhaps I did not know what I was getting myself into when I walked through the doors of this institution for the first time, looking for a place I could call home. “I’m curious and I love to learn,” I thought. Little did I know the perseverance, integrity, self-discipline, and emotional maturity required to be successful in completing my studies – fortunately, I had the resources to learn to rise to the challenge and enter a period of self-discovery and reinvention. Like the metamorphosis of a caterpillar into a butterfly, a gruesome transformation on the inside but a beautiful one from the outside. I am forever grateful for the opportunity for this experience and hope I live to see the day when education is no longer a privilege, but instead a human right on a global scale. The following are people who directly impacted my success throughout my studies in one way or another, and whom I have much respect and appreciation for.

I would like to thank Dr. Maxim Berezovski for his guidance, insight, and support over the course of my graduate studies. The knowledge and skills I have gained during the time in his group will be of value to me for the rest of my life. Thank you for giving me the opportunity to exercise leadership skills in your research group and for the long inspirational lectures you give periodically to the group.

I have greatly valued the support of the uOttawa facility technicians, Dr. Zoran Minic and Dr. Shahrokh Ghobadloo, who provided invaluable technical and personal guidance over the years. Without both of you, I would have been far more lost than I was (and still am). I am truly grateful for your willingness to mentor my colleagues and I, including but not limited to the critique of our presentations and thesis drafts.

I also thank the Science store for their cheerful assistant in shipping and receiving materials in a timely fashion. Thank you to Pierre and Alain for their impressively consistent positive attitude, and for pushing rush orders for me when I needed it most. Furthermore, I thank the administrative staff for their support and dedication to student success. Thank you to Chloe, Annette, and Jose for always welcoming me with open arms – no matter how many times I came to bug them.

To the lab members of the Berezovski group, both past and present, it has truly been an unforgettable experience working with you. I thank Yousef Risha for your support and encouragement, your cheerful energy, and admiration for your parents and work ethic is inspiring.

Your listening skills are out-of-this-world and had an enormous positive contribution to my sanity. Nico Hüttmann, you are an incredible friend and I admire your competitive spirit; you should know it prompted my likeminded spirit on numerous occasions. I should also thank you for the apples and protein bars you have donated to me, and I would have otherwise starved in despair. Emil Zaripov, I appreciate your humour and uniqueness that you bring to the lab. Your strong meme game and invaluable insight on lab protocols has been a critical part of my experience. I would like to thank Suttinee Poolsup and Lixuan Ren for being a source of feminine energy in a dominant androgynous space, and for sharing a love for Starbucks, Sephora and being future "sassy mamas". Yuchu Dou, thank you for your generosity, such as borrowing your car for my family emergencies or gatherings, I have always been able to count on you. Thank you to my undergraduate student Riya Shah, for your hard work and attention to detail – allowing me to produce a large amount of results in a short amount of time. To all, thank you for countless laughs, tears, and coffee breaks. I cherish our friendship, and I hope we keep in touch no matter where in the world life takes us.

To my mother: Thank you for migrating to Canada with a suitcase and a few dollars, in hopes of a better future for Anthony & I. Your utmost kind-heartedness and work ethic inspire me each day. To my father: thank you for gifting me skills of resilience at a young age in the form of athleticism. The characteristic of fighting for my personal best performance and standing back up off the ice despite injury, exhaustion or temporary loss of motivation has carried over in my academic and adult life. I will always be a firebird.

Finally, I would like to thank my best friend Loïc Muhirwa for seeing potential in me before I could see it in myself, and for being by my side every step of the way. If it were not for you, I would be back in my small hometown still living with the limiting belief that I was incapable of chasing my dreams because I am not among those gifted with a genius level IQ. You taught me anything is possible with the right approach; I truly would not be here without you.

List of Abbreviations

AptaBiD	Aptamer-Facilitated Biomarker Discovery
ACTG1	Actin
ATP1A1	Sodium/potassium-transporting ATPase subunit alpha-1
CLiC	Convex Lens-induced Confinement
CFSE	Carboxyfluorescein Succinimidyl Ester
CCAT2	Cancer-Associated Transcript 2
CID	Collision-Induced Dissociation
Cy5	Cyanine-5
DC	Differential ultracentrifugation
FDR	False Discovery Rate
FBS	Fetal Bovine Serum
FN1	Fibronectin 1
FASP	Filter-Aided Sample Preparation
FACS	Fluorescent Activated Cell-Sorters
ESCRT	Endosomal Sorting Complex Required For Transport Complex
ESI	Electrospray Ionization
ER/PR	Estrogen or Progesterone Receptors
EVs	Extracellular Vesicles
GPC1	Glypican-1
H1-4	Histone H1.4
HS	Horse Serum
HER-2	Human-Epidermal Growth Factor Receptor
ILV	Intraluminal Vesicle
IMR	Integrated Microbiome Resource
ISEV	International Society For Extracellular Vesicles
IAA	Iodoacetamide
KRT5	Keratin 5
LTF	Lactotransferrin
LFQ	Label-Free Protein Quantitation
MS	Mass spectrometry

m/lEV	Medium/Large EV
MFGE8	Milk Fat Globule-EGF Factor 8 Protein
MWCO	Molecular Weight Cut-Off
MVBs	Multivesicular Bodies
NTA	Nanoparticle Tracking Analysis
DDM	n-Dodecyl β-D-maltoside
NCL	Nucleolin
PBS	Phosphate buffer saline
PCR	Polymerase Chain Reaction
RAN	Ras-Related Nuclear Protein
sEVs	Small EVs
SDS	Sodium Dodecyl Sulfate
SELEX	Systematic Evolution of Ligands By Exponential Enrichment
TEM	Transmission Electron Microscopy
TCEP	Tris(2-carboxyethyl) phosphine
UC	Ultracentrifugation
UF	Ultrafiltration

LIST OF FIGURES

LIST OF TABLES

TABLE OF CONTENTS

BACKGROUND

Cancer is among the top ten global health threats in 2019, burdening over 15 million people between the ages of 30 and 69 globally and accounting for 70% of premature deaths.[1] Large scale efforts have been invested in the research and development of new treatments, [2] though there has been great success in personalized cancer therapies, they do not overrule the importance of early cancer detection. The time-sensitive nature of early cancer detection is analogous to a snowball rolling down a snowy hill. As the snowball rolls down the hill, it becomes larger and harder to stop or reverse. Similarly, the more advanced stage of cancer, the poorer the prognosis and treatment outcomes for the patient. There is some variation observed dependent on the cancer types. For example, colon and liver cancers abide by this trend predictably, whereas this is less true of prostate cancers and Hodgkin's lymphomas.[2,3] Strategies for early cancer detection should prioritize low-cost assays that minimize false positive and negative results, thereby increasing access of effective diagnostic services on a global scale.[4]

Extracellular vesicles (EVs) are an attractive candidate for early cancer detection because they are released by cancer cells in significant quantities,[5] are detectable in biological fluid,[6] mirror the surface proteins of the original cell and are stable in circulation.[7] More concisely, EVs carry cancer biomarkers on their surface that are reflective of their cancerous cell of origin, that may be isolated and detected from biological fluid. We are in the early stages of discovering cancer-related biomarkers on EVs with clinically relevant potential.

The thesis is structured in the following way. The **first chapter** serves as an introductory overview of the role of extracellular vesicles in cancer and biomarker discovery using an aptamer facilitated approach. The goal of this chapter is to outline the seminal work in the field as well as to provide relevant historical context. The **second chapter** describes the methods for isolation of extracellular vesicles derived from cell line tumour sources, human urine, and saliva. Then, the effectiveness and efficiency of the isolation strategies are assessed by characterization techniques. The **third chapter** describes the development validation of aptamer selection to cancer-derived extracellular vesicles. The **fourth chapter** describes the identification of the selected aptamer protein binding partner using proteomics and bioinformatics. Bioinformatics workflow was developed to identify a protein target that can be a good candidate as biomarker. Finally, among several candidates, the transmembrane protein ATP1A1 was identified on the surface of extracellular vesicles that may have future potential as a biomarker for cancer.

CHAPTER 1

INTRODUCTION

1. INTRODUCTION

Cancer is a group of diseases that may be characterized by unique molecular signature that may arise from any tissue in the body, but probabilistically more often in rapidly diving tissues. The underlying common denominator of all cancer subtypes are genetic instability, sustained proliferative signaling, evasion of growth suppressors, avoidance of cell death, enabling replicative immortality, induction of angiogenesis, and activating invasion and metastasis.[8] The process by which a normal cell progressively evolves to reach a neoplastic state is a multistep pathogenic process.[9] A neoplasm is an abnormal mass of tissue or collection of cells that rapidly divide and do not receive or respond appropriately to apoptotic cues.[10] A neoplastic mass is more commonly referred to as a benign tumour and may or may not progress into a malignant counterpart, ultimately becoming cancerous. A key question in the control and prevention of cancer growth or spread is the detection of the disease in its early critical stages. A biomarker is a quantifiable response that pertains to the physiological state of a cell at a particular time. [11] The measured response may be functional, physiological, biochemical, or molecular in nature. It is critical that in the pursuit of clinical applications, the validity of a potential biomarker is evaluated and not assumed. Furthermore, the relationship between the biomarker and the clinical endpoint should be well defined to be considered clinically relevant.[12]

Genome-based biomarkers have been heavily investigated as means of cancer detection, albeit there are many levels of post-processing that follow the genome. [13] Secondly, typical gene expression studies do not necessarily correlate with the relative abundance and variation of encoded proteins and are subject to downstream post-translational modifications.[14] This implies that studying the gene expression of potential biomarkers alone may not translate well into the reality of the final product in a biological system. Inevitably, all approaches have a set of pros and cons; EVs are promising in the future of non-invasive cancer detection because they are quantifiable, isolatable and reflect surface characteristics of their cell of origin in a realistic manner. EVs are released in quantifiable amounts into human biological fluids[6] such as urine, saliva and serum.[15] Transformed cells show evidence of secreting more EVs than healthy control cells influencing tumour initiation, progression, metastasis and drug resistance.[5] Understanding this relationship may allow future clinicians to have insight on a cancer profile and tendencies by investigating only the EV profile, instead of having to analyze the tumour itself.

1.1 Extracellular vesicles

Our understanding of EVs and their role has evolved immensely over the past half-century. Peter Wolf was first to publish an observation of what we now know as EVs; in the late 1960s from thrombocytes in human plasma where he initially believed was cellular debris. The scientific community's understanding of EVs has evolved since Wolf's "platelet dust" description. Two decades later, Pan and Johnson elegantly visualized the mysterious vesicles.[16,17] Interestingly, they observed that the vesicles retained the transferrin and other membrane-associated surface receptors which were shed from the cell of origin. However, the sophisticated nature of EVs was under-appreciated at this point in their history but instead, these vesicles thought to be operating as cellular garbage disposals.[18] Evidence on the contrary to the cellular garbage disposal hypothesis was discovered in the mid-1900s by Raposo and his colleagues when they made an important connection between the immunogenic response and extracellular vesicles.[19] Shortly thereafter, EVs as a topic of academic interest grew exponentially – revealing the complex and paramount role of EVs as transferring agents of biological information through cell-to-cell communication and the pathogenesis of disease. More specifically, EVs were found to be implicated in biological processes such as inflammation, lactation, cell proliferation, neuronal regulation, and the immune response.[20–22]

Selective pressures to protect biological cargo and signals likely lead to their encapsulation in a protective coating, shielding them from the harsh extracellular environment and allowing the delivery of messages. The resulting geometry of formation of lipid membrane vesicles is that of a sphere, ideal for carrying material as it elegantly maximizes internal space while minimizing the surface area and therefore tension, both a spontaneous and energetically favourable process.[23] EVs are a diverse and heterogeneous group of nanosized particles. They are characterized by a phospholipid bilayer and are released by most cells, containing bioactive molecules that can travel to a distant site and execute biological function.[24,25] The cargo of EVs continues to be an area of investigation but it may contain a range of lipids, DNA, RNA and proteins in different proportions depending on the cell type and subpopulation.[24,26] They do not contain a functional nucleus and thus are incapable of replication and must derive from a host cell. [27]

Classic definitions of EV subtypes were notoriously rigged with ambiguity, which called into action the International Society for Extracellular Vesicles (ISEV) to set more rigorous

guidelines. Traditionally, EVs were characterized by their experimentally determined size. The cut-off size was typically 150nm, vesicles being smaller being considered as exosomes, and vesicles larger being considered as microvesicles. This classification system was rejected by the ISEV, because it does not respect the known size overlaps between the groups. From a more fundamental perspective, the definitions of exosomes and microvesicles rely on the biogenesis pathway that will be discussed shortly, which are difficult to prove with currently available methods. The refined guidelines published in 2018 recommend categorizing EVs by physical characteristics, density, or biochemical composition. A detailed synopsis of the summary is described in **Table 1.1.**

Table 1.1 Summary of suggested EV characterization guidelines as of 2018. EVs may be classified by their size, density, biochemical composition, or cell of origin/conditions by which they were acquired. The method of the property chosen to characterize EVs is up to the researcher and could vary depending on downstream applications; however, it is critical for the subcategories to be well-defined. [27]

Characterization	Suggested Subcategories
Physical	Small EVs (sEVs) Medium/Large EVs (m/LEVs)
Density	Low Middle High
Biochemical composition	CD63+/CD81+ Annexin A5 +
Conditions/Cell of origin	Cell type origin (ex. Podocytes) Hypoxic EVs Apoptotic bodies Oncosomes

The term EVs encompass all exosomes, microvesicles, apoptotic bodies and each is defined by the biogenesis pathway of the vesicle.[23] Exosomes are derived from the plasma membrane budding inwards, forming endosomal multivesicular bodies (MVBs)[28] which then form smaller

internal vesicles eventually to be exocytosed from the host cell. This pathway requires endosomal sorting complex required for transport (ESCRT) complex and associated proteins as shown in **Figure 1.1**.[29] Microvesicles are derived from direct pinching off the cell membrane[24]in response to an increase in intracellular calcium[30] in contrast to membrane disintegration in the case of apoptotic bodies.[31]

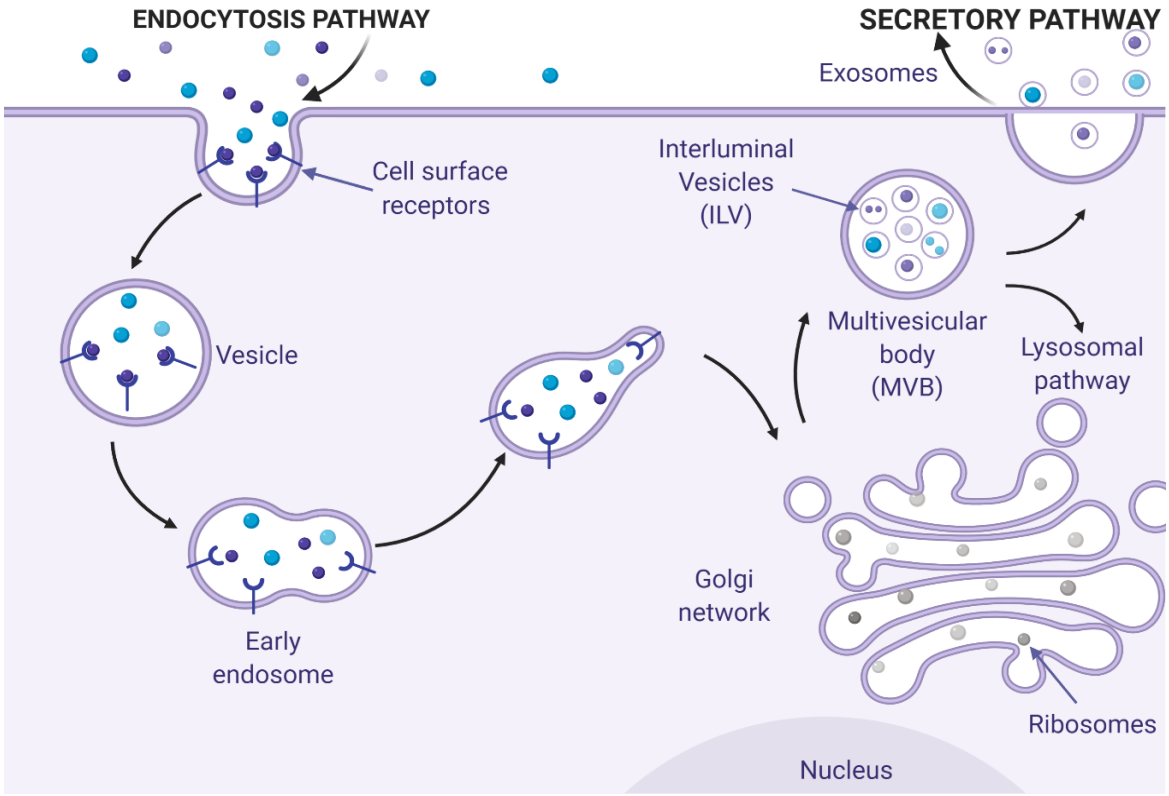

Figure 1.1 General schematic of exosome biogenesis. The cellular plasma membrane buds inward, forming early endosomes that are sent to the Golgi network. Multivesicular endosomes (MVE's) are also known as late endosomes and contain packaged intraluminal vesicles (ILV's). The MVE's then fuse with the plasma membrane, releasing the newly formed exosomes which then travel to the recipient cell.[32,33]

After they are released from the parent cell, both exosomes and microvesicles may travel to distant sites to release their cargo, having the ability to inspire biologically relevant changes to the recipient cell. Their uptake may happen via fusion of the EV with the plasma membrane of the recipient cell (an endocytosis-like mechanism) or by binding with a ligand on the surface of the cell eliciting a response by the cell.[33] EVs appear to have high variance in their cargo load, membrane composition, biogenesis, and biological function, thus giving rise to multiple subtypes

of EV populations. Due to significant overlap in size, challenges arise in studying these populations in isolation with currently available isolation techniques. To use the terminology exosomes or microvesicles should imply strong evidence of population separation, which is difficult to achieve if the vesicles were not observed in real-time being released from their cell of origin.[27] In order to respect the International Society for Extracellular Vesicles (ISEV) most recent guidelines, exosomes and microvesicles will be referred to as small to medium EVs for the remaining duration of this report.

Table 1.2 Main subtypes of EVs. Exosomes, microvesicles and apoptotic bodies. Important distinctions to make are the differences in size, composition and biological purpose or function.

	Exosomes	Microvesicles	Apoptotic bodies
Biogenesis	Endosomal route 1. ESCRT dependent pathway 2. Ceramide dependent pathway 3. Tetraspanin dependent pathway	Outward budding/ pinching of the cell membrane 1. Ca^{2+} dependent 2. Cell dependent	Blebbing of the cell membrane Apoptosis related pathway-dependent
Size	30-150 nm	100-1000 nm	50-5000 nm
Function	Protein sorting, recycling of bioactive molecules, transport, intercellular communication	Transport of bioactive molecules, intercellular communication	Decomposition of the cell, associated with apoptosis
Composition	Proteins, miRNA, mRNA, lipids	Proteins, miRNA, mRNA, lipids	Intact organelles, chromatin, nuclear fractions, DNA, coding and non-coding RNA, lipids

The composition of an EV gives insight into its host cell type can also give rise to an alternative classification system of subtypes. This composition may change depending on the EVs cell type origin or the subcellular compartment of origin, affecting the subsequent intercellular interaction once it reaches the recipient cell.[34]

The role of EVs in the development and metastasis of cancer is currently an area of extensive investigation. EVs are capable of supporting tumour growth by suppressing the body's immune system, regulating systemic and local processes and nurturing the tumour niche environment to favour metastatic and angiogenesis processes.[35–37] EVs may facilitate tumour growth and support by their ability of EVs to transfer mutated genetic material from healthy cells to affected cells[38] and functionally modifying "stem-like" cells.[37] The small size of EVs enhances their ability to be permeable and accumulate within the tumour microenvironment.[39] For instance, the phenotype of a more aggressive malignant cancer can be transmitted to less aggressive breast cancer through an EV dependent mechanism as shown in **Figure 1.2**.

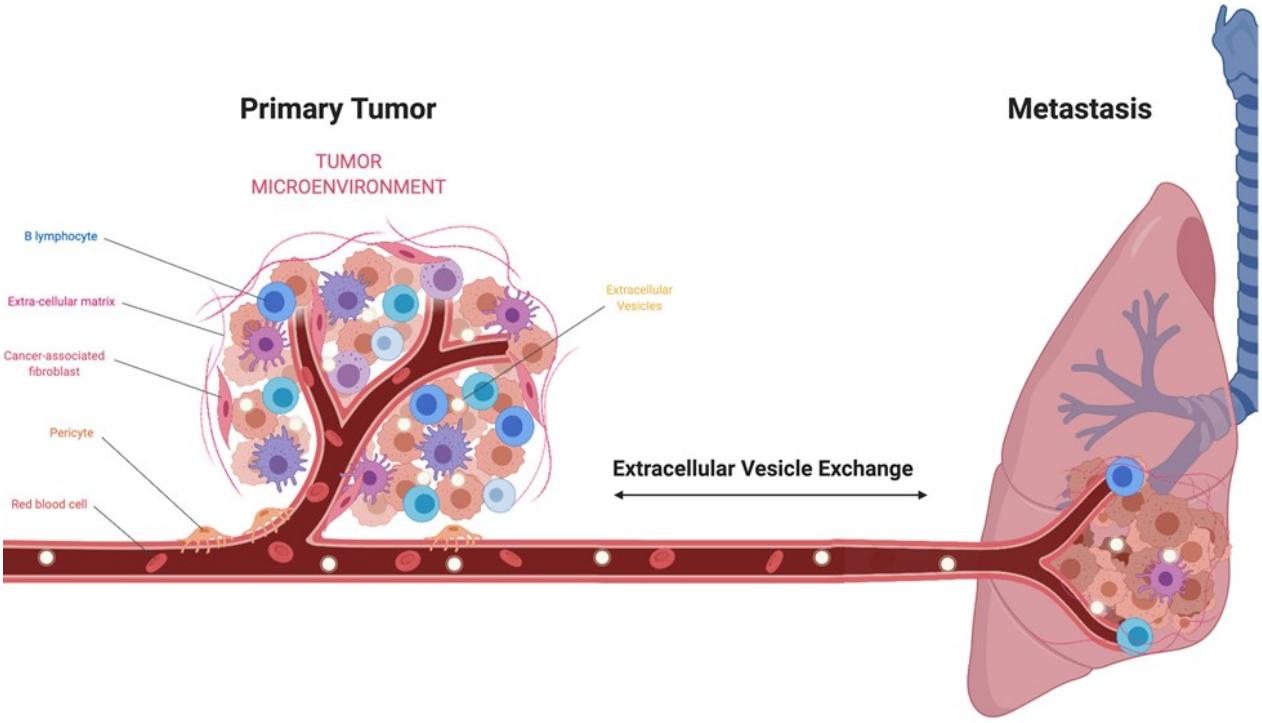

Figure 1.2. The supporting role of EVs in cancer metastasis. The tumour microenvironment is composed of a heterogeneous group of cancer cells, the supporting extracellular matrix and immune system cells in combat. EVs facilitate communication between primary tumour and metastasis site to further support tumour growth and may also transform unaffected cells. [40]

EXTRACELLULAR VESICLES AND BIOFLUID

Evidence supports detectable EVs in most human biological fluid including blood, amniotic fluid, cerebrospinal fluid, breast milk, saliva, urine, lymph, bile and abdominal cavity fluid in both health and diseased states.[41–43,43] Plasma is thought to be the most promising biological fluid for a protein biomarker approach because of its systemic nature, it is easily accessible and contains a high protein content. Though it is impractical to suggest that liquid-based biopsies would ever replace conventional surgical biopsies, however, this may serve as a platform for increasing access to screening and disease progression monitoring. This approach would particularly be advantageous for cancers in which surgical biopsy merits great risk to the patient if the tumour resides or is proximal to a vital organ.

EXTRACELLULAR VESICLES AND EARLY CANCER DETECTION

Both the primary tumour and metastatic site release EVs containing an abundance of cancer related molecular information into human biofluids. Thus, the enrichment of EVs from biological fluids to concentrate tumour signatures stands as a promising strategy for liquid based biopsy.[44] EVs are considered to be a rich source of biomarkers because each EV is bound to a lipid membrane with hundreds of bioactive transmembrane proteins as shown in **Figure 1.3**. This phenomenon was initially observed in 2008, where EVs derived from a glioblastoma tumour cell line were reported to be a snapshot of the RNA and protein load of the cell of origin,[35] Since this pivotal study, similar results have been reproduced in up to 60 different cancer types[45] demonstrating the similarly in cancer associated miRNA,[46] mRNA,[35,47] lncRNA[48] and post translational modifications[49] between the EV tumour and EV cell of origin. The potential of EV derived biomarkers has also been explored in plasma, serum, saliva, urine, and ascites fluid. Plasma has been investigated for lung,[50] pancreatic,[51] and gastrointestinal cancers.[52] Serum has been investigated for lung,[44] colorectal, and hepatobiliary cancers. Saliva has also been investigated for lung cancer.[53] Urine has been investigated for bladder,[54] renal,[55] and prostate cancers.[56,57,58] Ascites fluid has been investigated for colorectal[59] and ovarian cancers.[60]

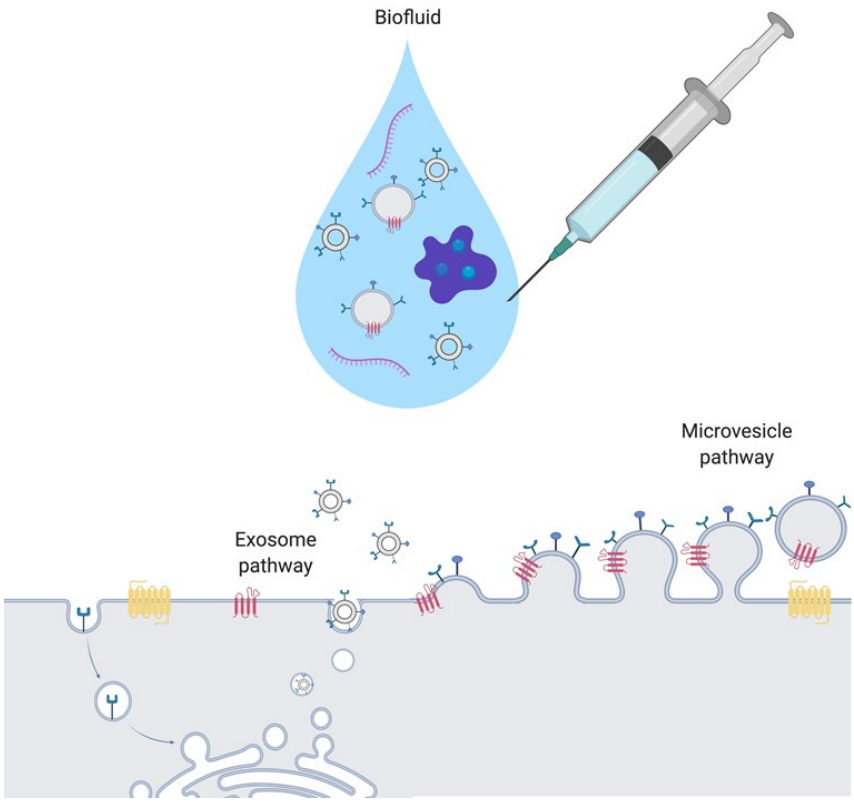

Figure 1.3. EVs share surface proteins with their cell of origin. Cells secrete surface proteins via EVs which can then be concentrated clinical samples and later detected, reducing the need for tissue biopsy.

To emphasize previous work that has made use of EVs as a biomarker source for early cancer detection, practical illustrations will follow. Cancer-Associated transcript 2 (CCAT2) was found to be upregulated in colorectal cancer EVs.[61] Developmental endothelial locus-1 (Del-1)[62], early breast cancer marker may offer a level of discrimination between breast cancer and benign breast tumours, respectively.[63] By the same token, CD24,[64] fibronectin[65] and have been proposed as general cancer marker. Proposed EV biomarkers have since then been demonstrated to have clinical potential for early cancer diagnostic assays in *in vivo* models. Pancreatic cancer was investigated by analyzing the presence or absence of tumour specific Glypican-1 (GPC1) positive EVs.[66] In the same year, the previously mentioned findings were supported when acute myeloid leukemia EVs were detected in circulation before leukemic blasts.[67] Detection of efficient biomarkers carried on EVs could be integrated into effective and simple biomarker diagnostic assays based on monoclonal antibody and aptamer-based methods,[68] allowing for cut backs on high-risk and expensive procedures.[69]

1.2 Aptamers

The use of nucleic acids for therapeutic targeting first emerged in the 90's, when an over-expressed transacting-response element resulted in the cells becoming resistant to the HIV virus. A single nucleotide mutation in the transacting-response element would no longer be able to provide the cell with resistance to the infection. It was predicted this was due to the change in 3-dimensional structure of the sequence, demonstrating the potential power of nucleic acids in therapeutics.[70] Aptamers are single stranded DNA, RNA or synthetic XNA molecules that can be developed to interact with a target of interest.[71] Aptamers each have a unique three-dimensional structure that is formed through intramolecular interactions. Base pairs interact predominantly through the Watson-Crick face but may also interact through the sugar edge between purines and the Hoogsteen edge of uracil (**Figure 1.4**).[72]

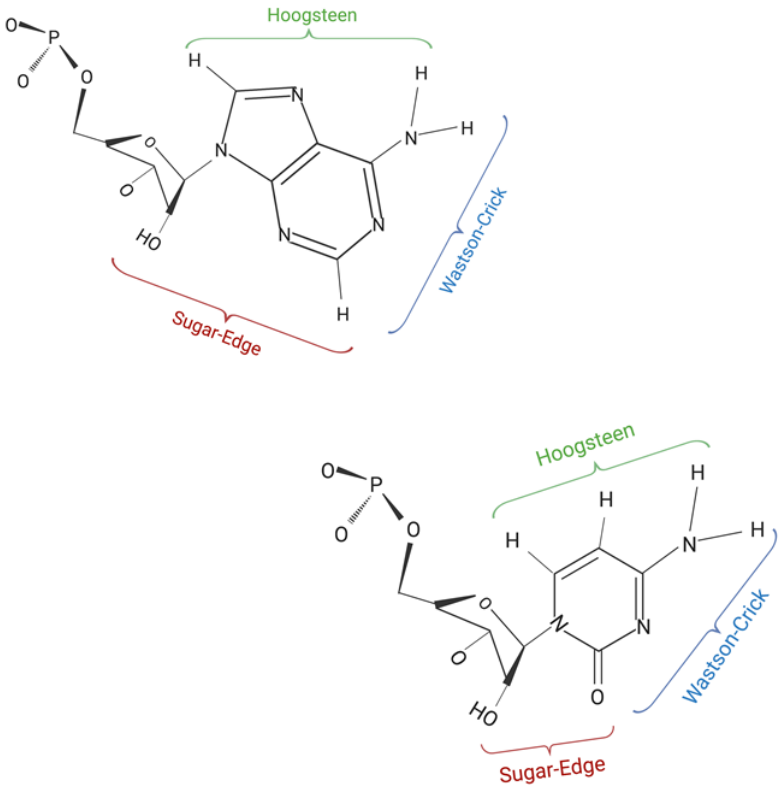

Figure 1.4 Nucleotide-nucleotide hydrogen bonding interactions between both purines and pyrimidines. Each base pair may interact with a neighboring base pair most often by the Watson-Crick face but may also interact by the Hoogsteen face or sugar edge.

DEVELOPMENT OF APTAMERS

Systematic Evolution of Ligand by Exponential Enrichment (SELEX) is used to develop crude nucleic acid molecules into functional aptamers. Tuerk and Gold initially described SELEX as a method one could generate high affinity ligands for proteins that bind nucleic acids as a function. The high affinity ligand was generated by starting with an initial variance of ligands, exposing them to alternate cycles of ligand selection, then amplification of bound ligands and discarding of the unbound. This process is done iteratively, representing the successive generations during an evolutionary process. Since the emergence of the field, improvements in methodology have been described, such as implementation of more stringent binding conditions as generations proceed to weed out poor aptamer bindings and select for aptamers with higher binding affinities and counter selection to develop aptamers that exhibit selectivity against chemically similar species. Finally, DNA pools are sequenced and analyzed by bioinformatics to cluster similar groups and strategically select strong candidates. (**Figure 1.5**)

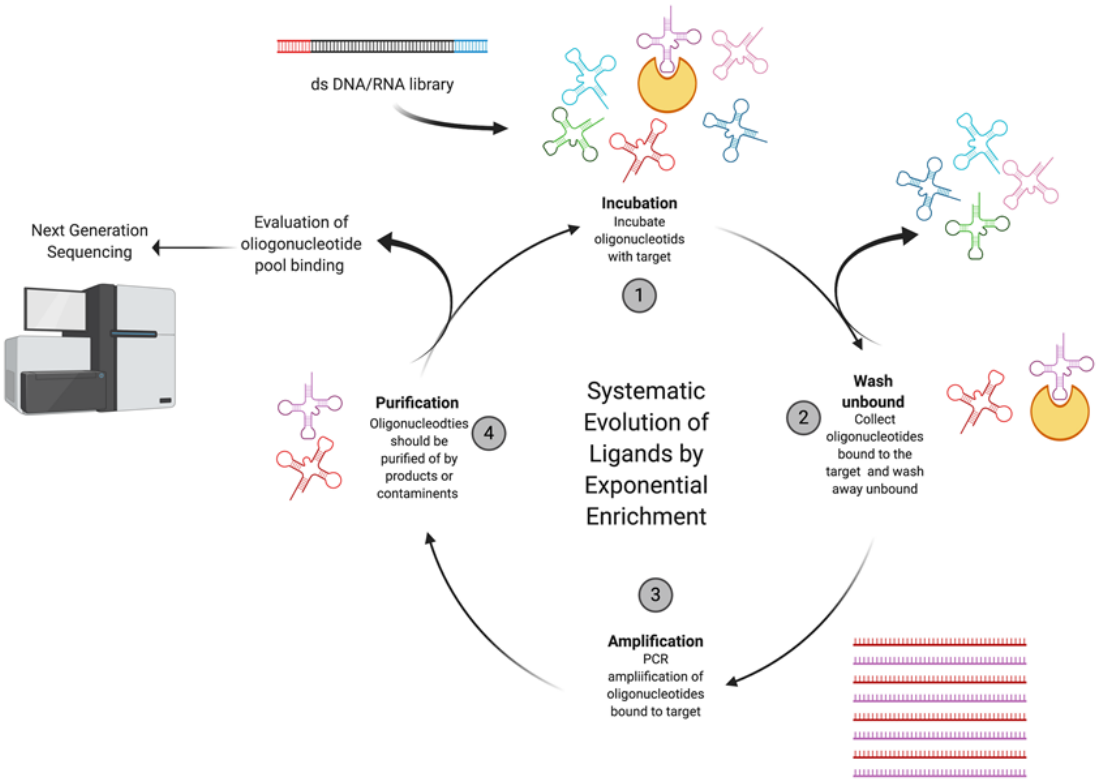

Figure 1.5. SELEX schematic for general target of interest. The workflow is divided into an incubation step, a wash step, an amplification step, and a purification step. The steps are repeated for several rounds then pools are checked by binding assay and sequenced for bioinformatic analysis.

The field of aptamers has further flourished by incorporating vast types of targets and chemically modified nucleic acids.[73] The use of chemically modified nucleic acids to give rise to more favorable physical characteristics such as an increase in stability and resistance to degradation of enzymes is another recent advancement in the field.[74] Several established modified SELEX methods for more specific applications also exist, such as live cell-based SELEX,[75] Fluorescent-Activated Cell Sorter based SELEX, capture-SELEX,[76] and tissue slide based SELEX.[77] Other non-SELEX based methods have also been previously described, which may be advantageous for non-clinical applications.[78]

APPLICATION OF APTAMERS TO EXTRACELLULAR VESICLES

Aptamers have been applied to the profiling, capturing,[79] detection[80,81] and anticancer targeting[82,83] of EVs. Moreover, aptamers have been applied to whole cancer cells in hopes of biomarker discovery, but not yet to EVs.[14] Biomarkers on whole cells do have their own set of useful applications, such as determination of molecular subtypes or discovery of new drug targeting, however, they lend little insight on detecting cancer by non-invasive methods since the detection of circulating tumour cells is an unlikely event and a consequence of a well-advanced cancer. EVs are a promising alternative because they offer a source of quantifiable and concentrated biomarkers that are related to their cell of origin. However, aptamers have yet been applied to EVs for novel biomarker discovery.

APTAMER-BASED TARGET IDENTIFICATION

Despite an industrial and clinical need for reliable biomarkers indicative of various diseases, there is little work done in academia that translates to the clinical environment.[84] One potential explanation for this discrepancy, is the lack of efficient methods for biomarker discovery. Most modern experiments rely on proteomic studies for the identification of novel biomarkers for disease. Though this is a powerful technique, it involves the global analysis of total protein or surface protein content. The advantage of combining aptamers with established proteomic methods offers an even higher degree of selectivity and a more focused approach. The idea of combining aptamers and a mass spectrometry-based approach for biomarker discovery was coined Aptamer-Facilitated Biomarker Discovery (AptaBiD) in 2008. [84] The most fundamental advantage of using an aptamer-based biomarker discovery approach is that it eliminates the need to have a preconceived notion of the binding partner. Theoretically, a selected aptamer that binds only

cancerous EVs but not to non-cancerous EVs, then the binding partner should be unique to the surface of cancerous EVs. A potential disadvantage of this approach is that there is little direct control over the binding partner of the aptamer on a biological and complex target. The discovered binding partner discovered may not be unique to the experimental group, or it may not be relevant to cancer. However, studies of this nature should persist despite the drawbacks because, EVs are relatively new field of research and thus there is enormous potential to deepen our understanding of EVs - regardless of the outcome.

Chapter 2

Extracellular Vesicle Isolation and Validation

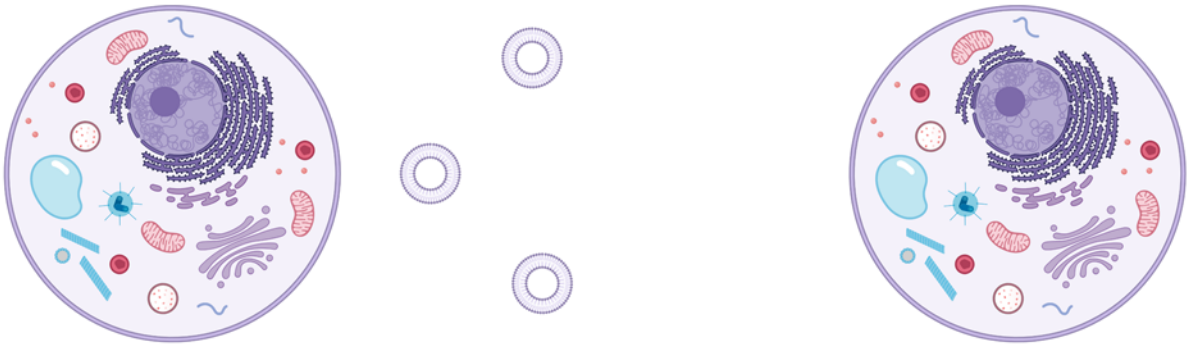

2. EXTRACELLULAR VESICLE ISOLATION AND VALIDATION

2.1 Objective

In this chapter, the rationale for the cell lines used throughout the thesis will be discussed. Then, it explores differential ultracentrifugation, density gradient separation and ultrafiltration as a means for EV isolation. The methods were compared for their effectiveness and efficiency. The established most reliable methodology for the isolation of exosomes was then used for EV characterization, achieved in collaboration with the Flow Cytometry and Robotic facilities and Dr. Sabrina Leslie at McGill University by checking for common small/medium EV markers (CFSE, CD81, CD63, CD9), transmission electron microscopy, convex-lens induced confinement microscopy, and nanoparticle tracking analysis. EVs were isolated from cell culture media, healthy human saliva, and urine (Approved Ethics Certificate No. H-08-18-980).

2.2 Introduction

Currently developed EV isolation methods may be categorized by: ultracentrifugation, density gradient separation, polymer-based precipitation, microfluidic or affinity-based methods.[85] It is important to select the appropriate isolation method for downstream applications. Methods may be used on their own or in combination – each carrying their own advantages and disadvantages as summarized in **Table 2.2.**

Table 2.1 EV isolation techniques. Comparison of ultracentrifugation, density gradient separation, polymer-based separation, immunoselection and microfluidics.

Method	Advantages	Disadvantages
Ultracentrifugation	• Commonly used therefore, protocols well established	• Time consuming and laborious • Large vesicle contamination • Aggregation of surface proteins could lead to the masking of antigens
Density gradient separation	• Better sample purity	• Requires special instrumentation
Polymer based separation	• High yield	• High risk of contamination (particularly with lipoproteins), especially in serum
Immunoselection	• Isolation of a subpopulation	• Costly • Impractical for large sample volume • Fails to consider heterogeneity of a sample
Microfluidics	• Compatible with small volumes	• Lack of evidence for efficiency or clinical downstream applications

ULTRACENTRIFUGATION

Centrifugation is a commonly used lab technique that allows for the separation of particles based on size and density as a result to being subject to a strong gravitational force. Ultracentrifugation (UC) applies the principal of centrifugation put at higher speeds, applying a centrifugal force up to 300,000-fold greater than gravity to a given sample.[85] Forces experienced by a particle on a circular path, identical to one inside of an operating centrifuge run are summarized in **Figure 2.1.**

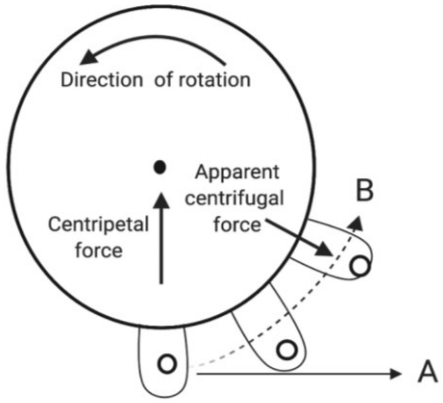

Figure 2.1. Forces experienced by a particle subject to centrifugation. The particle path is projected by arrow A – always tangent to the circular path. The centripetal force pulls the particle towards the center, causing the particle to deviate from its original trajectory of path A, and curve on its new path, B.

The velocity of a particle in centrifuge tube is dependent on the centrifugal force, Archimedes floating force and Stokes viscous drag force. The relationship between the parameters may be described mathematically by **Equation 2.1**.

$$v = g_{eff}\frac{d^2}{18\eta}(\rho - \rho_{solv}) \quad where \quad g_{eff} = \omega^2 R \tag{2.1}$$

Where, g_{eff} is the centrifugal force (acceleration), R is the radius of rotation, ω is the angular frequency of rotation, d is the diameter of a spherical particle, η is the viscosity of the solution medium, ρ and ρ_{solv} are the density of the particle and solution, respectively.

The particle will eventually reach terminal velocity (v_t) defined as the maximum velocity as if falls through the fluid, i.e. when the net forces acting on the object sum to zero. Then, we may arrive to sedimentation coefficient, s expressed more precisely in Svedberg's, where 1 Svedberg is equal to 10^{-13} seconds. The sedimentation coefficient allows for the comparison between particles of different size, different solution mediums and the rate at which they will sediment during a centrifugation protocol. The mathematical representation of the relationship may be described by **Equation 2.2,** where the m is the mass of the particle and r_0 is the radius of the particle. All other variables are defined similarly to **Equation 2.1**.

$$s = \frac{v_t}{rw^2} = \frac{m}{6\pi\eta r_0} \tag{2.2}$$

Protocols are generally are reported in terms of relative centrifugal force (RCF) expressed in units of gravity (g). Most centrifuges require a rotation speed in terms of revolutions per minute (rpm) and thus a conversion factor must be applied. The relationship between RCF and RPM is as described in **Equation 2.3**, where g is the relative centrifugal force, R is the radius of the rotor in centimeters, and S is the speed of the centrifuge in revolutions per minute.[86] This conversion considers differences in the rotor radius, which likely varies from rotor to rotor.

$$g = (1.118 \times 10^{-5})\ R\ S^2 \tag{2.3}$$

There is an inversely proportional relationship between the relative centrifugal force experienced by a sample and the size of the particle isolated. Therefore, a smaller particle requires a larger centrifugal force for it to be pelleted. When the centrifugation steps are planned in a chronological and logical fashion, we reach the fundamentals of density ultracentrifugation.

To compare rotor pelleting efficiency, the term k-factor should be introduced. Most research groups report the RCF used to isolate EVs but fail to consider that other groups could use a different rotor which would yield an entirely different centrifugal force. Without consideration of the k-factor, a different magnitude of force would be applied to the same sample despite

consideration of equation 1. This discrepancy would result in a variation of samples isolated and misleading results. K-factor considers maximum radius (r_{max}) and minimum radius (r_{min}) which both contribute to the maximum g force generated by the rotor. The mathematical relationship is described in **Equation 2.4**.

$$\text{k factor} = 2.533 \times 10^5 \times \ln\left(\frac{r_{(max)}}{r_{(min)}}\right)\left(\frac{RPM}{1000}\right)^2 \quad (2.4)$$

Differential Ultracentrifugation

Differential ultracentrifugation (DC) is regarded as the most reliable and commonly used technique for EV isolation.[87] The variation among published protocols and the laborious nature of this technique are the disadvantages of this technique. An optimized protocol for EV isolation should consider different rotors and their pelleting efficiency, volume of starting sample, viscosity of sample and nature the sample (ex. saliva sample would have a high concentration of amylase protein, which should be factored into the isolation protocol). If possible, it is best to optimize isolation protocol on a case-by-case basis of different sample types and starting volumes. Generally, a differential ultracentrifugation isolation strategy for EVs from cell culture media generally involves a primary centrifugation step to remove whole cells, followed by an ultracentrifugation step to remove intact organelles and large vesicles, subsequent a final ultracentrifugation step to pellet EVs as described in **Figure 2.2.**

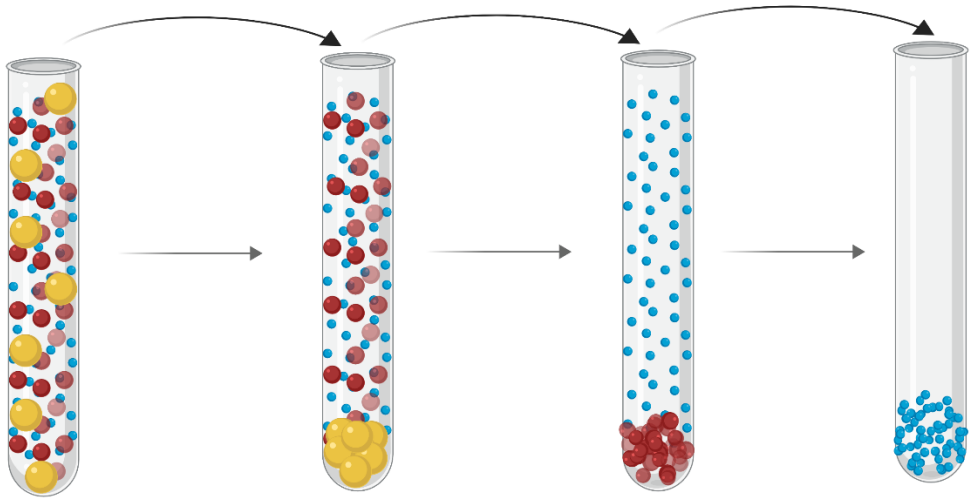

Figure 2.2. General schematic of differential centrifugation. Differential centrifugation is a technique commonly used to separate a smaller subset of particles from a complex mixture starting solution. It is carried out by spinning the sample at increasing speeds and discarding the pellet, until the molecule or species of interest is pelleted. The pellet is washed with a buffer and resuspended in an appropriate buffer solution.

DENSITY GRADIENT ULTRACENTRIFUGATION

Density gradient isolation involves creating a linear concentration gradient of a solvent molecule, typically sucrose, iohexol or iodixanol. Sucrose is commonly used density gradient for the isolation of EVs, perhaps because of its abundance in availability. A linear sucrose gradient of 2.0-0.25 M was created in an ultracentrifuge tube, then the EV sample isolated from DC is applied to the top of the gradient. As a result of ultracentrifugation, particles with different components of the sample will separate according to their density, by settling to their isodense fraction **(Figure 2.3).** Theoretically, better separation of EVs can be achieved from other components in the sample, as both size and density are considered.[88] Density gradients can be particularly useful for removing protein aggregates, perhaps more problematic in isolating EVs from certain biological fluids.[89]

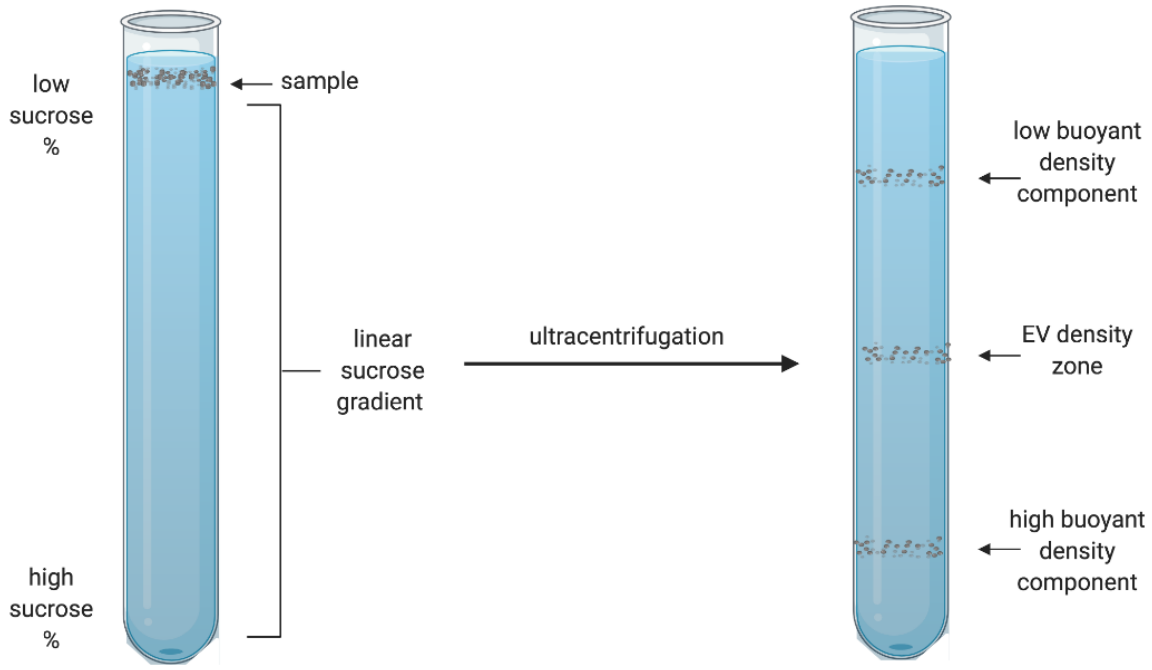

Figure 2.3. Schematic of sucrose gradient EV isolation. A linear gradient of sucrose is created in an ultracentrifuge tube. The EV sample pre-isolated from DC is applied to the top of the gradient. As a result of ultracentrifugation, particles with different components of the sample will separate according to their density, by settling to their isodense fraction.

ULTRAFILTRATION

Ultrafiltration (UF) is a method where membrane with a predetermined pore size is used to achieve separation by relative molecular mass. The selected filter allows solvents and small molecules to pass through the membrane, while retaining molecules with relatively higher molecular mass containing the molecule of interest. There is evidence to support UF is a valid method for EV isolation however, there is reason to doubt the purity of the isolated sample since is it exclusively a size-based technique, it does not discriminate against other molecules in a similar size range. Nevertheless, UF is an attractive method of EV isolation because of its relative affordability and convenience. [90]

Isolation of EVs must be followed with validation and characterization of the chosen method. This may be done quantitatively or qualitatively – it is recommended that several methods be used in conjunction with each other since each technique has its own set of limitations. [27] Quantitative methods commonly used for validation and characterization of isolated EVs are light

scattering techniques such as Nanoparticle Tracking Analysis or Dynamic Light Scattering, and immunoaffinity techniques such as western blot or flow cytometry. Qualitative methods that may be considered as additional validation are transmission electron microscopy and modified wide-field microscopy, such as convex-lens induced confinement.

NANOPARTICLE TRACKING ANALYSIS

Nanoparticle Tracking Analysis (NTA) is a light scattering technique that relates single nanosized particles to their Brownian motion in a solution by the Stokes-Einstein equation **(Equation 2.5).**[91,92]

$$D = \frac{RT}{N} \times \frac{1}{6\pi Z r} \tag{2.5}$$

Where D is the diffusion constant, R is the gas constant, N is Avogadro's number, T is the absolute temperature, Z is viscosity of the medium, and r is the radius of the diffusing particle. The Stokes-Einstein equation assumes that the particles in the solution move independently, are spherical in geometry, that their average kinetic energy is the same as gas molecules, and that the size of the molecules are proportionally small compared to the medium.[93] It should be noted that the same particle in a different medium will have a different radius according to the equation above, hence buffers should always be kept consistent when comparing samples.

The effective range of NTA is generally understood to be 30-1000nm, however the lower bound level of detection is depended on the refractive index of the particles. For biologically relevant such as EVs, NTA has been shown to be less effective at measuring particles equal or smaller than 70nm[94], problematic since many small EVs have been shown in the 70-90 nm size range.[95] NTA is also limited by the range of particle concentration that it can accurately detect, approximately 10^7-10^9 particles/mL, a narrower range than the competitor DLS technique.[96–98]

NTA exclusively quantifies particles in a non-specific manner, therefore it should be used in conjunction with other techniques to confirm the presence of EVs. Where there is EV isolation, there is almost certainly NTA – it is the most available, straightforward, and cost-effective technique.

Flow Cytometry

Flow cytometry is a powerful and widely applied technique that measures scattered light or fluorescent intensity. Particles are aligned in single file as they pass through a laser, where the light is scattered and detected giving information about their size and granularity (internal complexity). Cell components can be fluorescently labelled and then excited by a laser which allows the conclusion of whether the cell marker of interest is present.

Flow cytometry analysis of cells is common practice, however EV analysis by flow cytometry presents novel challenges because the majority of EVs fall below the lower level of detection. The method of EV analysis of by flow cytometry generally depends on the resolution of the instrument: lower resolution cytometers require the coupling of EVs to beads large enough to be detected, alternatively a higher resolution cytometer may carefully be used to analyze bare EVs but require careful use and an experienced technician.[99] Fluorescent Activated Cell-Sorters (FACS) are an example of a more powerful type of flow cytometer. In addition to light scattering information, FACS instruments can also separate different populations of particles based on their properties as shown in **Figure 2.4.**

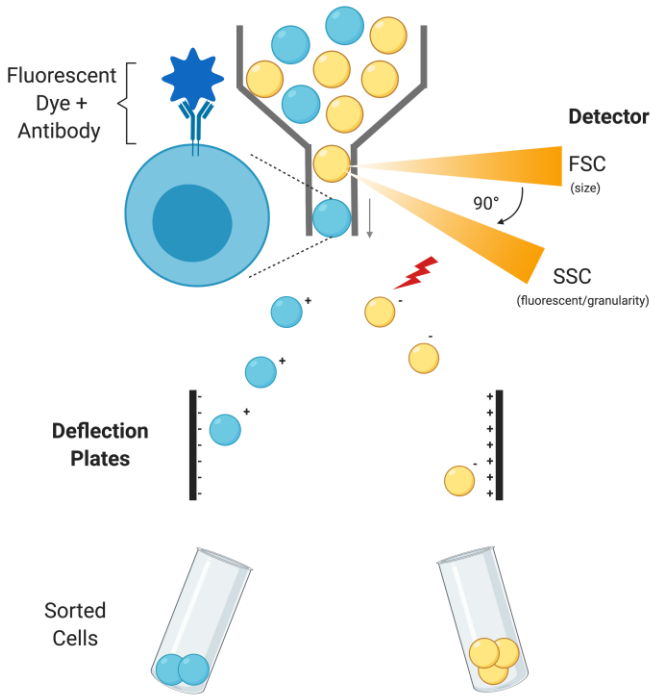

Figure 2.4. Schematic of Fluorescent-Activated Cell Sorting. The particles in the sample are forced into a single file as they pass the lasers. The particles then deflect light in a manner dependent on their physical

properties and are detected by the detector system. The particles are then given a charge assigned by the operator and particles can be separated into different samples.

The small size of EVs may result in multiple particles passing the laser at the same time, all being detected as a single event. This is known as the "swarm effect" and is more likely to occur when analyzing samples with a high particle concentration.[100] The swarming effect can be avoided by adjusting the sheath pressure of the sample depending on the relative concentration of particles. For instance, for relatively more concentrated sample, the sheath pressure should be reduced to decrease the likelihood that particles pass through the laser simultaneously.

Another physical phenomenon to consider is the small size EVs, therefore falling below the limit of diffraction of visible light.[101] This affects the type of scattering they give off after interacting with light rays. Larger particles follow Mie scattering pattern, where light is mostly scattered in the forward direction. In contrast, EVs are governed by Rayleigh scattering, considered to be elastic scattering since the energies of the scattered photons remains the same. Mie scattering and Rayleigh scattering patterns are shown in **Figure 2.5.** The refractive index of EVs is between 1.35 and 1.8.[101]

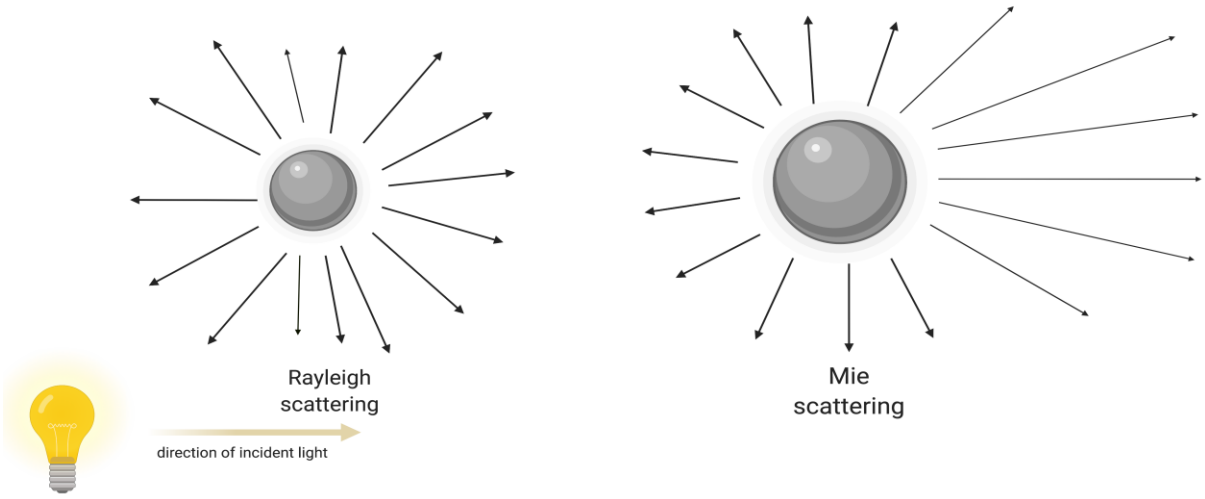

Figure 2.5. Rayleigh versus Mie Scattering. Very small particles <1/10 of visible wavelength obey Rayleigh scattering when interacting with light. Larger particles obey Mie scattering when interacting with light.

TRANSMISSION ELECTRON MICROSCOPY

Transmission electron microscopy (TEM) is a powerful technique used for the determination of morphology and structure of microstructures by ejecting a highly energetic electron beam through the sample of interest, the interaction between the electron and the sample forms an image. The components of a TEM instrument are the electron beam source, electromagnetic lenses and an electron detector as summarized in **Figure 2.6.** The electron source stimulates electrons to be ejected that are then accelerated and focused on the sample by the condenser lens. The electron beam passes through the sample whilst interacting with it, then reaches the objective lens where the electron beam is collected and then projected onto the detector by the projector lens to the computer for visualization of the sample.

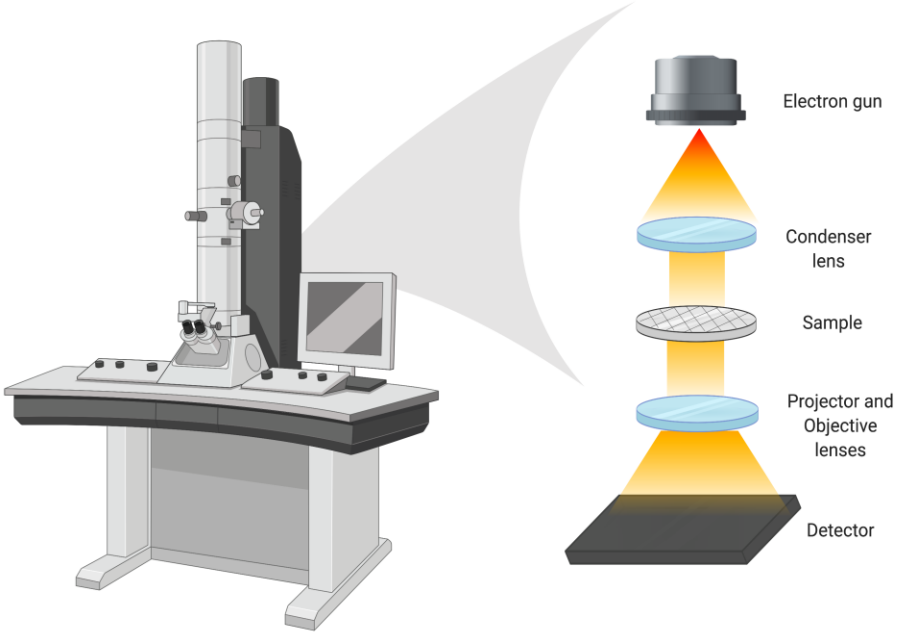

Figure 2.6. Schematic of transmission electron microscopy. TEM instrument is composed of the electron beam source, electromagnetic lenses, and an electron detector. The electron source is stimulated to eject electrons, that are then accelerated and focused on the sample by the condenser lens. The electron beam passes through the sample whilst interacting with it, then reaches the objective lens where the electron beam is collected and then projected onto the detector by the projector lens to the computer for visualization of the sample.

EVs fall below the limit of diffraction of visible light and thus it is impossible to view them using normal light microscopy techniques. TEM is widely use for the visualization of nanosized particles due to its nanoscale resolution, allowing for the visualization of EVs and discrimination from similar sized non-EVs particles.[102–104] Suboptimal resolution is a common challenge with

TEM since the negative staining required typically does not allow EVs to maintain their hydrated-native state. For this reason, Cryo-EM is a more suitable technique, however due to a lack of availability, it will not be evaluated in this report.[102]

Arguably, the use of TEM to assess the overall quality of a sample is a misuse of the technique, since the images obtained are selectively chosen by the operator have a high likelihood of bias. Instead, TEM is effective in confirming the presence of true EVs, by verifying the spherical morphology and lipid membrane bilayer, as opposed to debris or other irrelevant particles. [102]

FLUORESCENT MICROSCOPY IMAGING

Convex Lens-Induced Confinement (CLiC) imaging is the modified modern version of wide-field fluorescent microscopy. The technique of CLiC traps molecules inside of a nanoscale pit that is formed between a convex lens and a planar coverslip as shown in **Figure 2.7.** The shallow depth of the entrapment allows for reduced background fluorescence and eliminates out-of-plane diffusion compared to other microscopy techniques. [105]

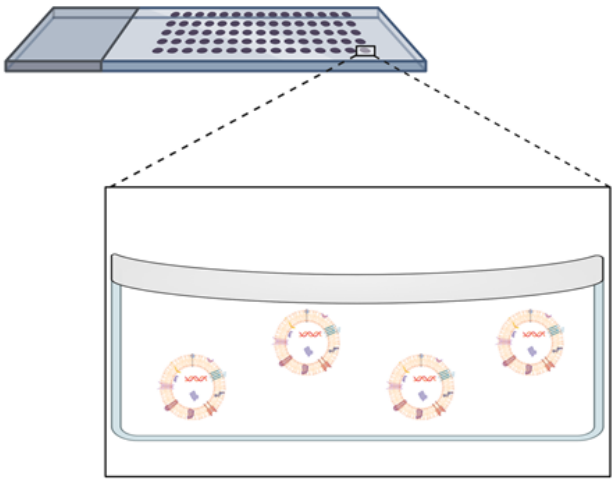

Figure 2.7. Convex lens-induced confinement technique traps molecules within a nanoscale glass well. The top arm piece pushes the top glass lens, forming a convex lens as it interacts with the planar glass coverslip.

The CLiC imaging system offers several unique advantages compared to other imaging techniques: molecules in a sample may be studied free in solution as well in real time, there is a relatively high throughput, better signal to noise ratio by the shallow depth of the pit, and the ability

to mimic physiological conditions inside of the flow cell. Eliminating out-of-plane diffusion by entrapping molecules in the glass pit results in an increased observed diffusion-limit observed per molecule.[105] A common drawback when using this system is that the glass of the cell wall where the sample is investigated has a net negative charge, thus positively charged molecules may spontaneously stick to the walls of the cell. Optimization of buffer conditions, dye concentration, if treatment to the glass well is required, removal of free dye should be assessed on a case-by-case basis. CLiC imaging technology has been applied to biomolecules such as DNA,[106,107] protein interactions[108] and single cells[109] but had not yet been applied to EVs.

2.3 Methods

CELL CULTURE

The cell lines used throughout the project were MDA-MB-231 (ATCC®, Cat No. HTB-26), HEK-293 (ATCC®, Cat No. CRL-1573™), MCF-7 (ATCC®, Cat No. HTB-22™), and MCF-10A (ATCC® CRL-10317™). Each cell line was grown in the ATCC recommended cell culture media except for MCF-7 and MDA-MB-231, instead cells were grown in DMEM/F12 to avoid differences in culture media influencing the expression of EV markers. Supplement recommendations by ATCC were followed. All culturing growth media specifications are included in **Table 2.2.** All cells were incubated at 37 °C in 5% carbon dioxide (CO_2) conditions. Cells were split when they reached 90-95% confluency and plated at 90-95% viability on 75 cm^3 vented cell culture flasks (ThermoFisher, Cat No. 156499) at approximately 10 million cells per plate. EVs were harvested only after incubation in EV free FBS. EV free FBS was prepared by a 1:1 dilution with the appropriate un-supplemented cell culture media to reduce the viscosity of the FBS for better pelleting efficiency of EVs. The 1:1 mixture was then spun at 100,000 g for 20 hours in the SW28 rotor (Beckman Coulter, Cat No. 342204) and the pellet was discarded. The prepared EV free FBS filtered with a 0.2 um syringe filter (MilliporeSigma, Cat No. SE1M179M6) to ensure suitable sterility for cell culture conditions and was stored at -20 °C for no longer than 2 months.

Table 2.2 Media Recipes for MDA-MB-231, HEK-293, MCF7 and MCF10A cell lines.

Cell line	Growth Media	Supplements (final concentration)
MDA-MB-231	DMEM/F12[3]	10% FBS [1] Antibiotic/Antimycotic[5]
HEK-293	EMEM[4]	10% FBS[1] Antibiotic/Antimycotic[5]
MCF-7	DMEM/F12[3]	10% FBS [1] Antibiotic/Antimycotic[5] Insulin (10µg/mL) [6]
MCF-10A	DMEM/F12[3]	5% HS[2] Antibiotic/Antimycotic[5] 100 ng/ml cholera toxin[7] Hydrocortisone (1mg/mL)[9] EGF (20ng/mL)[8] Insulin (10µg/mL) [6]

Additional information:

1. FBS = Fetal Bovine Serum (Sigma, Cat No. F2442)
2. HS = Horse Serum (Sigma, Cat No. H1270)
3. DMEM/F12 (ThermoFisher, Cat No. 11320082)
4. EMEM (ThermoFisher, Cat No. MT10009CV)
5. Antibiotic/Antimycotic (Sigma, Cat No. A5955)
6. Insulin (Sigma, Cat No. I-1882): Resuspended at 10 mg/ml in sterile dH2O then mixed for 10-15 minutes at 200 rpm. Aliquots stored at –20°C
7. Cholera Toxin (Sigma, Cat No. C-8052): Resuspended at 1 mg/ml in sterile dH2O and mixed for 10-15 minutes at 200 rpm. Aliquots stored at –20°C
8. EGF = Epithelial growth factor (Peprotech, Cat No. GMP100-15): Resuspended at 100 µg/ml in sterile dH2O. Aliquots stored at –20°C.
9. Hydrocortisone (Sigma, Cat No. H-0888): Resuspended at 1 mg/ml in ethanol. Aliquots stored at -20°C.

ULTRACENTRIFUGATION: EVS FROM CELL CULTURE

After harvesting cell culture media, EV isolation protocol was immediately carried out. Whole media was spun in for 10 minutes at 300 g to remove detached or dead cell. The supernatant was then spun in the same rotor for 30 minutes at 2600 g to remove cell debris. The supernatant was then spun in the SW28 (Beckman) rotor at 16,500 g for one hour to remove large EVs such as apoptotic bodies. The supernatant is then spun in the SW28 rotor at 100,000 g for 3 hours, which finally allows small and medium sized EVs to be pelleted. The last step washes the pellet with PBS to remove contaminants from the cell media. The EV pellet is resuspended in PBS and used for experiments within 1 week in 4°C storage conditions, or within 1 month in –20°C storage conditions. Differential ultracentrifugation steps are summarized as a schematic in **Figure 2.8.** [110]

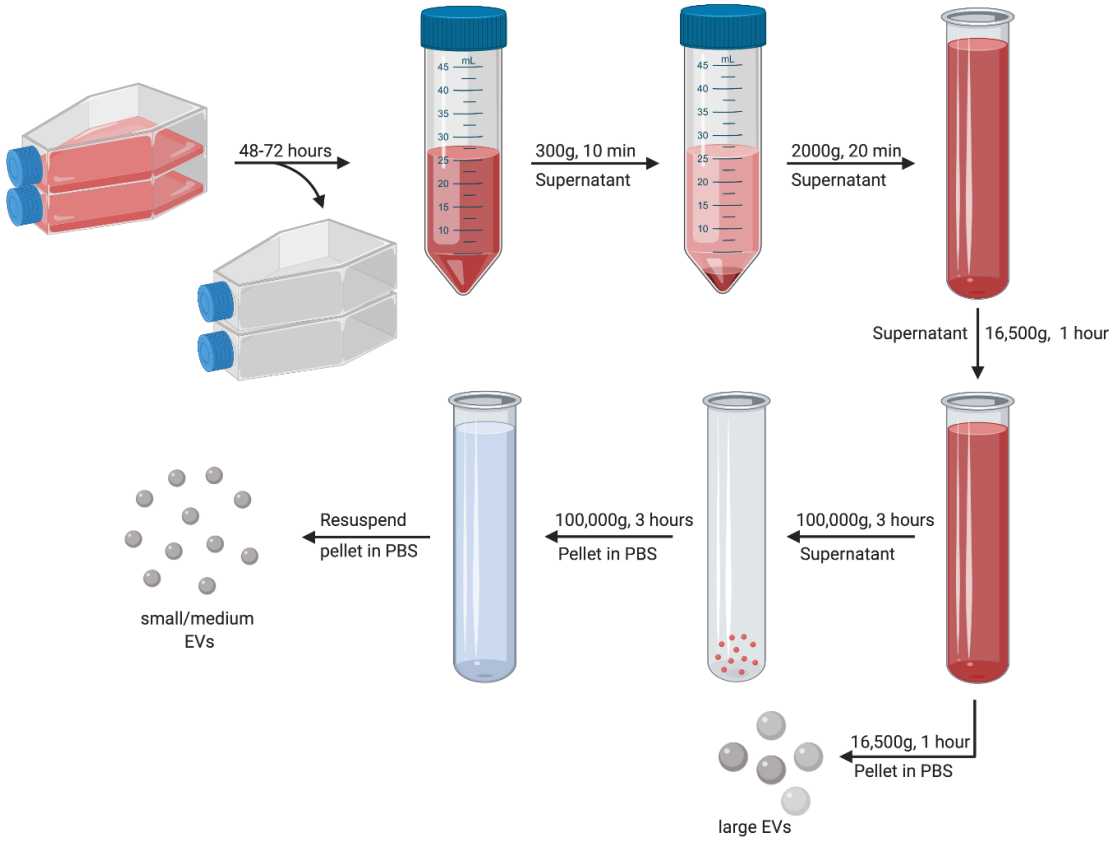

Figure 2.8. Isolation of small/medium EVs by differential ultracentrifugation. Cells that had reached ~30% confluency were incubated with EV free media for 48-72 until ~95% confluency. The cell media is harvested and spun at 300 g for 10 minutes to remove dead cells. The supernatant is then spun at 2000 g for 20 minutes to remove cell debris. The supernatant is then spun at 16,500 g for 1 hour to remove large vesicles, then finally small and medium EVs are pelleted at 100,000 g for 3 hours, washed, then resuspended in PBS.

ULTRACENTRIFUGATION: EVS FROM SALIVA

An in-house affinity chromatography was prepared by packing 0.5 g starch (Cat No. 9005-84-9, ThermoFisher) dissolved in 3 mL of PBS inside a syringe and then attached to a 0.2uM membrane filter. [111] Healthy donor criteria included: non-smoking male or female participants aged 18 to 60 with no history or current chronic medical conditions, including any acute respiratory infections. The donors were fasted or had not had food or drinks (except for water) for at least 1 hours and the donation was provided in the laboratory. The sample was processed immediately. 20 mL of saliva was collected from 5 different healthy donors and were pooled together. The saliva was diluted 1:1 with PBS then applied to the in-house chromatography plus filter system. The saliva was then treated by differential centrifugation using the same protocol as described for isolation of EVs from cell culture.

ULTRACENTRIFUGATION: EVS FROM URINE

Healthy donor criteria included: male or female participants aged 18 to 60 with no history or current chronic medical conditions, including any acute urinary tract infections, chance of pregnancy or sexual transmitted infections. The donors were asked to provide the first morning void and bring it to the laboratory within 1 hour of producing the sample. The sample was immediately stored in a 4°C fridge and processed within 24 hours. The 20 mL of urine was collected from 5 different healthy donors and were pooled together. The urine was then treated by differential centrifugation using the same protocol as described for isolation of EVs from cell culture.

ULTRAFILTRATION

Cell culture media was harvested and whole cells were removed by centrifuging the samples at 300 g for 10 minutes. The supernatant was collected and centrifuged at 2000 g for 20 minutes to remove cell debris. The supernatant was collected once more then transferred to Amicon® Ultra 30 kDa cut-off filter (Sigma, Cat No. UFC8030) and spun for 3000 g for 30 minutes as described in **Figure 2.9**.

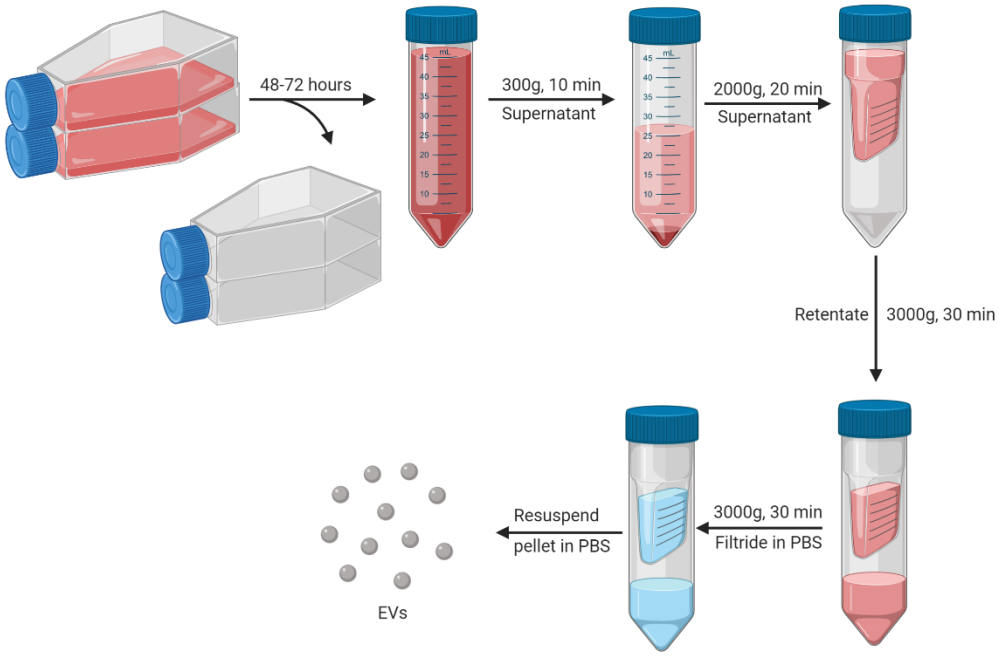

Figure 2.9. Schematic of isolation of small/medium EVs by ultrafiltration. Cell that had reached ~30% confluency was incubated with EV free media for 48-72 until ~95% confluency. The cell media is harvested and spun at 300 g for 10 minutes to remove dead cells. The supernatant is then spun at 2000 g for 20 minutes to remove cell debris. The supernatant is then spun at 2000 g for 20 minutes by 30 kDa filter until all the retentate has passed, washed twice with PBS, then resuspended in PBS.

Nanoparticle Tracking Analysis

The ZetaView nanoparticle tracking microscope PMX-110 (Particle Metrix) was used for determining the concentration and size distribution of exosomes at 85 and 40 camera shutter speeds. Data was acquired from 11 camera positions without exclusion unless recommended by the software. Polystyrene beads 102 nm in size (Microtrac, Cat No. 900383) were used to focus the camera and calibrate the instrument. Serial dilutions of isolated EV samples were prepared from 1:10 to 1:10,000 from all original samples to find the appropriate concentration of 10^8-10^9 particles/mL[112] for the instrument.

Transmission Electron Microscopy

Isolated EVs were fixed in 2.5 % glutaraldehyde in 0.1 M sodium cacodylate buffer (pH 7.4). Fixed suspensions were spotted on Formvar® coated copper grids (200 mesh; Canemco, Lakefield, ON, Canada) for 30 seconds. Samples were negatively stained with 2% aqueous uranyl acetate for 6 minutes and dried with filter paper. Vesicles were examined on a transmission electron microscope (JEOL JEM 1230, Japan) operated at 50 kV. The Feret's diameter of the particles was measured by analyzing the TEM images using ImageJ software.[113]

Flow Cytometry

FACS experiments were performed on Beckman Coulter MoFlo Astrios-EQ flow cytometer with 5 lasers (355, 405, 488, 561 and 640 nm wavelength) as summarized in **Table 2.3**. The CD63, CD9, CD81 and CFSE antibodies or dyes (**Table 2.4**) were excited and detected with the recommended lasers and PMTs depending on their fluorophore conjugate. 100 uL of isolated EV samples were stained with carboxyfluorescein succinimidyl ester (CFSE) with a 10 ug/mL dilution factor and CD63, CD81 and CD9 antibodies with a 2uL/100 uL dilution factor in filtered PBS buffer as per titration experiments performed by the technician. The samples were then incubated on a shaking plate at 4 °C and 300 rpm in the dark for 30 minutes before running any experiments. Approximately 50,000 events were acquired per sample and the flow rate was adjusted by the technician, as necessary. Raw .facs files were analyzed by Kaluza software. Gating for flow cytometry experiments included taking singlets only from FSC1 & FSC2 and singlets from SSC1 & FSC1 as well as positive populations for the above-mentioned antibodies. "Free" dye was accounted for by gating a sample containing dye and buffer only and then applying this gate to the rest of the samples.

Table 2.3 Lasers and photomultiplier tubes on the Beckman Coulter MoFlo Astrios-EQ flow cytometry (nm).

Lasers				**PMTs**			
355	448/59	620/29	692/75				
405	SSC	448/59	546/20				
488	SSC	513/26	576/21	620/29	664/22	710/45	795/70
561	SSC	579/16	614/20	692/75			
640	SSC	671/30	722/44	795/70			
FSC	FSC1	FS2					

Table 2.4. Chemical dyes and antibodies used in validating the presence of EVs after isolation by flow cytometry [a] or fluorescent microscopy [b].

	Chemical Structure	Binding mechanism	Fluorescent Conjugate	Excitation/ Emission
[a]CFSE[1]	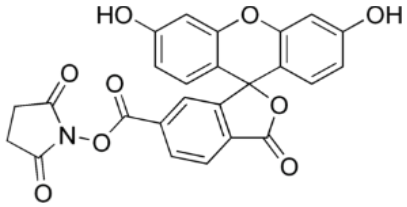	Intracellular amine groups	Not applicable	494 nm/ 521 nm
[b]YOYO-1[2]	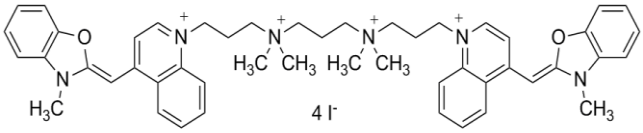	Double-stranded DNA	Not applicable	491 nm/ 509 nm
[a]CD63[3]	Biological	Transmembrane protein CD63	Allophycocyanin (APC)	650 nm/ 660 nm
[a]CD9[4]	Biological	Transmembrane protein CD9	Phycoerythrin (PE)	561 nm/ 578 nm
[a]CD81[5]	Biological	Transmembrane protein CD81	PerCP-eFluor 710	630 nm/ 710 nm

Additional Information:
1.CFSE (eBioscience™CFSE, Cat No. C1157)
2.YOYO-1 Iodide (Invitrogen, Cat No. N7565)
3.CD63 (ThermoFisher, Cat No.MA1-19786)
4.CD9 (ThermoFisher, 11-0091-82)
5.CD81 (ThermoFisher # 46-0819-42

CONVEX LENS-INDUCED CONFINEMENT (CLIC) IMAGING

EVs isolated from MDA-MB-231 cell line were concentrated using a 3 kDa filter (Millipore, Cat No. UFC900308) down to 50 µL. The sample was washed once with 0.2 µm syringe (Sigma, Cat No. Z290823) filtered PBS. From the new concentrated stock, a 1:10 dilution of the EVs were made and stained with 1:50 YoYo-1 dye. The sample was incubated on ice for 20 minutes in the absence of light. After incubation, the sample was filtered through a 0.2 µm syringe (ThermoFisher, Cat No. 13100108). The filtered, stained EV sample was then loaded in 1X TE buffer at pH 7.5 into untreated flow cell with 10, 25 and 50 um pits. Videos of the vesicles were taken on the after excitation of a 506 nm laser under 60X objective lens

DENSITY GRADIENT ULTRACENTRIFUGATION

The methodology of EV isolation by density centrifugation was adapted from Kazuya and colleagues published in 2016.[111] Five concentrations of sucrose (ThermoFisher, Cat No. 15503022), 61%, 49%, 37%, 25% and 15%, were prepared by dissolving sucrose in ddH2O. The prepared sucrose fractions were layered on top of each other as slowly and carefully as possible to minimize disturbances, with the highest concentration on the bottom to the lowest concentration on the top. Pre-isolated EVs from healthy human saliva source was isolated by differential centrifugation (as previously described) were attentively placed on the top layer of the gradient. The sample was ultra-centrifuged at 100,000 g for 18 hours at 4°C in an SW28 rotor. The fractions were then carefully separated, and each washed with PBS by spinning once more at 100,000 g for 1 hour. The fraction pellets were assessed for particle size by NTA.

2.4 Results and discussion

Breast cancer as an experimental group was strategically selected for this project, because it well classified of cancers among its molecular subgroups. Familiarity with breast cancer tumour markers allows for a meaningful comparison against EV potential biomarkers. MDA-MB-231 cell line was used as the experimental group as a model for human triple negative breast cancer. This subtype of breast cancer form of breast cancer is derived from epithelial cells of the mammary gland, and tests negative for Human-Epidermal Growth Factor Receptor (HER-2) and Estrogen or Progesterone Receptors (ER/PR). The aggressive nature of the triple negative breast cancer subtype alongside the lack of targeted treatment strategies yields a relatively low prognosis for affected patients. HEK-293 cell line was used as the main control cell line. This cell line is derived from human embryonic kidney cells – a completely different tissue type and thus in theory, should retain necessary EV surface markers but not ones pertaining to cancer. MCF-7 cell line was used as a breast cancer control cell line during validation experiments. MCF-7 is commonly used a model cell line for ER/PR positive breast cancer subtypes and is derived from epithelial cells of the mammary gland. MCF-10A cell line was an additional breast cancer control cell line used during validation experiments. MCF-10A is a non-tumourigenic cell derived from epithelial cells of the mammary gland that has been transfected for cell culturing purposes. Thus, this cell line is representative of "healthy" breast cells. EVs were isolated from 5 different mediums by UF, DC and density gradient centrifugation and then validated by NTA, flow cytometry and fluorescent microscopy techniques.

DIFFERENTIAL ULTRACENTRIFUGATION

The average particle size isolated by DC across different sources was 154.3 nm ± 12.9 nm. Results displaying particle size (nm) and particle concentration (per cm^3) across different EV sources isolated by DC are summarized in **Figure 2.10**, where it can be observed the natural variation in particle size as well as particle concentration. Though volume of starting material was kept constant, it is generally understood that different cell lines or sources may have a higher or lower EV concentration due to natural variation or innate tissues differences. It is also important to remember the limitation of NTA is that there is no direct correlation between particles and true

EVs. Therefore, it is likely that we are observing an over-estimation of the true concentration of EVs isolated.

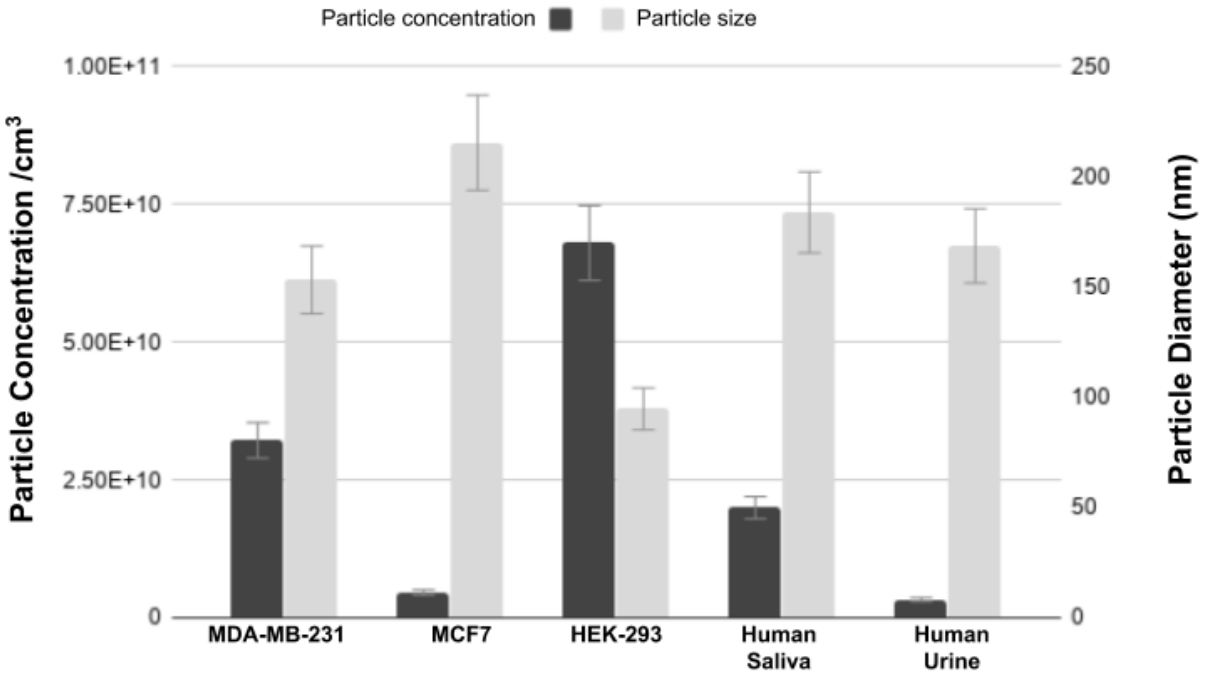

Figure 2.10. Mean particle concentration and diameter ± S.E across different sources using differential ultracentrifugation. Each source accounts for at least two biological replicates and a starting volume of ~233 mL, except for saliva has a starting volume of approximately one-half of the due to its high viscosity. Human saliva and urine samples were pooled among 5 healthy donors.

The high viscosity of human saliva makes brings forth new challenges in the isolation protocol. This bodily fluid is difficult to transfer, pipette and manipulate in general. Generating saliva samples in meaningful volumes is a tasking procedure for the donor. Amylase is one of the highly abundant protein in saliva that contributes to its increased viscosity.[88] The in-house affinity chromatography was previously shown to be effective in removing amylase from saliva during EV isolation prep, therefore it was added to our isolation method. The 1:1 dilution necessary for the isolation of EVs from saliva will affect the concentration of EVs isolated, presumably by one half. Interestingly, urine has yielded lower concentration despite twice the starting volume. These results should be repeated and validated by additional parameters, such as total protein content, immunoblotting or immunosorbent assays to draw more meaningful conclusions since to date there has not been a comparative study to quantify EVs in healthy human urine and saliva.

DENSITY GRADIENT ULTRACENTRIFUGATION

The density zone of most EVs lies in the low-density range (1.10-1.18 g/cm^3) [88] or the high-density range (1.26–1.29 g/cm^3).[114] Four out of five fractions of the density gradient isolation protocol were chosen for NTA analysis, as shown in **Figure 2.12.** Fractions containing 25% and 37% sucrose yielding particles in the most appropriate size range for small to medium EVs. There is an increase in average particle size the % sucrose increases. It appears that vesicles of in the size range of interest did settle in the appropriate fractions, however, there seems to be spill over into the 25% fraction as well. This could be a result of hand making the gradient since a specialized instrument is normally used for his purpose but was not available in our laboratory. The fraction of interest does not appear to be purer than DC alone, since the size range of particles from the pellet in both cases is approximately 150±55 nm. Furthermore, subpopulations of EVs with different densities have been identified, therefore it can simply be the case that we are seeing the different subpopulations of EVs based on density.[114] It is acknowledged that theoretically, density gradient density centrifugation should be a superior method of isolation in terms of vesicle purity, [115] however this is not the result observed and it does not give an advantage for the purposes of this work to isolate one subpopulation of EV densities over another. Therefore, traditional DC was a preferred method of isolation over density gradient centrifugation.

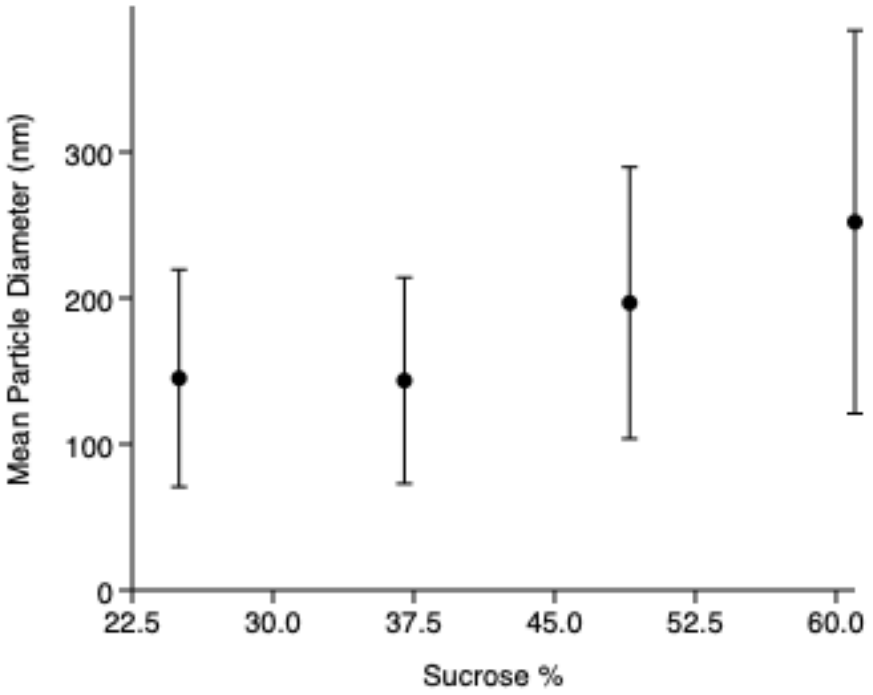

Figure 2.11. Mean particle diameter ± S.E. of sucrose gradient fractions isolated from healthy human saliva and analyzed by NTA. Each fraction was separated and washed with PBS; the pellet was then analyzed by NTA. From left to right, sucrose fractions 25%, 37% 49% and 61% are shown above.

ULTRAFILTRATION

On average, UF yields a higher particle concentration and larger particle diameter compared to DC method as demonstrated in **Figure 2.13.** This observation is expected since UF method theoretically will collect all particles equal or smaller than the 30 kDa cut off. Although DC is likewise isolating EVs with respect to their relative size to other particles in the medium, this method typically yields a cleaner sample with less contaminates.[116,117] One plausible explanation is that DC protocol has an additional 16,000 g step which is intended to remove larger vesicles and contaminants, but EVs are also likely to be lost at each step of transfer during the isolation protocol. Another explanation for the results observed may be that DC requires much high pressure to be exerted on the sample for separation which is known to be correlated with the rupture or damage of some vesicles. There is a tradeoff between concentration of particles isolated and sample purity – though purity of the samples were not assessed in this report, it has been shown to be the case in the literature.[118]

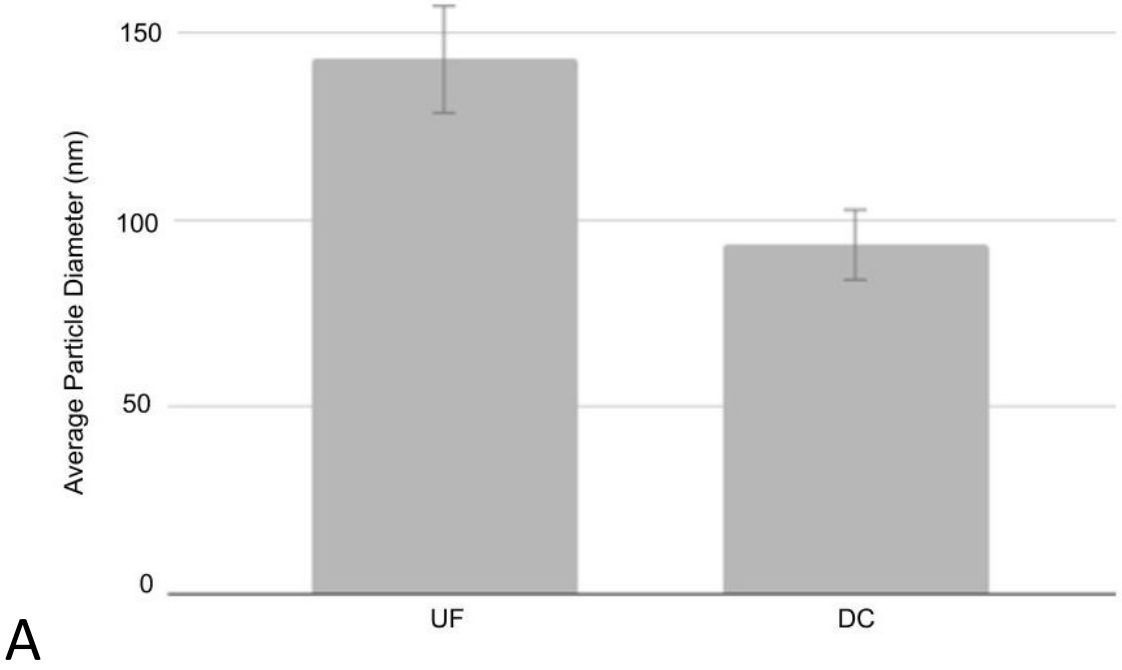

A

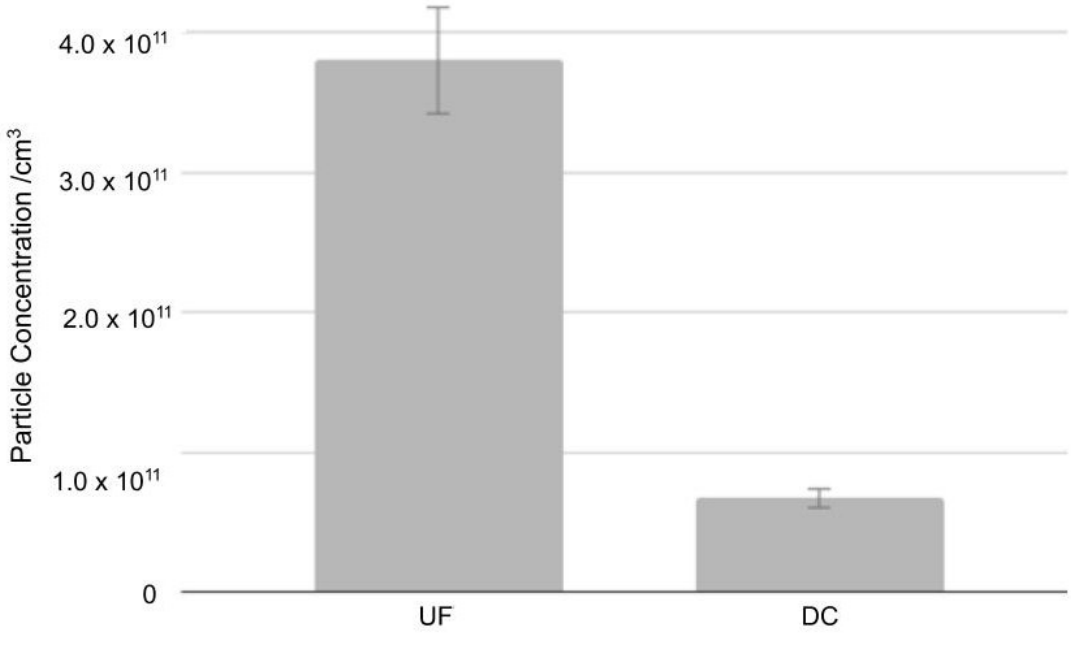

B

Figure 2.12 Comparison of ultrafiltration (UF) and differential ultracentrifugation (DC) methods for EV isolation by assessing mean particle size (A) and concentration (B) ± S.E by Nanoparticle Tracking Analysis. Data was acquired from two biological replicates of HEK-293 cell line derived EVs using the UF method and the DC method described.

NANOPARTICLE TRACKING ANALYSIS

DLS and NTA light scattering techniques nanoparticle tracking analysis are frequently used for comparing or assessing EV isolation protocols.[92,96,119]. NTA was the method used due to accessibility over DLS. Histogram NTA results of an EV sample isolated by UC (**Figure 2.14**) reveals a mean particle diameter of 129 nm, with a second peak of vesicles just under 100 nm and most of the particles within 50 to 200 nm diameter range. The literature reports that small/medium EVs reside in the 30-150 nm size range, though there is some inconsistency in the precise size range.[120]

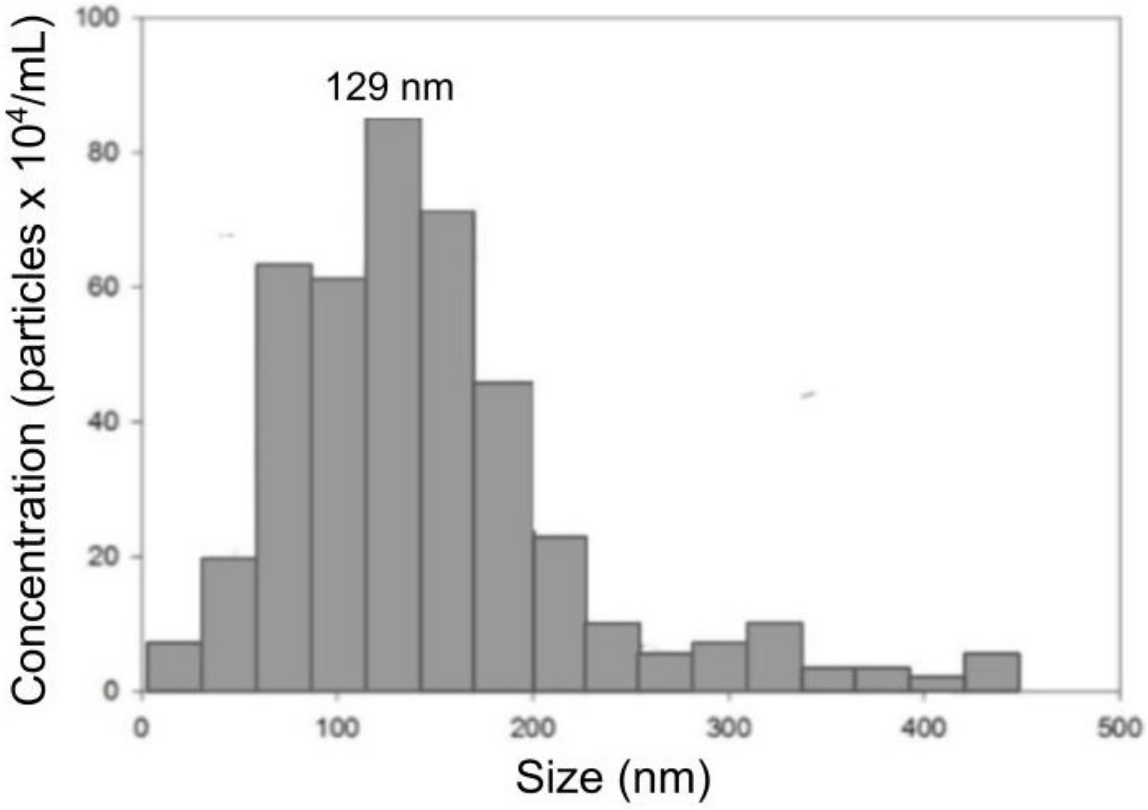

Figure 2.13. Validation of isolated extracellular particles by average particle size determined by nanoparticle tracking analysis. EVs were isolated from MDA-MB-291 cell culture media by ultracentrifugation protocol. The average diameter of the most abundant population is 129 nm. The original concentration of the sample was determined by the instrument to be 3.8×10^{11} particles/mL. There was an average of 76 particles counted per frame and 288 total particles traced. Data was acquired from 11 camera positions.

NTA data acquired for EV sample isolation characterization is an important consideration when comparing protocol efficiencies, however, it is not specific EVs, instead the instrument exclusively assesses particles detected by the scattered light. In this sense, it's important to remember that true EVs are likely a subset of the particles detects by NTA and the results should not be directly translated to true EV yield, instead it is important to interpret this data along other validation and characterization methods such as TEM and detection of exosome markers by flow cytometry.

Transmission Electron Microscopy

Transmission electron microscopy allows for visualization of the nanosized vesicles to characterize their morphology. **Figure 2.15** shows two vesicles in the field of view, where the top vesicle shows a diameter of 101.59 nm and the bottom vesicle shows a diameter of 98.63 nm. The diameters of the vesicles were approximated using Image J software.[113] The darker halo encircling the lighter color vesicle can be seen to be the lipid bilayer of the vesicles. The TEM result in **Figure 2.14** confirms the spherical morphology of EVs as well as their lipid bilayer. The diameter of the top and bottom vesicles in the field were calculated to be 101.59 and 98.63 nm, respectively. This result is consistent with literature values. However, it is a qualitative measure of EVs isolated to simply confirm their presence, not assess the quality of the sample isolated.

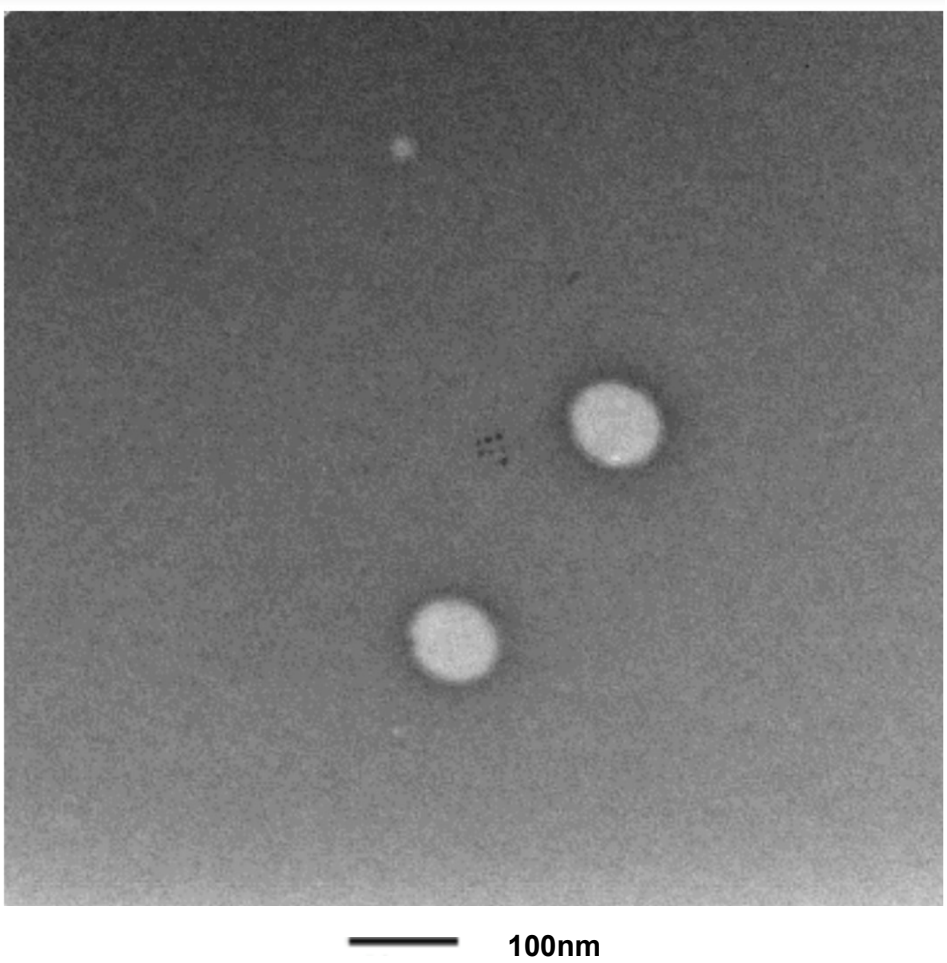

Figure 2.14 Transmission electron microscopy of urine EVs isolated by differential centrifugation. Samples were fixed in 2.5 % glutaraldehyde in 0.1 M sodium cacodylate buffer (pH 7.4). The fixed suspension was spotted on Formvar® coated copper grids (200 mesh; Canemco, Lakefield, ON, Canada) for 30 seconds. Samples were negatively stained with 2% aqueous uranyl acetate for 6 minutes and dried with filter paper. Vesicles were examined on a transmission electron microscope (JEOL JEM 1230, Japan) operated at 50 kV. The Feret's diameter of the particles was measured by analyzing the TEM images using ImageJ software, the top and bottom particle were measured to be 101.59 and 98.63 nm, respectively. The bar represents 100 nm.

FLOW CYTOMETRY

Antibodies chosen for validation of EVs by flow cytometry are summarized by **Table 2.4.** CFSE passively diffuses through the lipid bilayer and covalently couples with amine sources, such as lysine residues and the N-terminus region, thus staining intact lipid vesicles. The covalent coupling of this dye ensures that it does not leak back out of the membrane and affect neighboring vesicles.[121] Transmembrane protein markers (CD63, CD9 and CD81) are enriched on EVs in general, but there is heterogeneity among EVs and so the proportion of positive populations varies from source to source.[26] Yoyo-1 will be further discussed in the fluorescent microscopy section.

Experimental results obtained from analysis of EVs isolated from saliva, MDA-MB-231 and MCF7 sources are shown in **Figure 2.16.** Only events positive for CFSE were considered when looking at the other EV markers, CD9, CD63 and CD81 to reduce background noise that comes from particles other than EVs. Among EVs isolated from healthy human saliva, the % of events positive for CD9, CD63 and CD81 were 16.8%, 14.6% and 18.7%, respectively. Among EVs isolated from MDA-MB-231 cell culture media, the % of events positive for CD9, CD63 and CD81 were 9.3%, 6.4% and 12.1%, respectively. Among EVs isolated from MCF7 cell culture media, the % of events positive for CD9, CD63 and CD81 were 23.0%, 16.6% and 26.1%, respectively. The results are summarized in **Table 2.5.**

Table 2.5. Summary of events CFSE positive for common small/medium EV markers CD9, CD61 and CD81. EVs isolated from healthy human saliva donors and MDA-MB-231 and HEK-293 cell lines by differential ultracentrifugation. % Positive events for each antibody and cell line are summarized

EV marker	% Positive		
	Saliva	MDA-MB-231	MCF7
CD9	16.8	9.3	23.0
CD63	14.6	6.4	16.6
CD81	18.7	12.1	26.1

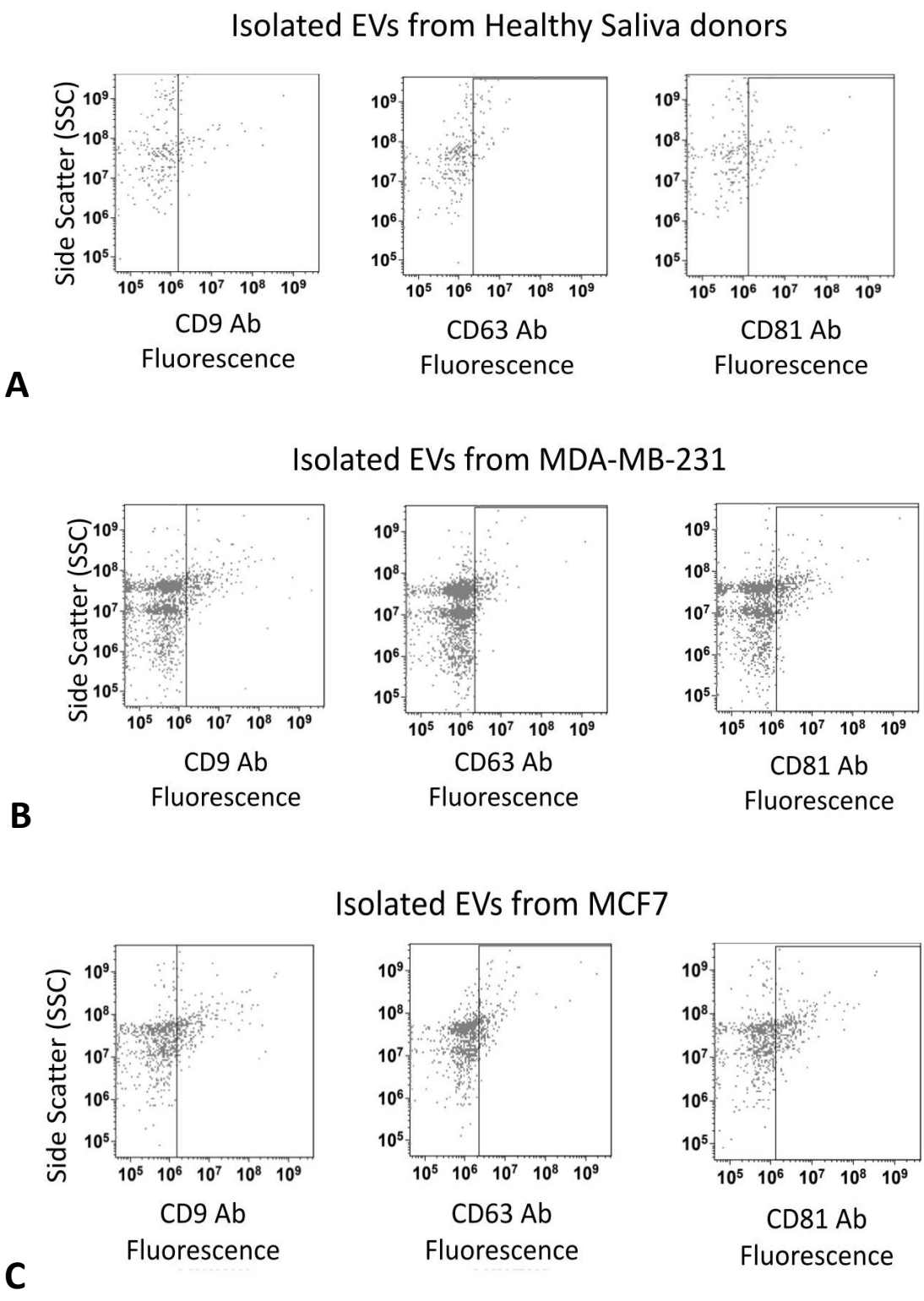

Figure 2.15. Analyzing EVs by flow cytometry across different sources (saliva from healthy human donors (A), MDA-MB-231(B) and MCF 7 (C) cell lines) by CD9, CD63 and CD81 antibodies. All graphs shown are displaying only CFSE positive events for better specificity of lipid membrane vesicles.

CONVEX-LENS INDUCED MICROSCOPY

EVs have been viewed under fluorescent microscopy,[122] though it is not a commonly used technique, likely because the challenges that are associated with imaging particles smaller than the diffraction limit. Convex-induced confinement microscopy is a modern wide field fluorescent microscopy technique designed for single molecule imaging.[105] EVs can be labelled by organic fluorescent dyes that are used for labelling of the cell membrane of cells. The fluorescently labelled molecules of interest are trapped in a glass well and an image is produced by capturing the fluorescence and a video is recorded to view the molecules in real time.

The lipid membrane dye CFSE was first attempted to label EVs, but the dye was too bright, and the image was unclear. YoYo-1 dye was used to stain double-stranded DNA of the EVs instead, there was better success with the latter dye. Our early attempts involved using an EV sample directly after DC however, few particles were observed, and it was concluded that the sample needed to be concentrated. After some trial and error, a 1:10 dilution of the concentrated isolated sample was the appropriate number of particles in the field of view. The next challenge we encountered was the particles were "sticking" to the glass wall instantaneously after closure of the glass well with the cover slip. We hypothesized that the net negative surface charge of EVs[123] interacts with the positively charged glass and that high salt concentration in PBS exacerbated this effect. We attempted to increase the pH of the buffer and treating the flow cell with Po Poly-L-Lysine graft PEG to decrease the interaction between the glass and the EV particles, but there was no improvement. We went back to an untreated flow cell and replaced PBS buffer for 1X TE buffer (10 mM Tris, 1 mM EDTA, pH 7.5) that resulted in a drastic improvement in EVs mobilization, likely because of the reduced salt concentration. There is no supporting evidence that EVs remain intact in TE buffer therefore, it was important that the sample was imaged immediately after buffer exchange. From the motion picture in **Video 2.1,** most EVs are mobile in the glass wells and some are trapped in between the coverslip and the glass. Some particles appear to be larger (and diffuse more slowly) than others, which could be EVs aggregates or simply larger EVs. The goal of viewing EVs by a novel platform and in-real time.

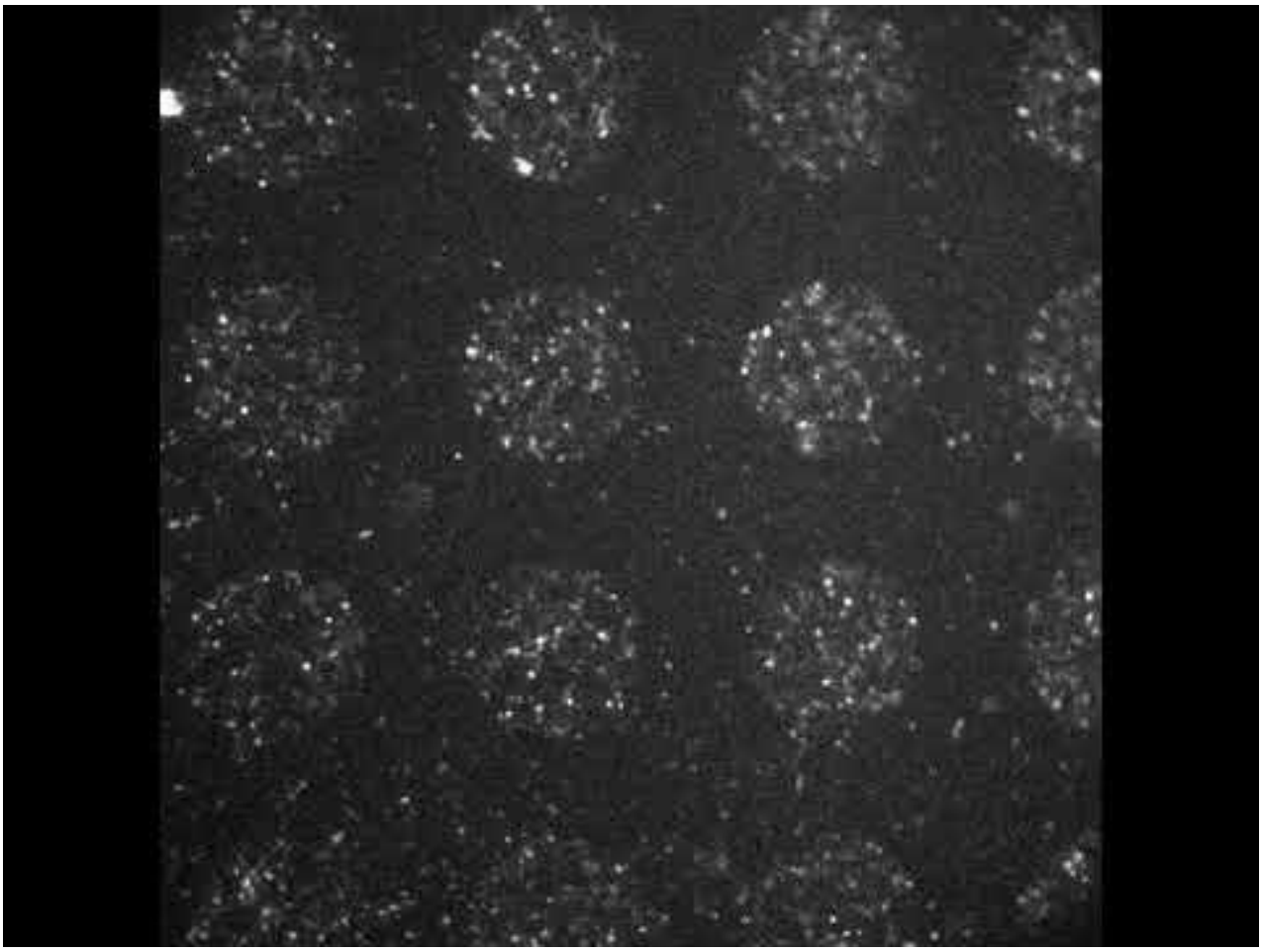

Video link: https://youtu.be/XIq6Pfn14Ro

Video 2.1. Convex lens-induced confinement microscopy of EVs. EVs isolated by differential ultracentrifugation from the MDA-MB-231 cell line with YoYo-1 staining (1:100 dilution factor) in 25 um untreated flow cells in TE Buffer at pH 7.5 under 60X objective lens, under the green channel (Emission filter: 525 nm).

2.5 Conclusion

DC is a lengthy and laborious procedure – therefore a poor trade-off for the small yield of EVs in comparison to the hours spent at the bench. However, it remains the gold standard for EV isolation as it produces the most consistent results and does not discriminate against EV subpopulations based on surface markers.[27] DC method was applied to cell culture media (MDA-MB-231, MCF7, HEK-293), urine and saliva. Saliva isolation required an additional step of affinity chromatography to remove extra starch, as well as a 1:1 dilution with PBS to reduce viscosity for better handling. A drastic range for particle concentration was observed depending on the source of the EVs. UF was compared to DC by analyzing particle concentration and diameter by NTA. UF yields higher particle concentration on average (3.8×10^{11}) in comparison with DC which yields a lower particle concentration on average (6.7×10^{10}). The average diameter of the EVs isolated were 143.1 nm and 95.1 nm for UF and DC methods, respectively. Despite higher particle yield and less laborious efforts, UF has been demonstrated in other works to contain a higher number of contaminates, potentially supported by the higher number of particles seen in UF samples.[118] Density gradient isolation is advantageous compared to traditional ultracentrifugation in that it has a higher capacity to separate particles efficiency, resulting in better sample purity. The limitations of this method are that it is incredibly time consuming, adding even more effort to an already laborious DC protocol. Additionally, the instruments typically used to prepare density gradients are expensive and take up a large amount of space, making it impractical without access to the equipment. An increase in particles of the appropriate small to medium EV size range were observed in the EV isotonic fraction (1.10-1.18 g/mL), however, it did not appear to be significantly purer than the DC method alone by assessing particle size. It should be noted that gradients were made by hand which increases the chances that there is mixing between layers. There was also a considerable amount of additional labor required with this protocol, without any noticeable pay off in quality of sample isolated. DC method was further validated by TEM and flow cytometry. Average particle diameter determined by NTA was reported as 154.3 nm ± 12.9 nm. Flow cytometry confirmed the presence of CFSE positive vesicles that exhibited positive populations for the commonly used EV marker CD63, CD9 and CD81. The reported % of each population varied depending on EV source, highlighting the heterogeneity of EVs. TEM was used observe the morphology of the vesicles isolated, spherical lipid membrane particles were observed. Finally, isolated EVs were observed in real-time by single molecule imaging. DC method for EV isolation has been successfully validated and will be used without modification for the remainder of the project.

2.6 Ethics approval

10/09/2019

Université d'Ottawa
Bureau d'éthique et d'intégrité de la recherche

University of Ottawa
Office of Research Ethics and Integrity

CERTIFICAT D'APPROBATION ÉTHIQUE | CERTIFICATE OF ETHICS APPROVAL

Numéro du dossier / Ethics File Number	H-08-18-980
Titre du projet / Project Title	ANALYSIS OF HEALTHY HUMAN URINE AND SALIVA EXOSOMES FOR FUTURE DIAGNOSTIC APPLICATIONS
Type de projet / Project Type	Thèse de maîtrise / Master's thesis
Statut du projet / Project Status	Renouvelé / Renewed
Date d'approbation (jj/mm/aaaa) / Approval Date (dd/mm/yyyy)	10/09/2019
Date d'expiration (jj/mm/aaaa) / Expiry Date (dd/mm/yyyy)	23/09/2020

Équipe de recherche / Research Team

Chercheur / Researcher	Affiliation	Role
Vanessa SUSEVSKI	Département de chimie / Department of Chemistry	Chercheur Principal / Principal Investigator
Maxim BEREZOVSKI	Département de chimie / Department of Chemistry	Superviseur / Supervisor
Nico HÜTTMANN	Département de chimie / Department of Chemistry	Co-chercheur principal / Co-principal investigator
Emil ZARIPOV	Département de biologie / Department of Biology	Co-chercheur principal / Co-principal investigator
Yousef RISHA	Département de chimie / Department of Chemistry	Co-chercheur principal / Co-principal investigator
Prabir Kumar KULABHUSAN	Département de chimie / Department of Chemistry	Co-chercheur principal / Co-principal investigator
Suttinee POOLSUP	Département de chimie / Department of Chemistry	Co-chercheur / Co-investigator

Conditions spéciales ou commentaires / Special conditions or comments

550, rue Cumberland, pièce 154 Ottawa (Ontario) K1N 6N5 Canada
550 Cumberland Street, Room 154 Ottawa, Ontario K1N 6N5 Canada

613-562-5387 • 613-562-5338 • ethique@uOttawa.ca / ethics@uOttawa.ca
www.recherche.uottawa.ca/deontologie | www.recherche.uottawa.ca/ethics

10/09/2019

Université d'Ottawa

Bureau d'éthique et d'intégrité de la recherche

University of Ottawa

Office of Research Ethics and Integrity

Le Comité d'éthique de la recherche (CÉR) de l'Université d'Ottawa, opérant conformément à l'*Énoncé de politique des Trois conseils* (2014) et toutes autres lois et tous règlements applicables, a examiné et approuvé la demande d'éthique du projet de recherche ci-nommé.

L'approbation est valide pour la durée indiquée plus haut et est sujette aux conditions énumérées dans la section intitulée "Conditions Spéciales ou Commentaires". Le formulaire « Renouvellement ou Fermeture de Projet » doit être complété quatre semaines avant la date d'échéance indiquée ci-haut afin de demander un renouvellement de cette approbation éthique ou afin de fermer le dossier.

Toutes modifications apportées au projet doivent être approuvées par le CÉR avant leur mise en place, sauf si le participant doit être retiré en raison d'un danger immédiat ou s'il s'agit d'un changement ayant trait à des éléments administratifs ou logistiques du projet. Les chercheurs doivent aviser le CÉR dans les plus brefs délais de tout changement pouvant augmenter le niveau de risque aux participants ou pouvant affecter considérablement le déroulement du projet, rapporter tout évènement imprévu ou indésirable et soumettre toute nouvelle information pouvant nuire à la conduite du projet ou à la sécurité des participants.

The University of Ottawa Research Ethics Board, which operates in accordance with the *Tri-Council Policy Statement* (2014) and other applicable laws and regulations, has examined and approved the ethics application for the above-named research project.

Ethics approval is valid for the period indicated above and is subject to the conditions listed in the section entitled "Special Conditions or Comments". The "Renewal/Project Closure" form must be completedfour weeks before the above-referenced expiry date to request a renewal of this ethics approval or closure of the file.

Any changes made to the project must be approved by the REB before being implemented, except when necessary to remove participants from immediate endangerment or when the modification(s) only pertain to administrative or logistical components of the project. Investigators must also promptly alert the REB of any changes that increase the risk to participant(s), any changes that considerably affect the conduct of the project, all unanticipated and harmful events that occur, and new information that may negatively affect the conduct of the project or the safety of the participant(s).

Marc Alain BONENFANT
Coordonnateur de l'éthique / Ethics Coordinator
Pour/For **Daniel LAGAREC** Président(e) du/ Chair of the **Comité d'éthique de la recherche en sciences sociales et humanités / Social Sciences and Humanities Research Ethics Board**

550, rue Cumberland, pièce 154 Ottawa (Ontario) K1N 6N5 Canada
550 Cumberland Street, Room 154 Ottawa, Ontario K1N 6N5 Canada

613-562-5387 • 613-562-5338 • ethique@uOttawa.ca / ethics@uOttawa.ca
www.recherche.uottawa.ca/deontologie I www.recherche.uottawa.ca/ethics

2.7 Acknowledgements

I would like to acknowledge Emil Zaripov, who had optimized an UF protocol prior to my arrival to our lab. I would like to thank Dr. Arkadiy Reunov, from the Cell Imaging & Histopathology Core Facility at the University of Ottawa Heart Institute, for his assistance in obtaining the exosome TEM images and to Yousef Risha for helping me prepare my samples. I also thank Dr. Derrick Gibbings for providing access to the NTA instrumentation and Ryan Reshke for pleasant management of this instrument. I would like to acknowledge Riya Shah for her diligent assistance in sample preparation and acquiring NTA data. I would like to acknowledge Dr. Sabrina Leslie in the Department of Physics at McGill University for allowing me as a guest in her lab to collaborate using her CLiC microscope. Thank you to Dr. Marty Kurylowicz for reaching out to me at the Chemical Biophysics Symposium at the University of Toronto and for hosting me in Dr. Leslie's laboratory during the month of June 2019. I would also like to acknowledge Dr. Radin Tahvildari for his academic leadership and expertise for his assistance provided to obtain the video of EVs in solution.

Chapter 3

Selection of DNA Aptamers to Tumour-Derived Extracellular Vesicles

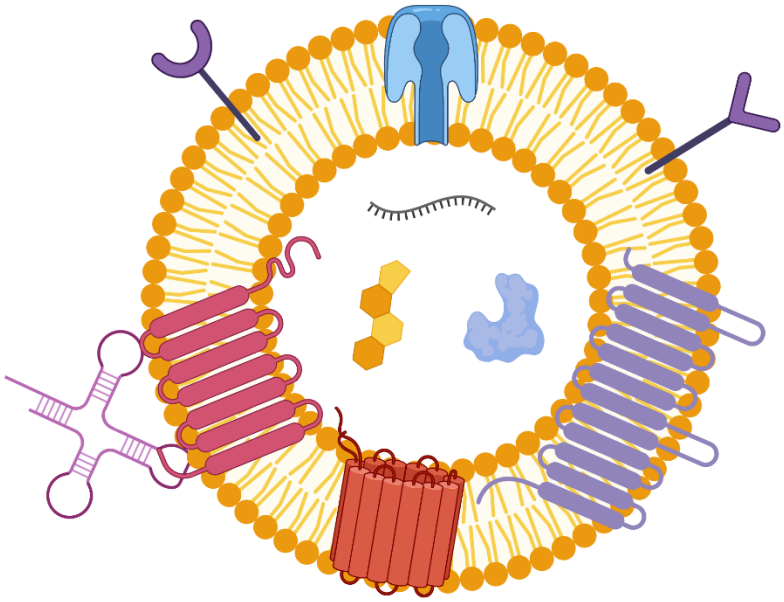

3. SELECTION OF DNA APTAMERS TO CANCER DERIVED EXTRACELLULAR VESICLES

3.1 Objective

Aptamers should be engineered by Systematic Evolutions of Ligands by Exponential Enrichment. The DNA sequences are determined by next generation sequencing and candidate aptamer sequences are selected based on enrichment throughout the selection process, predicted secondary structure and preserved consensus sequenced determined by bioinformatic analysis. Candidate aptamers are screened by flow cytometry to determine the aptamer that binds to the preferentially to the triple negative breast cancer EVs.

3.2 Introduction

The process of SELEX is inspired by evolutionary principals: variation, mutation, selection and time. In the theory of evolution, variation refers to a wide range of genetic variability which translates into vast phenotypic variation. In this manner, individuals in a population vary from one another. Variation synonymously seen in SELEX in the starting nucleic acid library – allowing each oligonucleotide to have its unique 3-dimensional structure. Mutations are essential to increasing genetic diversity in a population. Similarly, the process of PCR amplification introduces mutations into the library which may or may not help increase their binding affinity for the target molecule – the introduction of novel mutations can potentially give rise to aptamer candidates that were not in the initial library. Individuals with genetics that offer a better survival or reproductive factor, will have a greater likelihood of survival and thus passing on their genetic material to their offspring – this is known as selection. Selection is an evident process in SELEX, as oligonucleotide sequences with better binding affinity to the target will be more likely to persevere to subsequent rounds (generations) of selection. Similarly, some sequences will be favored by the polymerase enzyme (reproduction) and may persist through the selection process as a result. Evolution happens over time, rather than instantaneously. Likewise, success in developing an aptamer to a target of interest takes several rounds of selection and could not be achieved in solely one round.

SELEX can select for a range of targets of interest with high affinity by starting with a random DNA, RNA, or peptide library. The relative lack of diversity with oligonucleotides may be disadvantageous compared to peptides since there are fewer possible folding combinations with only 4 nucleotides, but they are simpler and more stable to work with. Work done on SELEX earlier on primarily used RNA libraries as they generally can produce more intricate 3-dimentional

structures. More recently, the focus has been shifted to DNA libraries, as DNA is better at resisting degradation since it lacks a 2'-OH group. [124,125]

Aptamer selection begins by incubation of the library with the target, then separate the unbound DNA from the bound, formally known as the partitioning step. The DNA bound to the target is amplificated by polymerase chain reaction (PCR)[73] and the DNA pool is extracted and purified in preparation for subsequent rounds. The partitioning, amplification and purification step is repeated for 8-12 cycles, or until evidence of binding can be drawn. The generated pools are sequenced by Next Generation Sequencing and analyzed by bioinformatics. Here, the SELEX method as described is applied to cancer derived EVs (EV-SELEX) as shown in **Figure 3.1.**

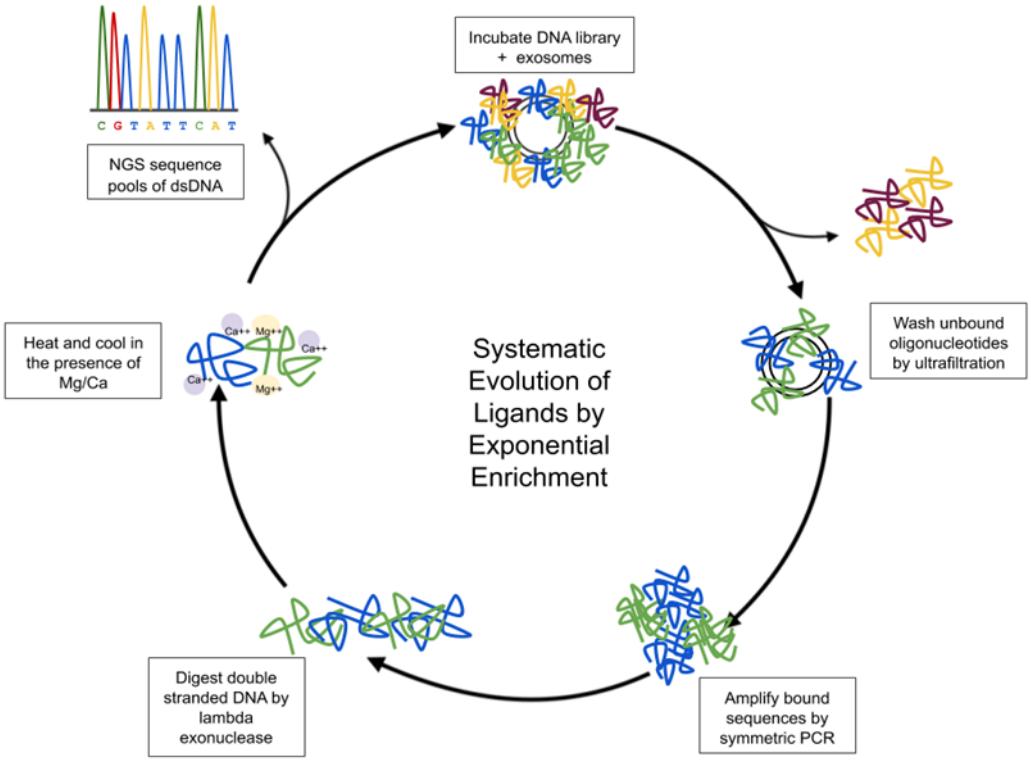

Figure 3.1. Schematic of workflow for SELEX to EVs. The DNA library is heated and cooled in the presence of Ca^{2+}/Mg^{2+}, followed by incubation with pre-isolated target EVs. Bound DNA is partitioned by size-cut off filtration then amplified by PCR. The double-stranded DNA is digested by lambda exonuclease enzyme to return single stranded copies. The process is repeated for 8-12 generations then the pools are assessed for evidence of binding in the presence of the target. The pools are sequenced by Next Generation Sequencing and then analyzed by bioinformatics.

3.3 Methods

SYSTEMATIC ENRICHMENT OF LIGANDS BY EXPONENTIAL ENRICHMENT

Harvard DNA Library (Integrated DNA Technologies) template is 5'-CTC CTC TCG TAA CCA CG(N1:45054505) (N3:05450545)(N1)(N3) (N1)(N3)(N1) (N3)(N2:25252525)(N2)(N2) (N1)(N3)(N1) (N3)(N1)(N3) (N1)(N3)(N1) (N3)(N1)(N3) (N2)(N2)(N2) (N1)(N3)(N1) (N3)(N1)(N3) (N1)(N3)(N1) (N3)(N2)(N2) (N2)(N2)(N1) (N3)(N1)(N3) (N3)(N1)(N3) (N2)(N2)(N2) (N1)(N3)(N1) (N3)(N1)(N3) (N1)(N3) G CAT AGG TAG CC AGA AGC C -3', where N1 has a composition of C:A:G:T of 45%:05%:45%:05%, where N2 has a composition of C:A:G:T of 25%:25%:25%:25% and N3 has a composition of C:A:G:T of 05%:45%:05%:45%. The library was resuspended in PBS and stored in -20 °C. 100 µL of DNA library in 1X PBS with Ca^{2+} / Mg^{2+} was heated to 95 °C for 5 minutes, then the DNA is cooled on ice for an additional 10 minutes. 100 µL of isolated EVs was added to 100 µL to the DNA library and incubate for 1 hour while shaking at 200 rpm at room temperature. The mixture was then transferred into Amicon® Ultra 50 kDa cut-off filter and centrifuged at 2600 g for 1 hour or until the filtrate has passed. The concentrate was washed once with PBS and then collected by ensuring thorough washing of the membrane via aspirating at least 20 times against the membrane.

SYMMETRIC PCR

PCR master mix was prepared to the manufacturer's instructions as well as the additional PCR reaction components as summarized in **Table 3.1** and symmetric PCR was carried out in MasterCycler (Eppendorf). The template denaturation step occurred at 95°C for 2 minutes, the primer annealing occurred at 65°C for 15 seconds and DNA elongation step occurred at 72°C for 35 seconds. The number of cycles was determined for each round as described in the PCR optimization section.

Table 3.1. Master mix recipe for PCR of DNA library.

	Final Concentration	Volume (µL) per 10 reactions	Catalogue Number
ddH_2O	--	266	-
5x Phire Buffer	1X	100	F-527L
dNTPs	0.4 µM	0.4	R1121
DMSO	7%	35	-
Forward primer[1]	0.4 µM	2	Integrated DNA Technologies
Reverse primer[2]	0.4 µM	2	Integrated DNA Technologies
Phire II Hot Start DNA Polymerase 4U/µL	1U/25 µL	5	F122L
DNA template	2.5 pg − 25 ng	-	-

Additional Information:
1. Forward Primer: 5'-/5CY5/ CTC CTC TGA CTG TAA CCA CG-3'
2. Reverse primer: 5'-/5Phos/ GGC TTC TGG ACT ACC TAT GC-3'

PCR Optimization

PCR master mix was prepared to the manufacturer's instructions as well as the additional PCR reaction components as summarized in **Table 3.1**. The optimal number of PCR cycles was determined each round of selection to minimize by-product and maximize product yield. This was determined by sampling 6 through 22 cycles by multiples of 2. A 5 µL aliquot was taken from the sample every other cycle and stored on the side until all cycles were complete. The samples were stained with 1X Gel Red (Invitrogen, Cat No. 41003) and run on 1% agarose gel at 120 V for 30 minutes. Image the gel under the RGB channel and assess for the optimal number of cycles. The lane with the sharpest and most intense band at the appropriate migration rate relative to control with minimal by-product bands was chosen as the optimal number of cycles.

Exonuclease Digestion

After the optimal number of PCR cycles, all samples were combined and 10x exonuclease reaction buffer and lambda exonuclease (ThermoFisher, Cat No. EN0561) were added to the combined samples according to **Table 3.2.** The samples were re-divided into PCR tubes and the digestion protocol was performed in MasterCycler (Eppendorf) at 37°C for 400 minutes, at 95°C for 25 minutes and 4°C for 10 minutes.

Table 3.2. Exonuclease digestion reaction recipe.

	Final Concentration	Volume (µL) per 50µL reaction	Catalogue Number
Exonuclease reaction buffer	1X	2	EN0561
Lambda Exonuclease 10U/µL	10U	1	EN0561

Gel electrophoresis

The single stranded DNA product from the previous steps was loaded onto a 1% agarose gel into one giant well, alongside the library and primer as controls. The library and DNA product were stained Gel Red (Invitrogen, #41003) to a final 1X concentration. The samples were run on the gel in 1X TBE buffer at 120 V for 35 minutes, or until clear separation was achieved.

Purification of DNA

Two possible methods of DNA product purification were explored: Cutting the product directly out of the gel and allowing it to diffuse out passively and by making use of an automated robot to extract DNA of a desired size. These two methods will be referred to as method A and B, respectively. The concentration of DNA was determined throughout this experiment by NanoDrop 2000c spectrometer.

Method A: Gel cutting

The single stranded DNA product was run on a fresh gel according to the method described in the gel electrophoresis section. The only difference is that one large well was prepared for the product, instead of having several wells (for several samples). The product is then cut into small cubes using the same scalpel and was transferred to a 15 mL falcon tube and incubated at room temperature in ddH_2O at 200 rpm overnight. The liquid was carefully removed from the gel cubes and imaged to check if diffusion had been completed. Diffusion was said to have reached completion if there were no longer any fluorescence visible from the gel cubes when imaged under the red-green-blue channel. If diffusion was not completely, more ddH_2O was added to the falcon tube and again incubated overnight under the same conditions as before. This process was repeated until diffusion was complete and the samples were dehydrated at 60 °C until dry. The DNA was resuspended in 50 µL of ddH_2O. The concentration of DNA was determined by NanoDrop spectrophotometer 2000c.

The liquid collected from gel diffusion step was combined in preparation for DNA purification by ethanol precipitation. The dilute DNA solution was divided by adding 200 µL to 1.5 mL Eppendorf tube. The final number of Eppendorf tubes varied depending on the starting volume. Each sample tube received 5 µL of 5 M ammonium acetate and 150 µL of cold absolute ethanol. All samples were stored in -20°C overnight. Samples were then centrifuged at 16,000 g for 30 minutes and the supernatant was discarded. The DNA pellet was then washed with 200 µL of 70% ethanol, stored in -20°C for 10 minutes, then centrifuged at 16,000 g. The pellet was air dried completely in a clean fume hood until dry, ~1 hour. Finally, the pellet was resuspended in 30 uL ddH_2O.

Method B: Size exclusion robot

A maximum of 50 µL of DNA product was loaded into wells 1 through 8 in a 2% agarose gel cassette (Costal Genomics, [CG-10600]- [10600]-[02]-[06]-[14]) as well as 50 µL of DNA ladders 500 and 50 base pairs in size are added to each well. The samples were run at 100 V for 40 minutes and the data was visualized using Venous software. The extracted DNA was solubilized in 1x TBE buffer. The retrieved DNA product was concentrated to a final volume of 100 µL by a 3 kDa filter (Millipore, UFC900308) and washed once with PBS.

Validation of Pool Binding

After 8 rounds of selection, each DNA pools 1 through 8 were screened for evidence of binding using Coulter MoFlo Astrios EQ Cell Sorter as previously described in the "Flow Cytometry" method section. Each round of aptamer pools was prepared as previously mentioned to a final concentration of 1 uM. Isolated EVs were vortexed to ensure uniform concentration across samples. 100 uL of isolated EVs was mixed with DNA in PBS buffer to give a final DNA concentration of 500 nM. Data was acquired for was targeted to reach 100,000 events per sample. Raw .fcs files were analyzed by Kaluza software as per the Flow Cytometry Data Analysis section.

DNA Pool Sequencing

DNA pools 1 to 8 were sequenced by Illumina Next Generation Sequencing at the Integrated Microbiome Resource (IMR), Dalhousie University using the same forward and reverse primers as mentioned in the PCR methods section, without chemically added modifications.

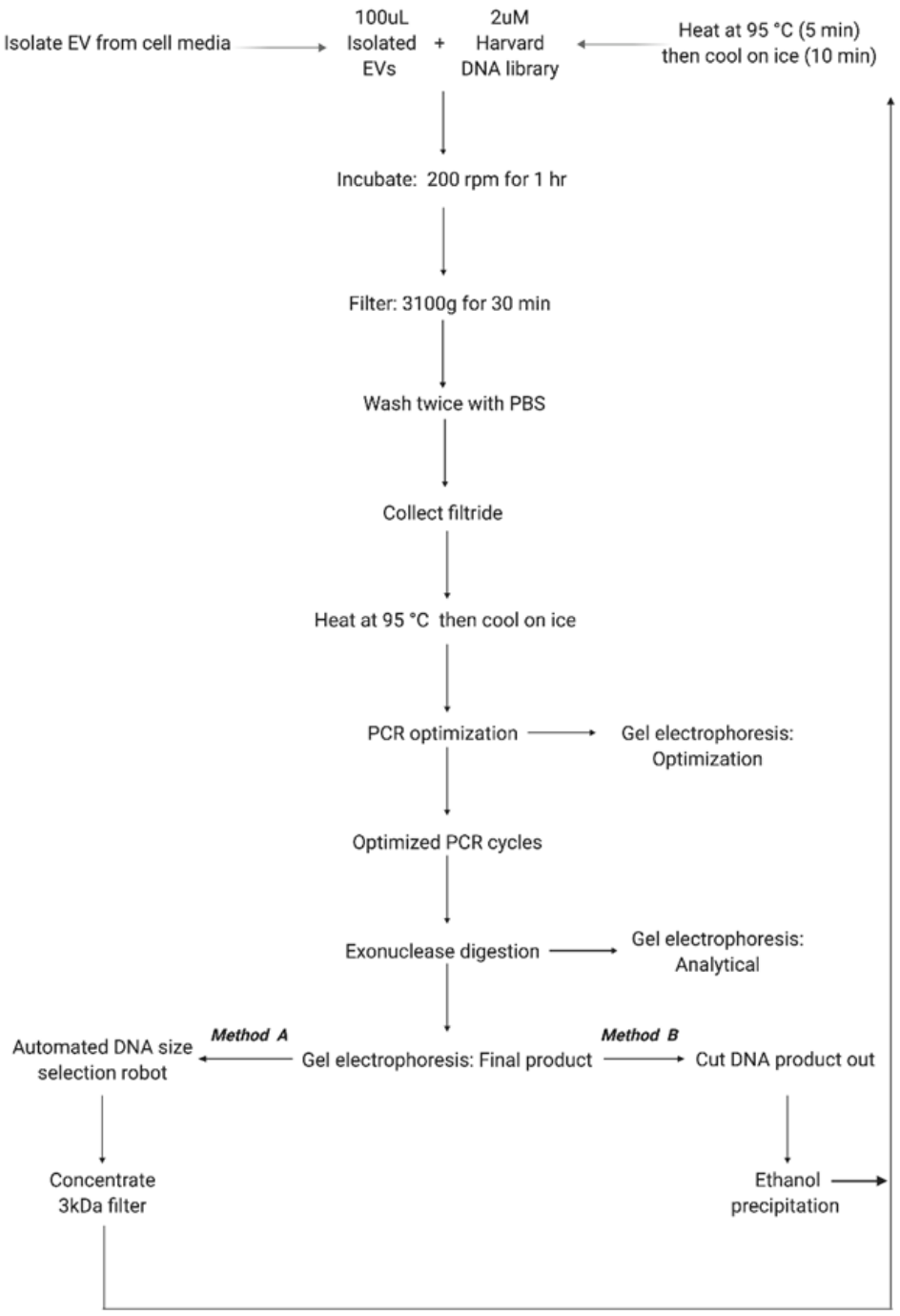

Figure 3.2. Flow chart of protocol used for the selection of DNA aptamers to EVs. The DNA library is heated and cooled in the presence of Mg^{2+} and Ca^{2+} ions to initiate folding into their 3-dimensional structure. Incubation between the DNA library and target for 1 hour on a shaking plate allows for interaction between the two species. The DNA bound to the target is then separated by the unbound by a 50 kDa filter. The bound DNA is then amplified by polymerase chain reaction. The number of cycles is optimized each round to ensure minimal by product and maximum desired DNA product. The double-stranded DNA is subject to exonuclease digestion to return single stranded DNA. The product is then visualized by gel electrophoresis, then the product is isolated (Method A or Method B) and purified.

APTAMER CANDIDATE SELECTION

Data was obtained from Dalhousie University via a drop box containing .fastq files. All files were preprocessed using the open source galaxy program (https://usegalaxy.org/). The fastq files were converted to .fasta then, both template and coding strands were analyzed by changing the R2 file into the complimentary sequences then the R1 and R2 file were then merged together. Sequences were trimmed of both forward and reverse primer sequences and any primer dimers identified were removed. Only sequences 100 base pairs ± 2 in length were analyzed. Low abundant sequences were defined to be sequences that only appeared once and were removed from the data set for more efficient processing. The clean files were imported into CLC Genomics Workbench 12, aligned to discover consensus sequences. The aligned sequences were then used to construct a circular phylogenetic tree. The tree was constructed using the Neighbor-Joining method and the nucleotide distance measure used the Jukes-Cantor algorithm.

Aptamer candidates were chosen based on 3 criteria: relative abundance across the selection process, stability of predicted secondary structure and abundance of consensus sequence within a pool. CLC sequence viewer 8 (open source) was used to align the sequences in families according to their sequence similarity. Sequences were organized using phylogenetic tree analysis. Sequences were assessed for their abundance within each pool, whether they had evolved from the previous round and their predicted secondary structure.[126] DNA sequences that were that were present in pools from both cell lines were excluded in order to potentially select aptamers more specific to their respective cell line. 4 potential candidates to bind MDA-MB-231 EVs but not the non-cancerous control EVs were selected and tested by flow cytometry.

VALIDATION OF APTAMER BINDING

The 4 chosen aptamer candidates VBS-1, VBS-2, VBS-3 and VBS-4 were purchased from Integrated DNA Technologies with the CY5 modification on the 5' end. The candidates were tested against EVs isolated from MDA-MB-231, HEK-293 and MCF10A cell lines by flow cytometry assay. Each candidate aptamer was mixed with 100 μL of EVs for a 1μM final concentration. EVs were incubated with CFSE (1:100 dilution factor) in the dark for 20 minutes, then immediately run on the Coulter MoFlo Astrios EQ Cell Sorter as previously described in the "Flow Cytometry" method section.

3.4 Results and discussion

EV-SELEX

The Harvard DNA library was incubated with pre-isolated EVs from either MDA-MB-231, MCF7 or HEK-293 cell line. It should be noted that selection was only successful for HEK-293 and MDA-MB-231 and was terminated at round 4 for MCF 7 after several failed attempted to amplify the bound DNA without success. The reason for this result is unknown, however perhaps it could be due to the relative low yield of extracellular particles produced by the MCF7 cell line, as shown in **Figure 2.7.** Therefore, successful selection with this cell line likely requires an increased starting volume of cell culture media and number of cells, though this was not attempted. For the two other cell lines, 8 rounds of selection as described were completed.

BINDING

The Harvard DNA library was selected as the starting library instead of an entirely random one because of its elegant design which incorporates regions more probabilistically to exhibit self-complementary, and thus a hairpin secondary structure with stem loops. It is hypothesized that a successful aptamer candidate is more likely to arise from a strategically designed library, in contrast to an entirely stochastically determined one, though this idea has never been proven experimentally. At the start of every round, the DNA library was heated to 95°C to interrupt hydrogen bonds, then cooled in the presence of PBS buffer with calcium and magnesium ions to facilitate 3-dimensional folding of the DNA. The incubation between the DNA and the EV target occurred in PBS buffer (pH 7.4) to ensure stability of the EVs. The incubation occurred at room temperature to simulate conditions that would be required of a clinical diagnostic test.

PARTITIONING

An EV-SELEX protocol was adapted from CELL-SELEX protocol. The main difference is that the target is magnitudes smaller, so simple ultracentrifugation cannot be used to separate the DNA-target complex from the free-floating DNA because this method is too inefficient and results in excessive DNA loss that affects the subsequent rounds. Isolation of EVs by streptavidin coated magnetic beads coupled to biotinylated CD63 was attempted, but this method would exclude a large subgroup of EVs. Moreover, it was a relatively convoluted and error prone protocol since it required having beads coupled to the primary antibody, then bound to the EVs, and finally a second antibody for their detection. This led us to pursue UF for the recovery of bound DNA, isolating the DNA-target complex primarily based on a size cut off. The 50kDa cut-off filter was chosen because the 100 base pair library has an approximate size of 30kDa, consequently any unbound DNA will pass through the filter and will not be retained on the membrane.

AMPLIFICATION

Hot Start II Polymerase was chosen to amplify the DNA library. A polymerase with a lower fidelity is desired to mimic the mutation prone process of natural selection, allowing the new mutations to be introduced that may offer a binding advantage to the target. The forward primer design was a Cyanine-5 (Cy5) fluorophore modification at the 5' end to allow detection of the DNA during flow cytometry or visualization on gel electrophoresis. The reverse primer design was a phosphate group modification at the 5' end to allow for recognition of lambda exonuclease for double-stranded to single stranded DNA digestion. A visual summary of the details that occurred during the PCR reaction are shown in **Figure 3.3.**

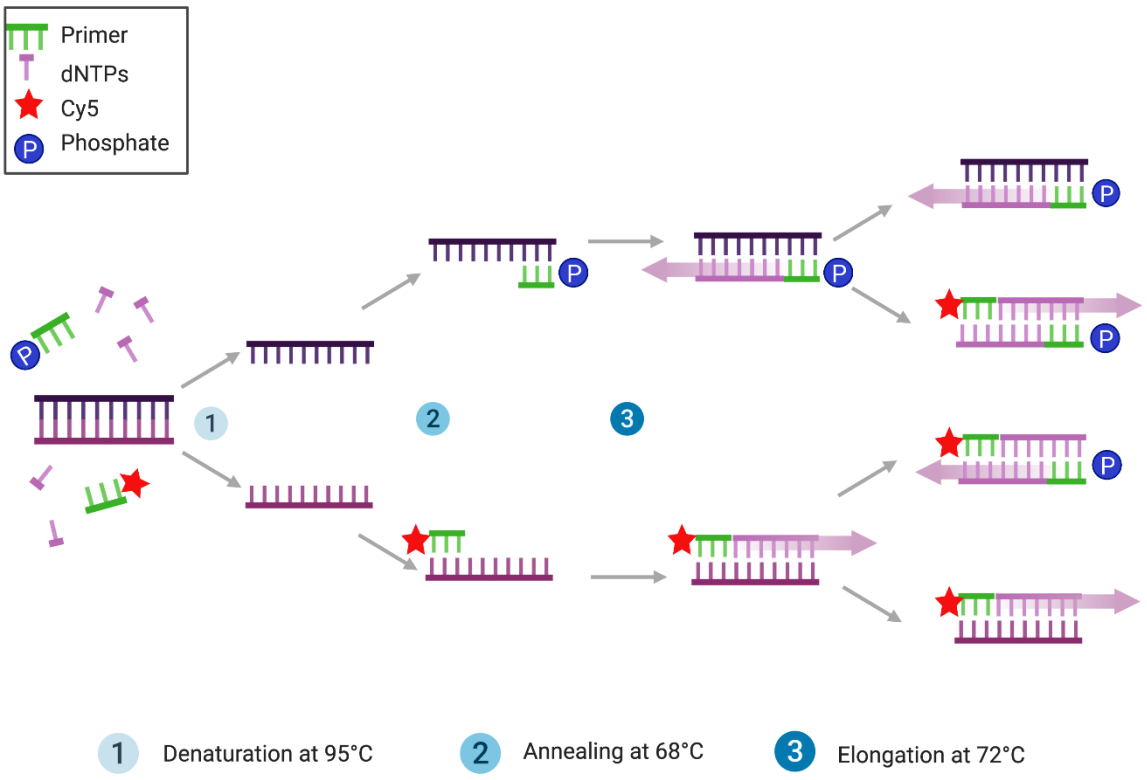

Figure 3.3. Schematic for polymerase chain reaction with forward and reverse primer design. The denaturation step separates the complementary DNA strands and is carried out at 95°C. The annealing step occurs at 68°C and allows the primers to bind to the template strand. The elongation step allows the DNA polymerase to add nucleotides according to the template strand.

PCR yields double-stranded DNA; however single stranded DNA is required for aptamer selection to allow for secondary structure folding. The exonuclease digestion protocol reverts the DNA back to its single stranded state. The reverse primer incorporated phosphate group on the coding strand during PCR. In the presence of Mg^{2+} lambda exonuclease is highly processive exodeoxyribonuclease that digests the complimentary strand in the 5' to 3' direction, yielding dNMPs and phosphate as the products of the reaction. It is in this fashion **(Figure 3.4)** that the original coding strand is recovered.

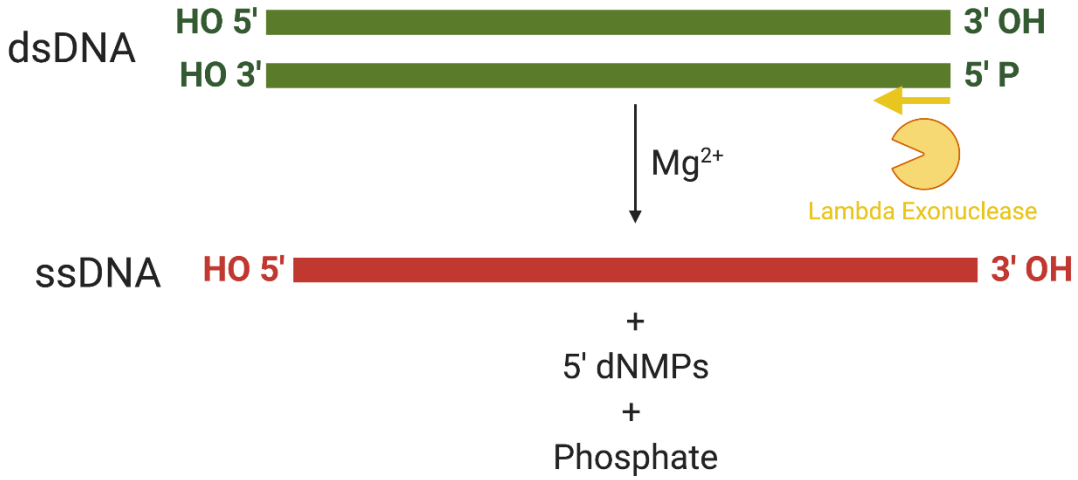

Figure 3.4. Schematic for lambda exonuclease activity on double-stranded DNA. Coding strand receives a phosphate group on the 5' end of the DNA after incorporation of the reverse primer in PCR. In the presence of Mg^{2+} Lambda exonuclease chews from the phosphate end of the DNA, yielding single stranded DNA 5'dNMPs and phosphate groups as the products of the reaction.

PCR OPTIMIZATION

The PCR optimization step is important for minimizing by product created by the PCR reaction and maximizing the amount of product produced. Gel electrophoresis is used to visualize the product quality from PCR and compared to the library sample to ensure the desired product was indeed amplified. The first experiment done was to determine if the PCR optimization step could be done without exonuclease step, in essence, if the visualization of the double-stranded DNA yielded immediately after PCR was a good estimate for the single stranded DNA that would be a result of the exonuclease digestion. **Figure 3.5** shows the results of this experiment. Panel A shows a slightly slower migration rate than the library because its double-stranded nature, as expected. The samples in panel B shows a similar pattern as panel A, therefore we may use the double-stranded DNA to determine the optimal number of PCR cycles. The logic for selecting the optimal number of PCR cycles is as follows: select the number of cycles that yields the brightest band which corresponds to the library, that has the least or no high molecular by product or remaining primer. Therefore, the optimal number of cycles as per the results in panels A and B are 16 and 12 cycles, respectively.

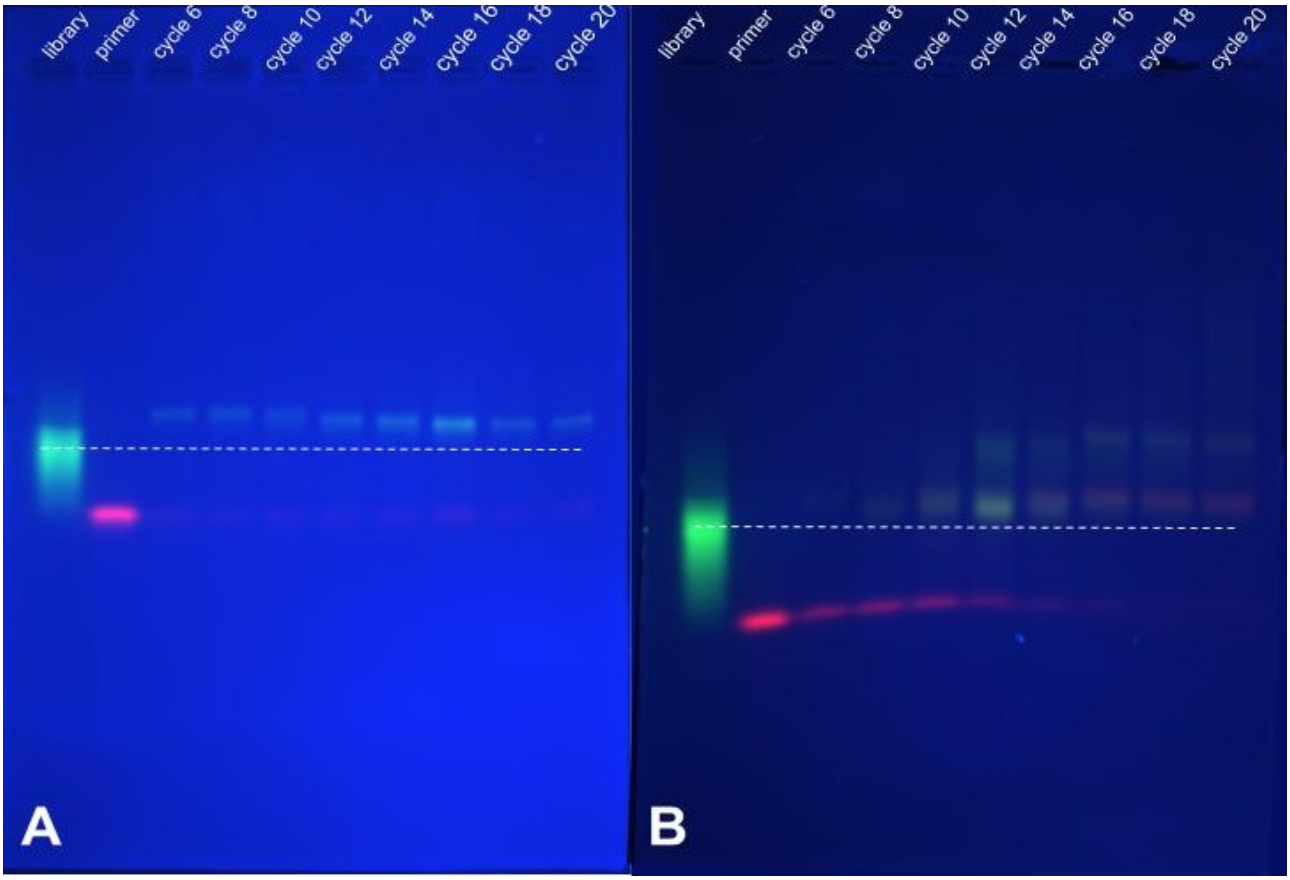

Figure 3.5. Optimization of the number PCR cycles with (B) and without (A) exonuclease digestion. Results shown from round 1 from HEK-293 selection protocol. 1% agarose gel electrophoresis of PCR optimization comparing the results before and after exonuclease digestion. Samples were loaded according to the labels on the top of the gel. The DNA was stained with 1X gel red and run at 120V for 35 minutes.

The remainder of the work presented, gel electrophoresis following PCR optimization of the double-stranded DNA will be used to approximate the results of the single stranded DNA as shown in **Figure 3.5.** The resulting PCR optimization of MDA-MB-231 and MC7 cell line derived EVs for rounds 5 and 2 were taken to be 10 and 8 cycles, respectively.

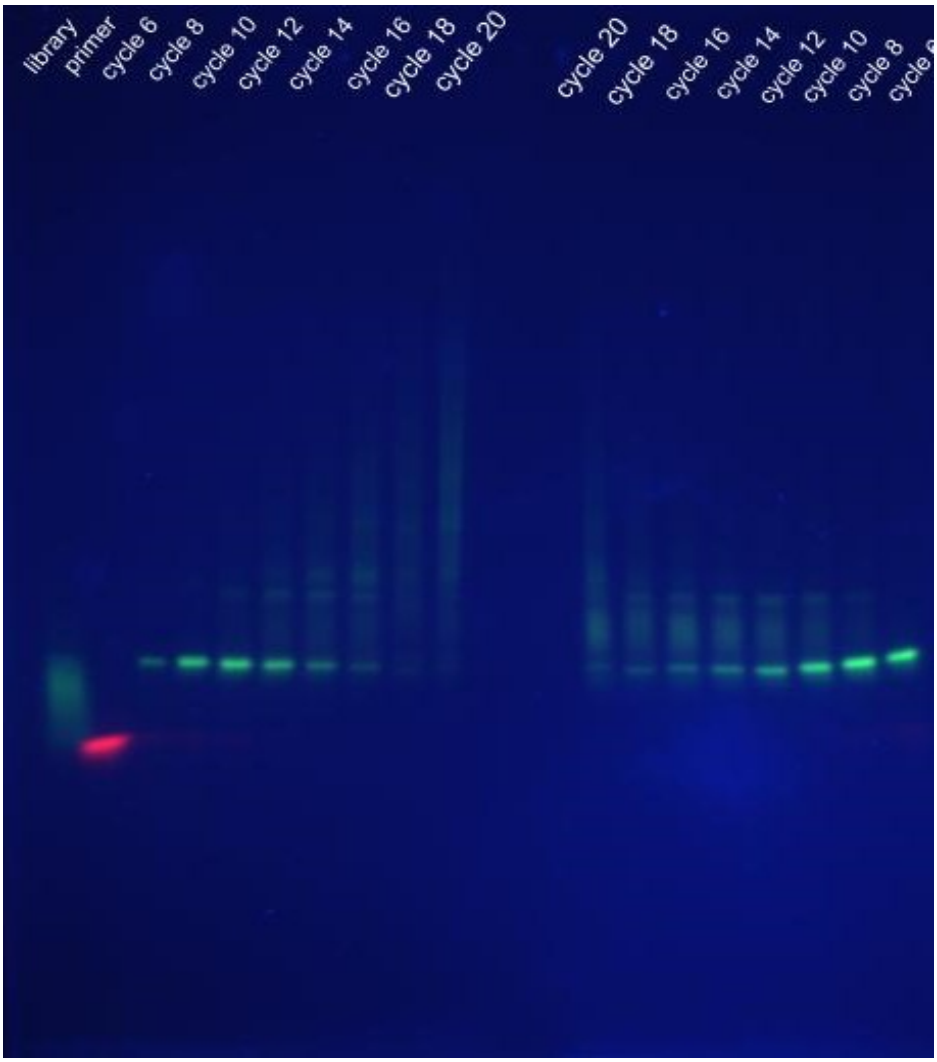

Figure 3.6. PCR optimization of MDA-MD-231 and MCF7 selection for rounds 5 and 2, respectively. 1% agarose gel electrophoresis of PCR optimization. Samples were loaded according to the labels on the top of the gel. The DNA was stained with 1X gel red and run at 120 V for 35 minutes.

After PCR optimization, the appropriate number of PCR cycles is carried out on the remaining DNA then digested by exonuclease to return single stranded DNA. A final quality check gel was performed before moving on to cleaning up and retrieval of the DNA pool, to ensure clean product was achieved.

RETRIEVAL OF DNA PRODUCT

Method A: Manual DNA extraction from agarose gel

The single stranded DNA product from the previous steps was loaded onto a 1% agarose gel into one giant well, alongside the library and primer as controls. The gel was then visualized in a dark room under a UV light and the DNA product was cut using a stainless-steel scalpel. **Figure 3.7a** is the gel before cutting out the product and **Figure 3.7b** is the gel after cutting out the product.

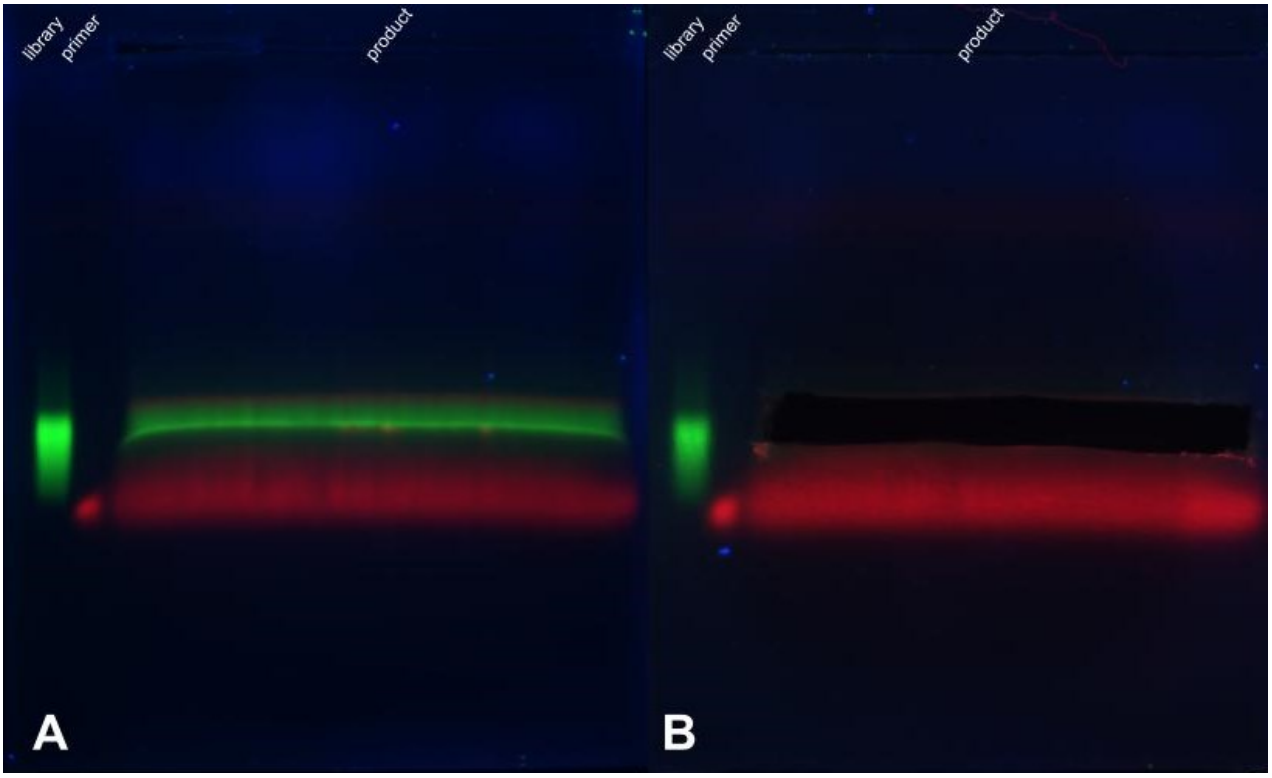

Figure 3.7. DNA product before (A) and after (B) extraction from the agarose gel for round 1 with MDA-MB-231 EVs. 1% agarose gel electrophoresis for gel extraction. Samples were loaded according to the labels on the top of the gel. The DNA was stained with 1X gel red and run at 120V for 35 minutes. DNA product band was cut using a stainless-steel scalpel under UV light.

The product is then cut into small cubes using the same scalpel to increase the surface area of the gel, increasing the rate of passive diffusion of the DNA from the gel into the surrounding solution. The gel cubes were transferred to a 15mL falcon tube and incubated at room temperature in ddH_2O at 200 rpm overnight. The ddH_2O was exchanged for a fresh solution every day until

diffusion was complete. When there was no longer a fluorescence signal when the gel cubes were imaged compared to falcon tube containing only ddH_2O as the control as shown **Figure 3.8.**

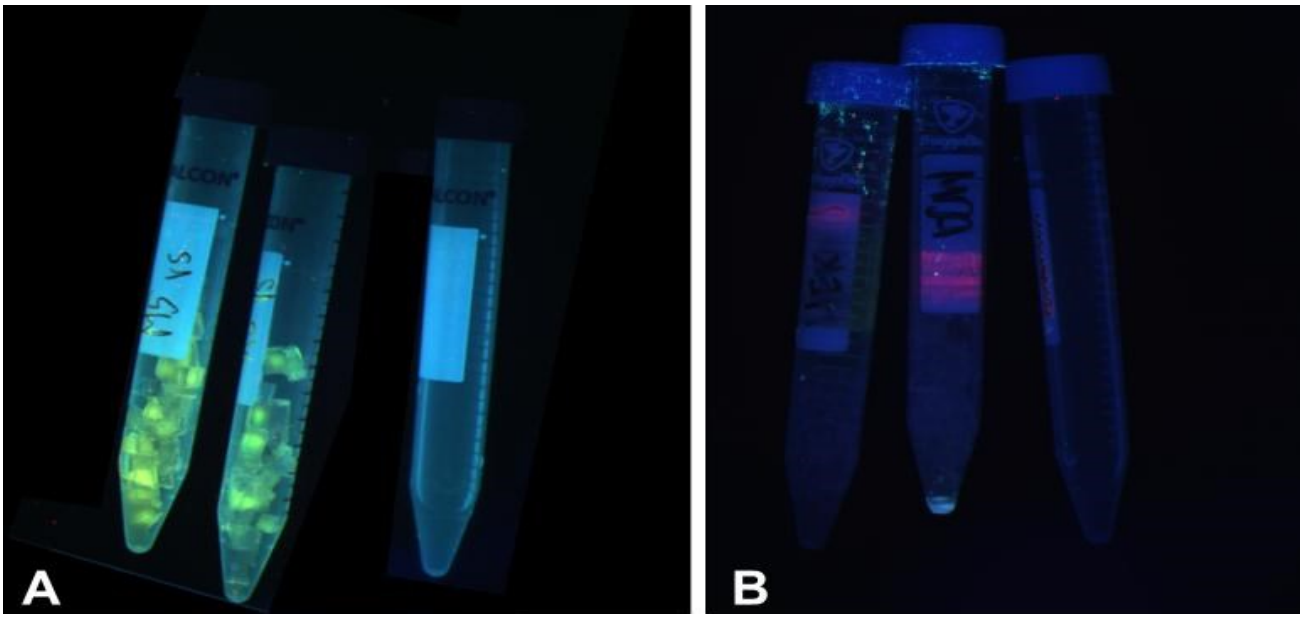

Figure 3.8. Passive diffusion of DNA product from agarose gel (A) into solution (B). From left to right, MDA-MB-231 round 5 DNA product are in the two left most samples, the right most sample is dd H_2O. A) Pre diffusion – The DNA product is inside of the gel cubes. B) Post diffusion – The DNA product has diffused out of the gel cubes and into the surrounding solution (not shown) that was removed and stored.

The ddH_2O reserved liquid from gel diffusion step was combined in preparation for DNA purification by ethanol precipitation. The dilute DNA solution was divided by adding 200 µL per 1.5 mL Eppendorf tube. Each sample tube received 5 µL of 5 M ammonium acetate and 150 µL of cold absolute ethanol. All samples were stored in -20°C overnight. Samples were then centrifuged at 16,000 g for 30 minutes and the supernatant was discarded. The DNA pellet was then washed with 200 µL of 70% ethanol, stored in -20°C for 10 minutes, the centrifuged at 16,000 g. The pellet was air dried completely in a clean fume hood until dry, ~1 hour. Finally, the pellet was resuspended in 30 uL ddH_2O.

Method B: Automated DNA size exclusion robot

The second explored method for extraction of the DNA product is by automated DNA size exclusion robot. The separation DNA molecule by size is achieved by relative migration compared to DNA markers with known size and voltage modulation to allow for synchronization of desired product based on size at the extraction well. **Figure 3.9** shows the anatomy of the instrument.

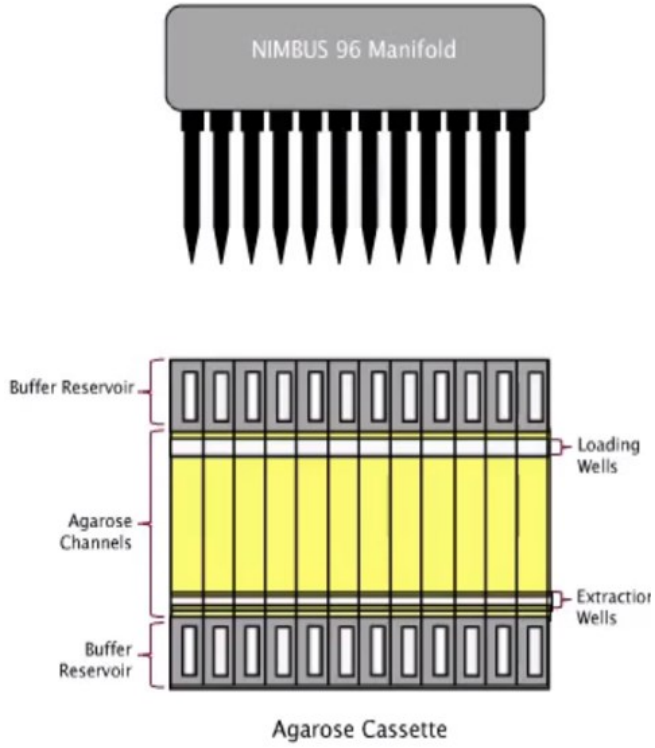

Figure 3.9. Anatomy of robotics size exclusion instrument used for DNA extraction. The sample is loaded in the loading well of the precast agarose cassette and migrates towards the buffer reservoirs through the agarose channels when voltage is applied. The NIMBUS 96 Manifold is responsible for extracting the samples from the extraction wells, when appropriate.

A gel image of the DNA product retrieval (**Figure 3.10**) by robotic size exclusion show a significant amount of DNA product in wells 4-7. The voltage allows the synchronization of DNA of relevant number of base pairs at the extraction well. Disadvantages of the size exclusion robot method were that the DNA extracted resulted in a very low concentration that had to be concentrated and that it required a technician to operate the instrument. However, the automated size exclusion robot was a more precise method, time efficient and less laborious protocol for DNA extraction after each round of SELEX.

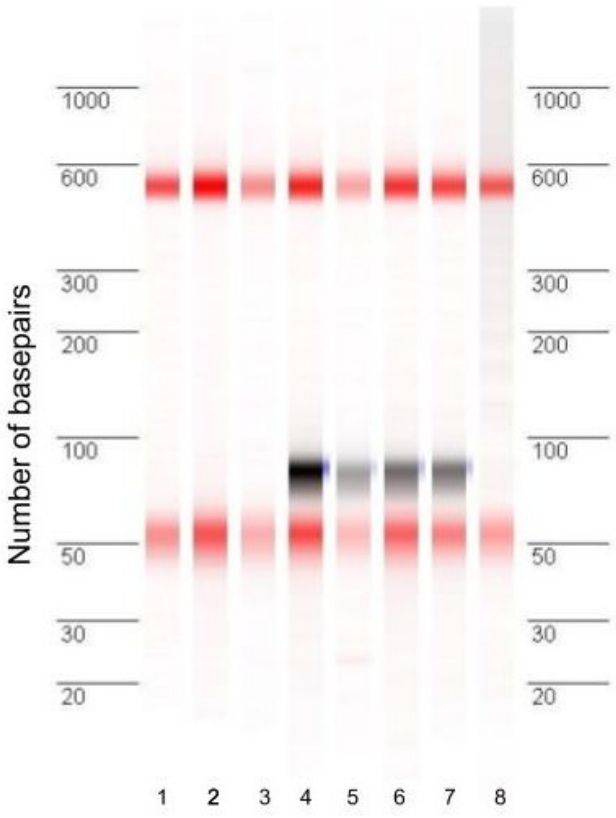

Figure 3.10. DNA product retrieval from Nucleic Acid Size Selection Robotic System. 1% precast agarose gel (Costal Genomics) was loaded in wells 1-8 with DNA markers (red bands) of 50 and 600 bp and DNA product (black bands). Samples were run at 120V for 40 minutes and the data was visualized with Venous software.

VALIDATION OF DNA POOL BINDING

DNA pool binding is assessed by flow cytometry to determine whether the SELEX method has been successful. This experiment reports the "average" fluorescent intensities of CY5 of the DNA pools – not individual aptamer capacities. Though this experiment does not reveal candidate aptamers, it gives insight on if the DNA pools are ready for Next Generation Sequencing analysis, or if more rounds of SELEX should be carried out. The DNA oligonucleotides are detected by CY5 fluorescence (ex/em: 649 nm/666 nm). The 5' end of the forward primer (Integrated DNA Technologies) has the CY5 chemical modification and incorporates itself into the product DNA strand from the PCR reaction.

Raw .facs files obtained from the Beckman Coulter MoFlo Astrios EQ Cell Sorter and analyzed using Kaluza software. Non-singlet events determined by a non 1:1 FSC-height-1 vs

FSC-height-2 ratio or a non 1:1 FSC-height-1 to SSC-area-1 ratio were excluded from the analysis. We assume that non-aggregated events that stained positive for CFSE were small or medium extracellular vesicles of interest, since a size range of 50nm-300nm was observed. Only events positive for CFSE (as determined by the negative control sample of only CFSE + buffer) were considered when analyzing the CY5 fluorescent intensity shift. Data is always displayed as % gated to account for slight variation in the number of events recorded and natural variation among the number of events that meet the gating criteria.

Since events identified as non-aggregated lipid vesicles are exclusively included in the analysis, it may be concluded that a right ward shift in fluorescent intensity positively corresponds to binding events. The stronger the rightward shift observed, the more CY5 fluorescence is detected by the instrument suggests more labelled DNA is interacting with the target, therefore we may infer better binding between the DNA molecules and the target EVs. The % increase in CY5 fluorescent intensity of the DNA pools was calculated by mean intensities as reported by the Kaluza analysis software by exporting the data as .cvs files. The formula for calculating the relative % intensity shift is shown in **Equation 3.1.**

$$100 \times \frac{Mean\ Fluorescent\ Intensity\ CY5_{(pool)} - Mean\ Fluorescent\ Intensity\ CY5_{(library)}}{Mean\ Fluorescent\ Intensity\ CY5_{(library)}} \quad (3.1)$$

Observed relative CY5 florescence intensities for DNA pools rounds 1 through 8 are summarized in **Figure 3.11** for HEK-293 and MBA-MB-231 cell lines. The DNA pools are compared to the DNA library as a control because it demonstrates binding the baseline of DNA to the EV target before selection pressures were put in place.

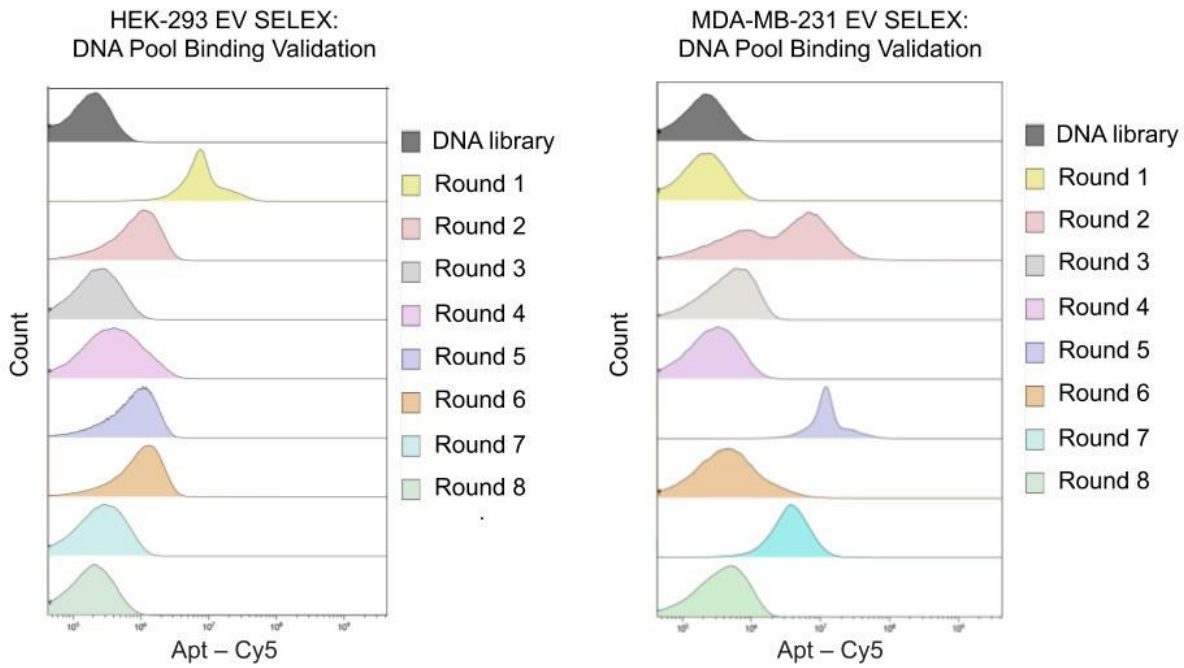

Figure 3.11. An overlay of DNA library + round 1-8 DNA pools detected CY5 fluorescent intensity selected to HEK-293 control and MDA-MB-231 cell line derived EVs. DNA is detected by CY5 fluorescent shift after gating for non-aggregated singlet events and excluding events negative for the lipid membrane dye CFSE.

The general trend for the pools generates to the HEK-231 cell line EVs can be described as an increase in the average fluorescent intensity, then it reaches a peak, then finally retreat towards the control shift. On average, the willingness to bind of the DNA pools increased as they became more selective to their target through the selection process before the maximum is reached. Afterwards, the mutations acquired in selection rounds 6-8 were less beneficial which is why we see the decreasing trend. This trend excludes round 1, showing an unexplainably strong rightwards shift in intensity. It would be reasonable to expect earlier rounds of SELEX are composed of relatively diverse DNA sequences; thus, the strong shift is not evidence of good binding since it has not experienced a great deal of selection pressure. A more detailed side-by-side comparison of the three pools with the largest shift relative to the DNA library control are shown in **Figure 3.12** DNA pools 1, 5 and 6 generated to the HEK-293 cell line show the largest difference in detected fluorescent intensity shift relative to the control. A 99%, 12% and 16% rightward shift relative to the DNA library control were calculated for rounds 1,5 and 6, respectively.

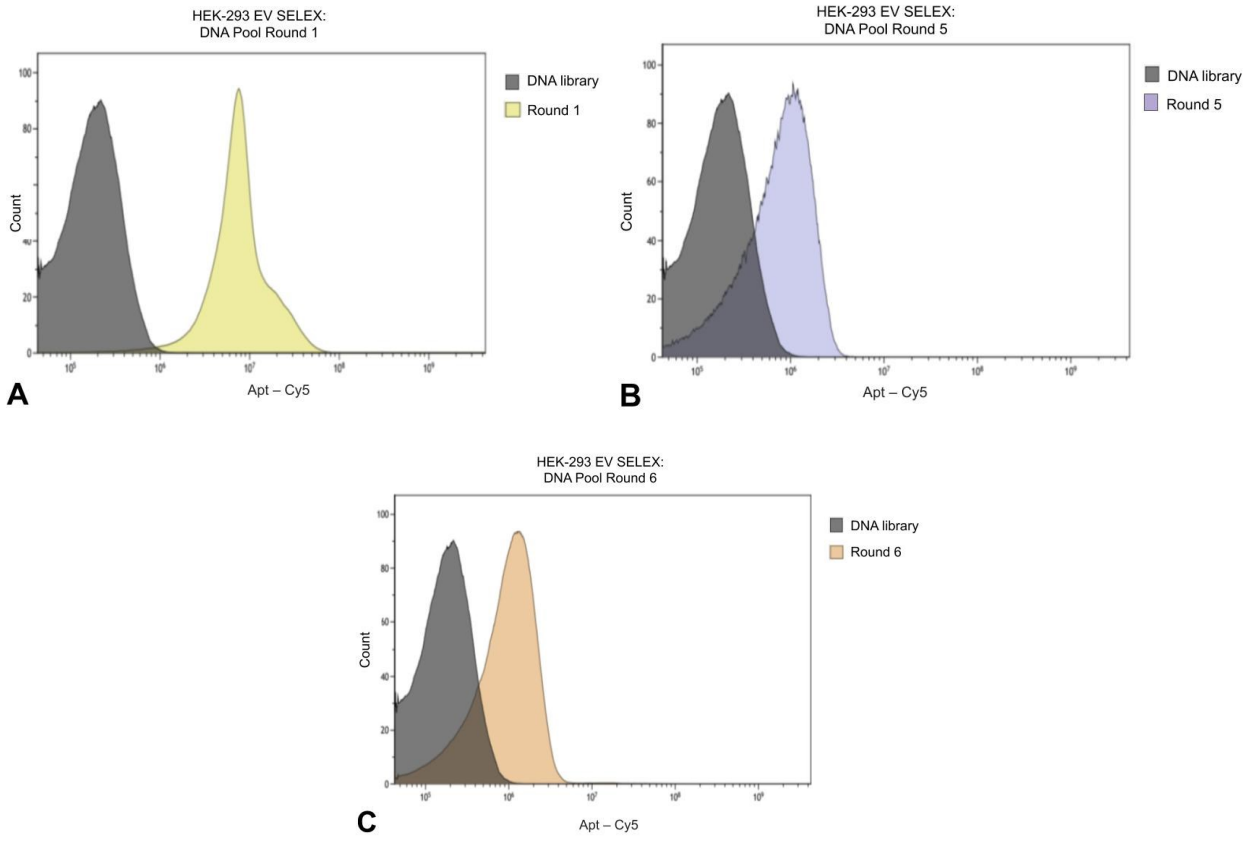

Figure 3.12. An overlay of round 1, 5 and 6 DNA pools selected to HEK-293 EVs with the largest detected CY5 fluorescent intensity shift compared to the DNA library. The % increase in shift for rounds 1, 5 and 6 are 99%, 12% and 16%, respectively.

A pattern is less apparent for the average fluorescent intensities of the pools generates to the MDA-MB-231 cell line EVs. An increase in affinity for the EV target is observed early in the second generation of SELEX but soon thereafter retreats towards the control, and then rightwards shift is observed again in the late rounds of selection. A more detailed side-by-side comparison of the three pools with the largest shift relative to the DNA library control are shown in **Figure 3.13.**

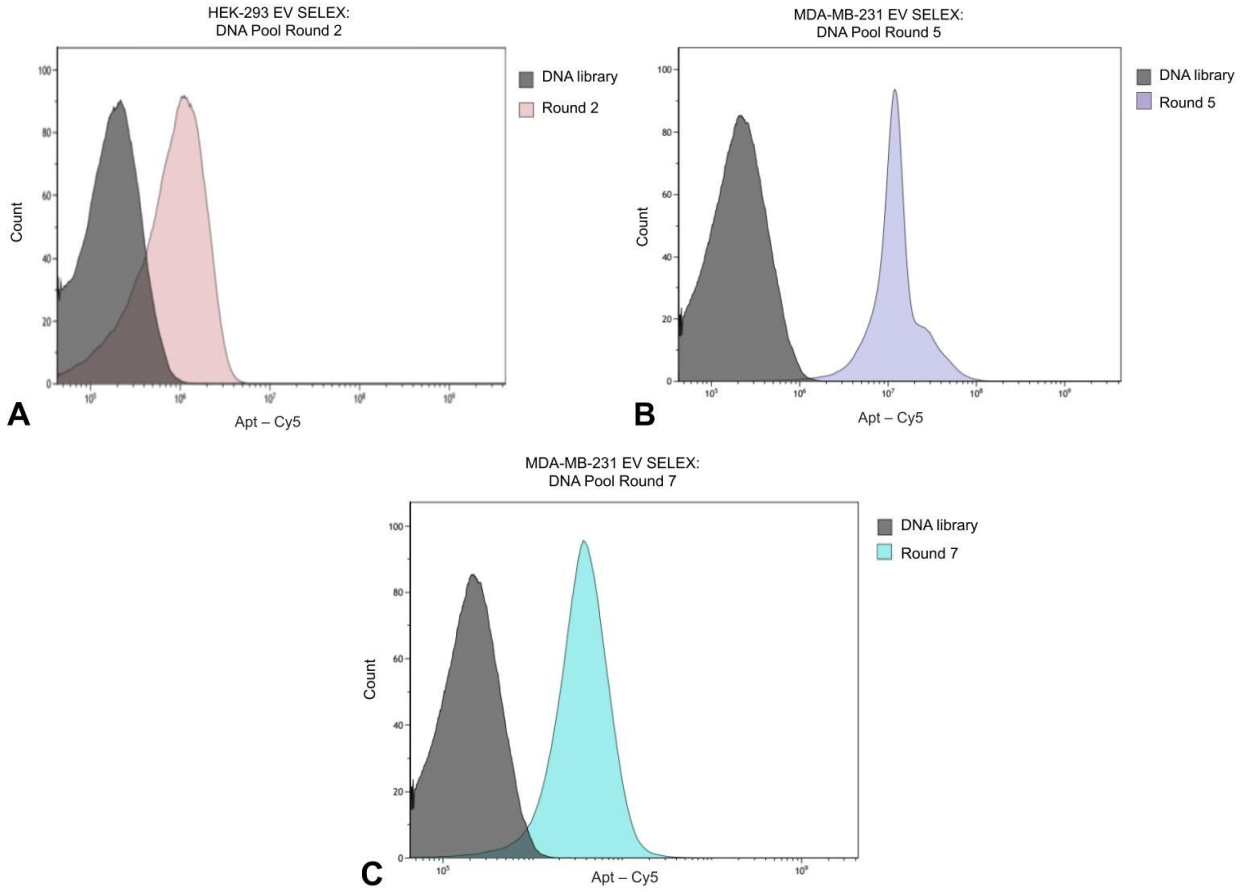

Figure 3.13. An overlay of round 2, 5 and 7 DNA pools selected to MDA-MB-231 EVs with the largest detected CY5 fluorescent intensity shift compared to the DNA library. The % increase in shift for rounds 2, 5 and 7 are 47%, 130% and 37%, respectively.

SELECTION OF CANDIDATE APTAMERS

DNA sequences were not generally observed to have an enriched abundance until round 4 or 5 since earlier on in the selection process there are fewer selection pressures. The top 5 abundant sequences that appeared in the sequencing data for both cell lines is summarized in **Table 3.3.** Interestingly, the 4th most abundant sequence in the MDA-MB-231 pools was the 3rd most abundant in the HEK-293 pools. Moreover, the 5th most abundant sequence in the MDA-MB-231 pool was the 4th most abundant in the HEK-293 pool. Interestingly, the same sequence evolved in parallel to slightly different targets. This may be because there are many similarities across all EVs and therefore we speculate that if these two sequences were successful aptamers, they may recognize EVs from both cell lines and likely bind to a common protein. Since we were looking for a candidate aptamer that specifically recognizes EVs from the cancerous cell line, the

sequences were disqualified. Candidate aptamers should not be determined by abundance alone since DNA polymerases may have innate amplification bias towards certain sequences during PCR.

Table 3.3. Top five most abundant sequences for MDA-MB-231 and HEK-293 shown without primer regions. Abundance rank 1 is the most abundant sequence in all 8 rounds of selection, 2 is the second most abundant, etc.

Abundance Rank	MDA-MB-231	HEK-293
1	CGTGGTTACAGTCAGAGGAGATGGCTTCTGGACTACCTATGCCGTGGTTACAGTCAGAGG	CGTGGTTACAGTCAGAGGAGCGTGTCCGTGCGTGGATGGCTTCTGGACTACCTATGCCGT
2	GTGCAGCATAGGTAGTCCAGAAGCCATCACGTAGCGACGACCTCCTCTGACTGTAACCACGG	CGTGGTTACAGTCAGAGGAGGTCACGTGGCTTGACGTGGCTTCTGGACTACCTATGCCGT
3	CGTGGTTACAGTCAGAGGAGCGTGGTTACAGTCAGAGGAGATGGCTTCTGGACTACCTAT	CGTGGTTACAGTCAGAGGAGGTCACGTGCCTTGACGTGGCTTCTGGACTACCTATGCCGT
4	CGTGGTTACAGTCAGAGGAGGTCACGTGCCTTGACGTGGCTTCTGGACTACCTATGCCGT	CGTGGTTACAGTCAGAGGAGCGTGACCGTGCGTCATGGCTTCTGGACTACCTATGCCGTG
5	CGTGGTTACAGTCAGAGGAGCGTGACCGTGCGTCATGGCTTCTGGACTACCTATGCCGTG	TGCAGCATAGGTAGTCCAGAAGCCATCACGTAGCGACGACCTCCTCTGACTGTAACCACG

Point mutations, deletions or insertions will accumulate throughout the 8 rounds of selection, therefore relying on abundance of sequences along would also result in missing important sequences. Phylogenetic tree analysis can be constructed by clustering the DNA sequences based on the relatedness of their sequences. Conserved regions of sequences may then be considered for candidate validation.[127] The consensus sequence for EVs derived from the HEK-293 cell line is shown in **Figure 3.14b.** The degree to which each nucleotide is conserved is described by the conservation panel, and the sequence logo shows an alternative visual of the same information. There is little overlap between the consensus sequence resulting from the selection of both cell lines, suggesting that they experienced different selection pressures. The consensus sequence for aptamers selected to non-cancerous derived EVs seems more conserved based on higher reported conversation % on average than the sequence selected to cancerous derived EVs.

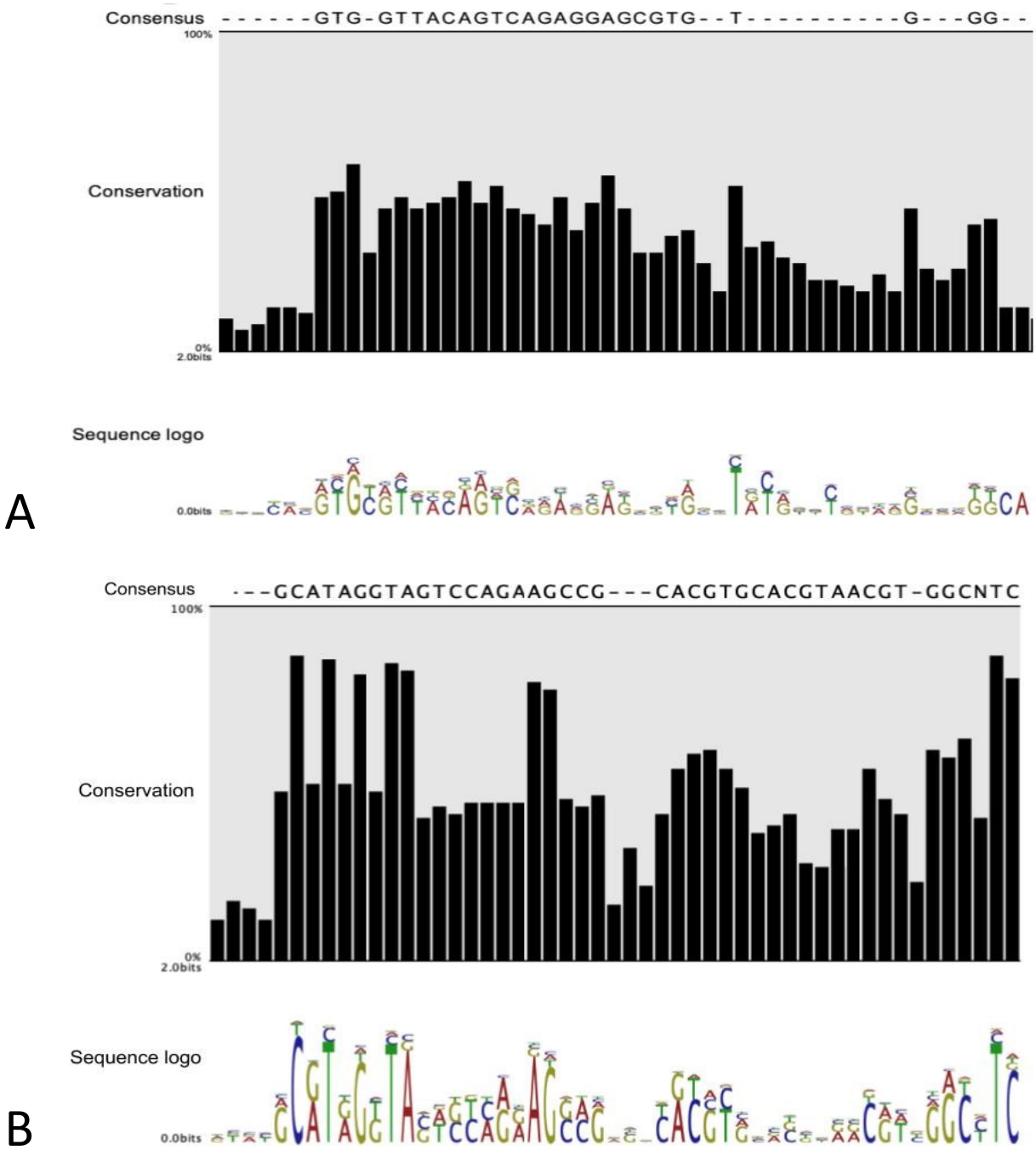

Figure 3.14. Fifty most conserved nucleotides from 8 rounds of SELEX to HEK-293 (A) and MDA-MB-231 (B) EVs across all DNA pools. Consensus sequence denotes the net most conserved nucleotides, Conversation denotes the % likeliness of each nucleotide from 0 to 100 to appear in that position. Sequence logo is an alternative visual representation of the data, the larger the nucleotide letter, the more prominent it appears in the given position. A dashed line represents a nucleotide below the conservation threshold of 40%. “N” within the consensus sequence denotes ambiguity.

Since loop regions of aptamers are not involving in usual base pair interactions, they are "available" to interact via non-covalent interactions with the target of interest. Thus, loop regions should be favored when selecting aptamer candidates.[128,129] For this reason, predicted secondary structure of the candidate aptamers should be considered. It is worth noting that the predicted secondary structure of an oligonucleotide is an oversimplification since it does not account for tertiary structure. Secondary structures of candidates believed to have potential was determined by OligoAnalyzer Tool (Integrated DNA Technologies, open source) as shown in **Table 3.4.**

VALIDATION OF CANDIDATE APTAMER BINDING

The four aptamer candidates were chosen to screen for evidence of binding selectively to the cancerous MDA-MB-231 EVs, but not the control cell line derived EVs. The % gated events (non-aggregated, CFSE particles) were plotted against CY5 fluorescent intensity to assess binding of candidate aptamers. The relative shift in intensity was compared to the original DNA library. The results are shown in **Figure 3.15.**

Table 3.4. Summary of candidate aptamers chosen after screening for abundance, consensus sequence and favorable predicted secondary structure.

Candidate Aptamer (5'--> 3')	ΔG(kcal•mole^{-1})	T_M (°C)	OligoAnalyzer predicted 2D structure
CTCTGACTGTAACCAC GTGGTTACAGTCAGAG GAGATGGCTTCTGGAC TACCTATGCCGTGGTT ACAGTCAGAGGGCATA GGTAGTCCAGAA	-41.91	83.2	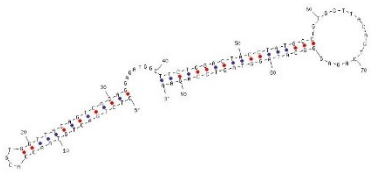
CTCCTCTGACTGTAAC CACGGTATGTACTGAG TGCCAAAGCTTCCCTA TGCACGTGCAGGGTGC ACGCGGGGGTGTAGAC GCATAGGTAGTCCAGA AGCC	-17.61	57.7	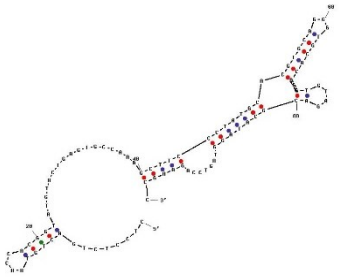
CTCCTCTGACTGTAAC CACGACGCATGTTTTC ATGGGTACAAGCCGTG TATACGTTCTCGCTTG GGCTTTGTGGATACTC GCATAGGTAGTCCAGA AGCC	-19.69	57.4	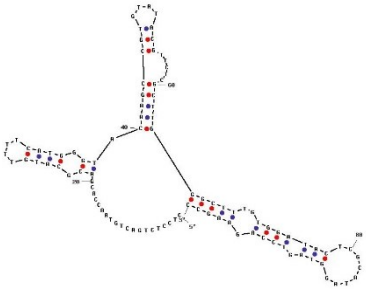
CTCCTCTGACTGTAAC CACGTGCAGCATAGGT AGTCCAGAAGCCATCA CGTAGCGACGACCTCC TCTGACTGTAACCACG GCATAGGTAGTCCAGA AGCC	-10.58	46.9	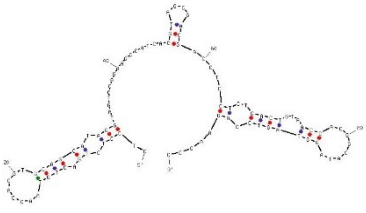

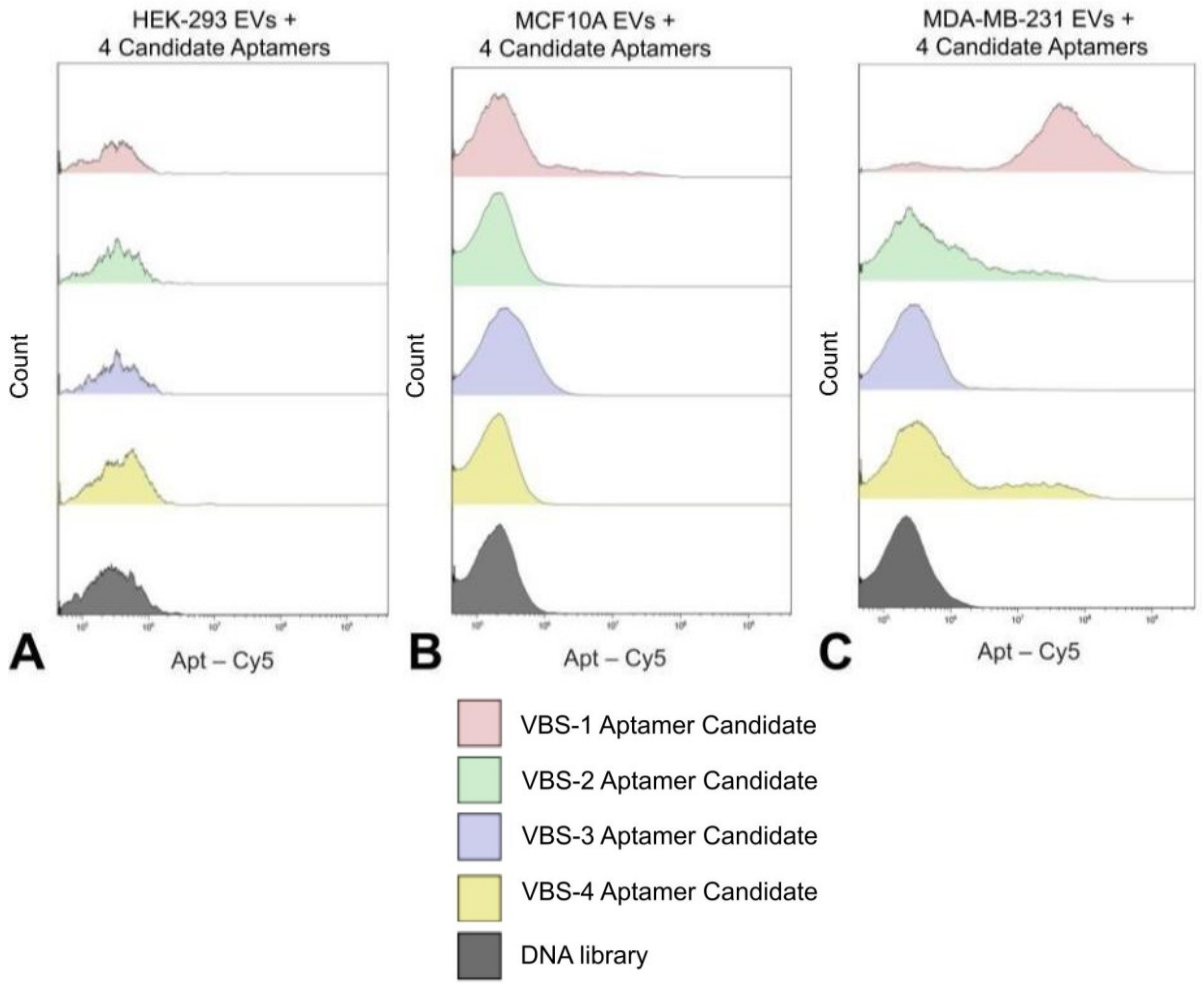

Figure 3.15. Screening of four candidate aptamers binding to EVs derived from A) HEK-293, B) MCF10A, C) MDA-MB-231 cell line. 1uM of 4 DNA aptamer candidates + 100uL of isolated EVs in PBS from each cell line.

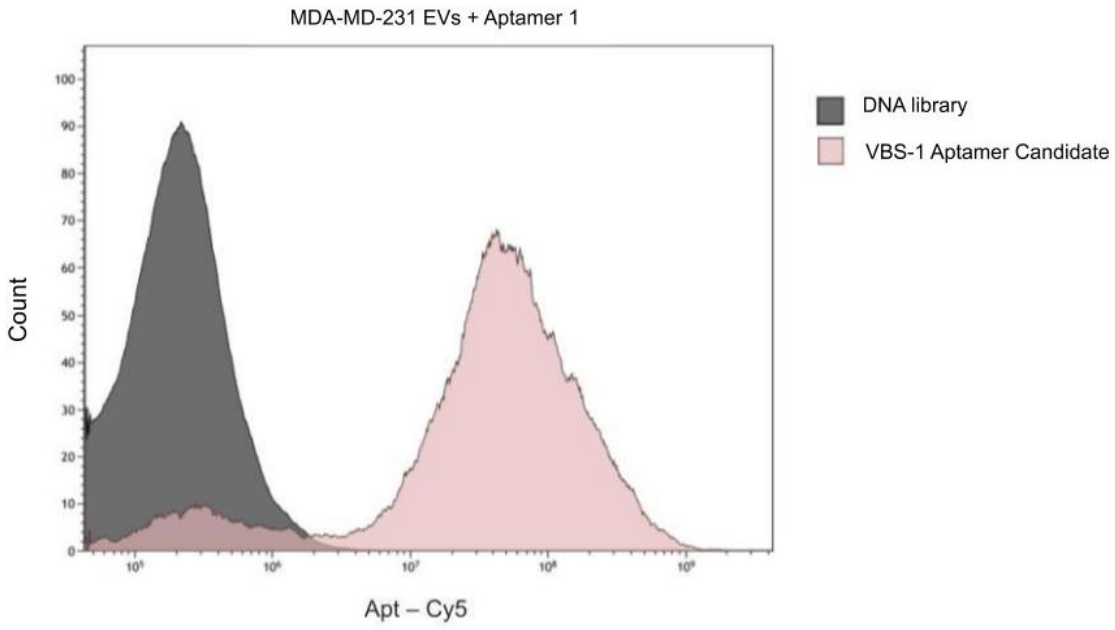

Figure 3.16. Screening of four candidate aptamers binding to EVs derived from MDA-MB-231 cell line. 1 uM of 4 DNA aptamer candidates + 100uL of isolated EVs from HEK-293 (A), MCF10A (B) and MDA-MB-231 (C) cell lines.

VBS-1 aptamer candidate binds selectively to MDA-MB-231 cell line, since the shift is observed exclusively in panel C. VBS-2 and VBS-4 aptamer candidates show little potential in panel C, but not as significant of a shift as the VBS-1 candidate. VBS-3 aptamer candidate does not show a shift and can thus be the first candidate to be eliminated. An overlay of the DNA library and the VBS-1 aptamer candidate are shown in **Figure 3.16.** The relative shift in intensity was 150% and displays the best potential as an aptamer. Therefore, VBS-1 was chosen for further investigation in Chapter 4.

3.5 Conclusion

The VBS-1 DNA aptamer was selected from a DNA library to bind to cancer (MDA-MB-231) and that does not bind non-cancer derived (HEK-293) EVs by systematic evolution of ligands by exponential enrichment. The binding of DNA aptamer pools was validated by flow cytometry where DNA pools 1 and 4 for the experimental cell line had the best relative shift compared to the DNA library control. All sequences were determined by Illumina Next Generation sequencing. The DNA sequences were aligned and sequences appearing in both control and cancer pools were rejected and only ones appearing exclusively in the experimental group were considered. Finally, four candidate aptamers were chosen by relative abundance, stability in predicted secondary structure and consensus sequence. Finally, four candidate aptamers named VBS-1, VBS-2, VBS-3 and VBS-4 were screening for selective binding. VBS-1 was the most successful candidate showing a relative binding shift of 150% compared to control and thus was further investigated to find the protein target in Chapter 4.

3.6 Acknowledgments

Next Generation Sequencing was performed at the Integrated Microbiome Resource (IMR) at Dalhousie University and I thank Andre Comeau for his excellent and personable customer service. I'd like to acknowledge the Flow Cytometry and Robotics Core Facility manager Dr. Shahrohk Ghobadloo for operating the automated DNA size exclusion robot and taking the time to explain the system to me. I would like to acknowledge Emil Zaripov for sharing his SELEX protocol and showing me how run gels during my first months in the lab. Lastly, I would like to acknowledge Dr. Prabir Kulabhusan for optimization the ethanol precipitation protocol for our DNA product.

Chapter 4

Aptamer-Facilitated Biomarker Discovery

4. APTAMER-FACILITATED BIOMARKER DISCOVERY

4.1 Objective

The objective of this chapter is to identity the protein on EVs derived from the MDA-MB-231 cell line that is bound by the VBS-1 selected aptamer described in Chapter 3 by an aptamer-based pull-down experiment. The target transmembrane protein identified by LC-MS/MS was shown to be present on MDA-MB-231 cell derived EVs by flow cytometry.

4.2 Introduction

It has been investigated that EVs could be the source of potential cancer biomarkers since the nature of their biogenesis provides them with similar surface proteins – thus allowing us to detect biomarkers on the surface of EVs instead of on the surface of whole tumour cells. Antibodies are useful for the detection of known protein, but do not have the capacity to identify novel proteins. The identification of the aptamer binding partner may strategically allow us to identify novel biomarker candidates if the aptamer candidate chosen binds selectively to cancer derived EVs.

LC-MS/MS-based methods are predominately used for protein identification. Sample preparation for proteomic analysis involves EV membrane lysis are denatured by physical (ex. heat) or chemical methods (ex. Urea) in order to interrupt hydrogen bonding, stripping the proteins of their tertiary structure, rendering the amino acid sequences more accessible for downstream processing. The proteins are solubilized in a detergent, such as sodium dodecyl sulfate (SDS), n-dodecyl β-D-maltoside (DDM), or Triton X-100. Solubilization allowing for a more thorough digestion by denaturation of proteins and thus exposure of cleavage sites.[130–133] In a bottom-up proteomics approach, proteins are solubilized (e.g. by detergents) then proteins are denatured by chemical methods. For example, urea is a commonly used denaturing agent that interrupts hydrogen bonding, stripping the proteins of their tertiary structure, rendering the amino acid sequences more accessible for downstream processing. Once lysis has occurred, the proteins are reduced and alkylated in preparation for enzymatic digestion. MS Trypsin is the most widespread protease used for enzymatic digestion, with its cleavage site at the carboxyl terminus of lysine and arginine. Thereafter, a desalting step should take place to prevent contamination of liquid chromatography and mass spectrometry equipment. The sample should then be evaporated and resolubilized in a formic acid solution - ensuring a positive charge on digested peptides. The

peptides are then fractioned by reverse phase chromatography techniques, allowing for their separation which is advantageous particularly for diverse and complex samples such as those derived from EVs. A general schematic of a general proteomic workflow is found in **Figure 4.1.**

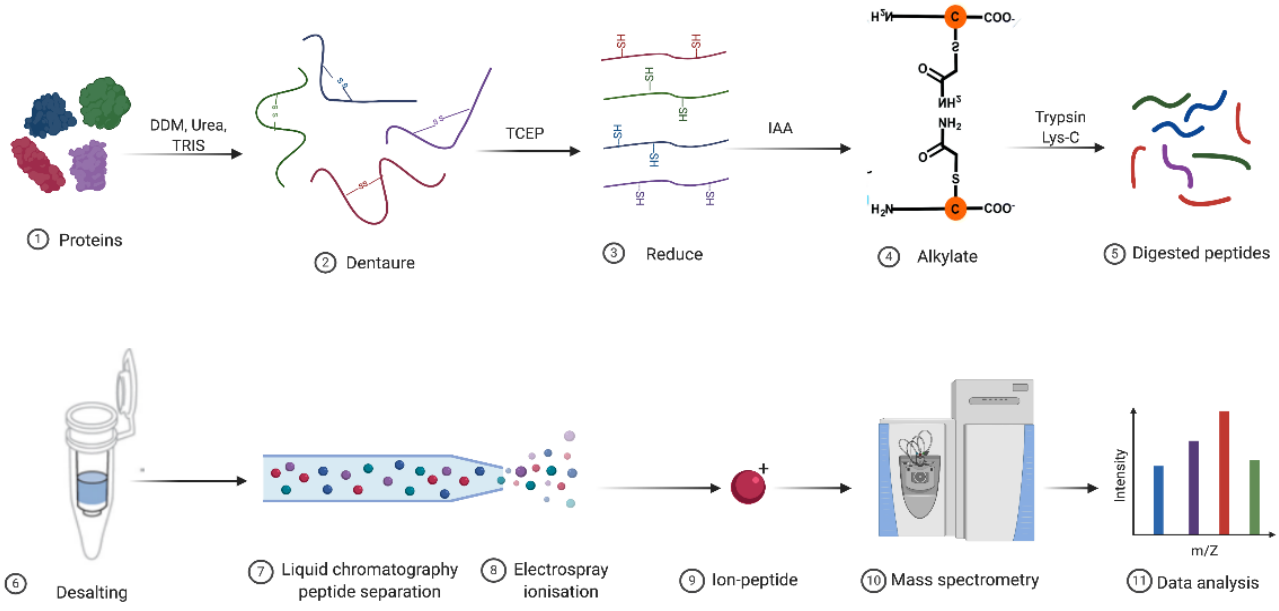

Figure 4.1. Schematic for bottom-up proteomics workflow for protein identification using a label-free quantitative LC-MS/MS approach. Proteins are denatured, reduced, and then alkylated. Proteins are then digested, and the sample is desalted to avoid contamination of the MS instrument. Chromatography separates peptides and then they are subject to a soft ionization source and analyzed by MS.

4.3 Methods

APTAMER-BIOMARKER PULL-DOWN

The following protocol describes two approaches for aptamer target identification on exosomes. In Method 1, aptamers are incubated with intact exosomes while for Method 2, aptamers are incubated with protein lysate. Each approach requires exosomes worth of 60 µg protein content. This amount is then divided into 6 x 10 µg for three target aptamer pull-down experiments and three control DNA library pull-down experiment. A schematic workflow summary is provided in **Figure 4.2.**

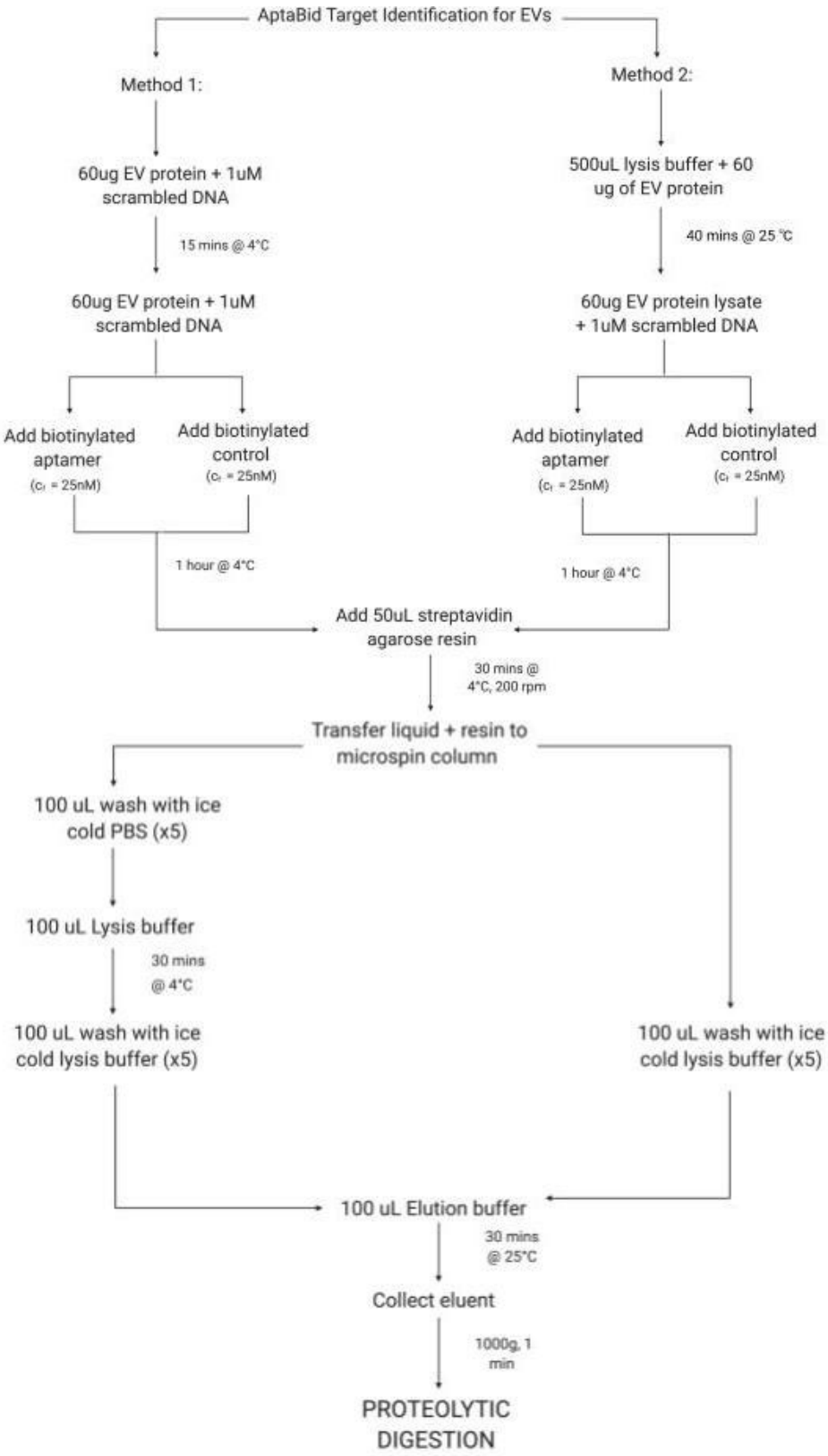

Figure 4.2. Schematic and comparison of Method A and B for aptamer-based pull-down workflow. Lysis buffer: 0.1% DDM in PBS, pH 7.4. Elution buffer: 8M Urea, 50mM TRIS-HCL, pH 8.

Method 1: Intact EVs + Aptamer

Scrambled DNA library was incubated with 60ug intact EVs to a final concentration of 1uM for 15 minutes at 4°C. The sample was then partitioned into 6 Eppendorf tubes to have 3 biological replicates of both the target aptamer and control aptamer groups. The 3 experimental samples each received a final concentration of 25nM of VBS-1 aptamer to a final volume of 100 ul and incubated for 1 hour at 4°C. The 3 control samples received the same treatment with scrambled biotinylated library of the same length instead of the target aptamer. 50uL of slurry streptavidin agarose resin (ThermoFisher, Cat No. 20349) was added and incubated for 30 minutes at 4 °C while on a shaking plate to avoid sedimentation of the resin. The whole liquid plus resin mixture was then transferred to spin columns (Micro Bio-Spin Chromatography Columns, Bio-Rad) ensuring everything has been transferred by washing once with PBS. Each sample is washed 5 times with 100uL of ice-cold PBS. 100uL of lysis buffer (0.1% DDM in PBS, pH 7.4) was added to each sample and they were incubated for 30 minutes at 4°C. The samples were then washed four additional times with 100uL of ice-cold lysis buffer. After the final wash, the samples were incubated with elution buffer (8M urea, 50mM TRIS-HCL, pH 8) and incubated for 30 minutes at 25°C. The column was washed 5 times with ice cold lysis buffer and the elutant was collected by centrifugation at 1000g for 1 minute and the column was washed once more with 100 uL elution buffer and centrifuged at 1000g for 1 minute.

Method 2: EV lysate + Aptamer

60 ug of isolated EVs were incubated in 500uL of lysis buffer at 25°C for 30 minutes. The sample was divided into two groups: aptamer and control, each with 3 biological replicates for a total of 6 samples. Biotinylated aptamer and biotinylated control were added to their respective samples for a final concentration of 25nM and final volume of 100uL and incubated for 1 hour at 4°C. 50uL of streptavidin agarose resin (ThermoFisher, Cat No. 20349) was added and incubated for 30 minutes at 4°C while on a shaking plate to avoid sedimentation of the resin. The whole liquid + resin mixture was transferred to (Micro Bio-Spin Chromatography Columns, Bio-Rad) and the residual mixture was transferred by one wash of PBS. Each sample was washed 5 times with 100uL ice cold lysis buffer then replaced with 100uL of elution buffer and incubated for 30 minutes at 25°C. The elutant was collected by centrifugation at 1000g for 1 minute and the column was washed once again with 100 uL of elution buffer and centrifuged at 1000g for 1 minute.

IN-SOLUTION DIGESTION OF PROTEINS

Eluted proteins from aptamer pull-down experiments were prepared for mass spectrometry analysis using an adjusted filter-aided sample preparation (FASP) protocol.[134] 200 uL eluate were added on top of a 10 kDa molecular weight cut-off (MWCO) filter (Microcon® 10K device, Cat No. MRCPRT010, Millipore) and mixed with 8 µL 100 mM tris(2-carboxyethyl) phosphine (TCEP) (Pierce™ TCEP-HCl, Cat No. 20490, ThermoFisher) to reduce proteins. Incubation for 30 minutes at 25°C was followed by a 15 minute centrifugation step at 14,000 g to concentrate proteins. Subsequently, the concentrate was diluted with 100 µL digestion buffer (1.5 M Urea, 50 mM TRIS-HCL, 0.6% glycerol, pH 8) and alkylated by 4 µL 0.5 M iodoacetamide (IAA) (Cat No. GERPN6302, SigmaAldrich) and incubated for 45 minutes at 25°C in the dark followed by a 15 min centrifugation step at 14,000 g. Proteins were again diluted with 100 µL digestion prior to starting the digestion by adding 0.3 µg Trypsin/Lys-C (Cat No. V5072, Promega) resulting in a minimum enzyme: substrate ratio of 1:33. Proteins were digested on the filter devices for 12 hours at 37°C and digests were collected by two repeated centrifugation steps for 10 min at 14,000 g rinsing in between with 40 µL digestion buffer. Peptides were acidified with 2 µL of 100 µL formic acid and desalted for MS analysis using C18 TopTip microcolumns (Cat No. TT2C18, Glygen) according to the manufacturer protocol. Purified peptides were vacuum dried and frozen in -20°C.

NANO-LC-MS/MS

Samples were analyzed by Orbitrap Fusion (Thermo Fisher Scientific) coupled to an Ultimate3000 nanoRLSC (Dionex, Thermo Fisher Scientific). Peptides were separated on an in-house packed column (polymicro technology), 15 cm x 70 µm ID, Luna C18(2), 3 µm, 100 Å (Phenomenex) employing a water/ acetonitrile/ 0.1% formic acid gradient. Samples were loaded onto the column for 105 minutes at a flow rate of 0.30 µl/min. Peptides were separated using 2% acetonitrile in the first 7 minutes and then using a linear gradient from 2 to 38 % of acetonitrile for 70 min, followed by gradient from 38 to 98 % of acetonitrile for 9 minutes, then at 98 % of acetonitrile for 10 min, followed by gradient from 98 to 2% of acetonitrile for 3 minutes and wash 10 minutes at 2 % of acetonitrile. Eluted peptides were directly sprayed into a mass spectrometer using positive electrospray ionization (ESI) at an ion source temperature of 250°C and an ionspray voltage of 2.1 kV. The Orbitrap Fusion Tribrid was run in top speed mode. Full-scan MS spectra (m/z 350 – 2000) were acquired at a resolution of 60 000. Precursor ions were filtered according

to monoisotopic precursor selection, charge state (+2 to +7), and dynamic exclusion (30 s with a ± 10 ppm window). The automatic gain control settings were 5×10^5 for full FTMS scans and 1×10^4 for MS/MS scans. Fragmentation was performed with collision-induced dissociation (CID) in the linear ion trap. Precursors were isolated using a 2 m/z isolation window and fragmented with a normalized collision energy of 35%.

DATA ANALYSIS

MS raw files were analyzed using the MaxQuant[135] software in combination with the Andromeda search engine.[136] Peptides were searched against a human UniProt FASTA file containing 20,412 entries (03.01.2019) and a default contaminants database. Default parameters were used if not mentioned otherwise. N-terminal acetylation and methionine oxidation were set as variable modifications and cysteine carbamidomethylation was set as a fixed modification. A minimum peptide length of 6 amino acids was required and false discovery rate (FDR) was set to 0.01 for both the protein and peptide level, determined by searching against a reverse sequence database. Enzyme specificity was set as C-terminal to arginine and lysine with a maximum of two missed cleavages. Peptides were identified with an initial precursor mass deviation of up to 4.5 ppm and a fragment mass deviation of 20 ppm. The 'Match between run algorithm' in MaxQuant[137] was performed between all samples to increase peptide identification rate. Proteins and peptides matching to the reverse database were discarded. For label-free quantitation (LFQ), a minimum ratio count of 2 was required.[138]

Peptide counts and unnormalized protein intensities were used for the data analysis. A scoring system was designed based on 5 parameters: log2 fold-change, p-value, peptide count difference, presence difference, and abundance rank difference. Each protein's score consists of its relative performance in each category which is then averaged across the best 3 parameters and assigned one final score. Each parameter is assigned equal weight. The scoring scale ranges from 0 to 1, where 0 is a protein unlikely to be the true aptamer binding partner, and 1 is a protein likely to be the true aptamer binding partner. P-value was computed by a student's t-test. Log2 fold change was calculated by **Equation 4.1.** Peptide count difference was calculated by **Equation 4.2.** Presence difference was calculated by **Equation 4.3.** Presence difference was calculated by

equation X. Abundance rank difference was calculated by **Equation 4.4.** The 4 equations are summarized in **Table 4.1.**

Table 4.1. Four of the five parameters and their equations used to calculate protein score in the aptamer-based pull-down experiment.

Equation	Parameter	Equation
4.1	Log2-fold change	$log_2(fc) = log_2(\frac{\sum abd_{apt}}{n_{apt}} / \frac{\sum abd_{ctrl}}{n_{ctrl}})$
4.2	Peptide count difference	$\Delta peptides = \frac{\sum peptides_{apt}}{n_{apt}} - \frac{\sum peptides_{ctrl}}{n_{ctrl}}$
4.3	Presence difference	$\Delta n_{ident.} = \frac{\sum n(p_i > 0)_{apt}}{n_{apt}} - \frac{\sum n(p_i > 0)_{ctrl}}{n_{ctrl}}$
4.4	Abundance rank difference	$\Delta r(abd) = \frac{\sum \frac{r(abd_i)_{apt}-1}{n_{prot.}-1}}{n_{apt}} - \frac{\sum \frac{r(abd_i)_{ctrl}-1}{n_{prot.}-1}}{n_{ctrl}}$

Additional Information:
1. Apt = aptamer
2. Ctrl = control
3. n=number of samples
4. r= rank
5. Abd = abundance

The list of proteins obtained was reduced by removing targets that were evidently non-binding. Proteins were removed if: they were present in less than 50% of aptamer replicates, they were calculated to have a negative presence difference, they were calculated to have a negative abundance rank difference, they were calculated to have a negative log2-fold change or if they were calculated to have a negative peptide difference. After reducing the list of proteins, the remaining proteins within each sample are ranked from highest score (potential binding target) to lowest score (unlikely binding target) and exported including all parameters.

VALIDATION OF ATP1A1 ON EVS

ATP1A1 primary antibody conjugated to Alexa 488 was purchased from Santa-Cruz biotechnology (Santacruz Biotech, Cat No. sc-48345 AF488). The antibody was diluted in 1: 500,000 1:50,000 1:5,000 1:500 1:50 ratios and incubated for 20 minutes in the dark with MDA-MB-291 and HEK-293 pre-isolated EVs in PBS buffer. A blank control sample of only buffer and antibody was also included. All samples were run on Beckman Coulter MoFlo Astrios EQ Cell Sorter. The data was analyzed by Kaluza software. Separation index between the positive and negative populations were calculated according to **Equation 4.5** and plotted against varying concentrations.[139] A 1 in 5000 dilution factor was used during the validation experiment.

4.4 Results and discussion

Technical and biological variability should be considered within a proteomics MS based experiment. Technical variability is concerned with the reproducibility of the experiment due to slight variations in sample extraction, label, technician, reagent batch or instrumentation. Biological variation is a consequence of the innate biological differences between samples in a study such as subtle differences in EVs produced by the cells.[140] Three technical and biological replicates were considered.

The aptamer-based pull-down experiment was conducted by two slightly different methodological approaches to embody the advantages and disadvantages of both, in order to gain well-rounded understanding and avoid any biases that may arise from only examining one approach over the other. Method A involves aptamer incubation with intact EVs, preserving intra-EV and extra-EV components, thus is better representation of how the aptamer interacts with its target. Method A also has 5 extra washing steps, which can be assumed to result in a washing away more proteins, thus a stronger aptamer biding is required. Method B on the other hand, solubilized proteins before incubation with the aptamer, which may allow for better accessibility than when they are embedded in the membrane. This can be seen in **Figure 4.3** where the number of proteins identified by LC-MS/MS by both methods is shown in a Venn diagram. Method A identified 199 proteins, whereas method B identified 237 proteins. Additionally, there is a significant overlap of 185 proteins identified by both methods, with 14 and 52 proteins detected only in method A or B, respectively. This reinforces that both methods are valid approaches but give slightly different perspectives of the binding partner.

Figure 4.3. Number of proteins identified in method A verses method B by LC-MS/MS. Method A identified 199 proteins, whereas method B identified 237 proteins. 64 proteins are exclusively identified by either method A or method B.

Both methods share significant overlap in the proteins that were identified. Evidently, we can expect that the proteins exclusively found in the control sample will not be the true aptamer binding protein, since there is no evidence that suggest they are binding to the aptamer. Instead, they may be proteins that have a net positive charge under the buffer conditions and consequently bind to the net negative charge of DNA in a non-specific fashion, or they were simply not identified by the aptamer by chance. Proteins that appear in aptamer only or aptamer and control samples are of interest for investigation as potential binding partners. Proteins in aptamer only samples are not necessarily a top priority, since a protein could be present in the control sample and be enriched several folds in the aptamer sample. Thus, a systematic approach must be used to determine which proteins are strong candidates.

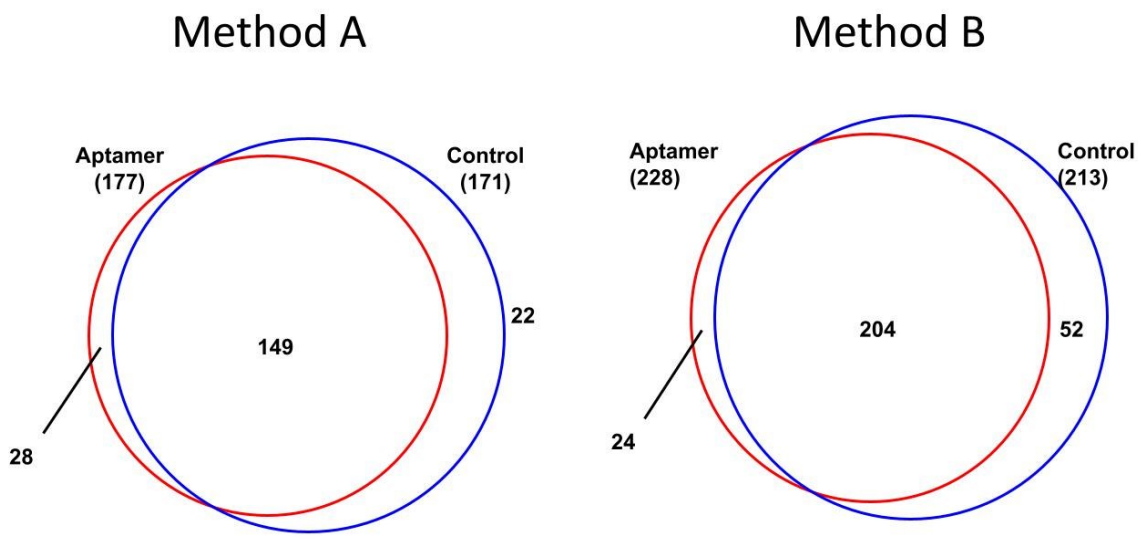

Figure 4.4. Method A vs. Method B: Proteins in control and aptamer samples identified by LC-MS/MS. Method A identified 199 proteins, 149 of which were shared between the aptamer and control sample and 50 proteins are unique between the two groups. Method B identified 237 proteins, 149 of which were shared between the aptamer and control sample and 76 proteins are unique between the two groups.

Five parameters (**equations 4.1-4.4)** were strategically chosen to rank proteins obtained and to create meaningful order: p-value, log2fold-change, peptide count difference, presence difference and abundance rank difference. The mean difference in abundance relative to the variance yield the p-value. The p-value tells us if the abundance differences between the control and the aptamer samples are significant therefore consistent or due to random chance. [141] The p-value is computed from the LFQ intensity for each protein.

Fold change is the ratio of changes between the final and original value, over the original value. The Log2-fold change parameter commonly used in the analysis of –omics data to measure the mean change in different conditions. Log2 fold-change was computed from the protein abundance for each protein. The mean number of identified peptides in the control samples were subtracted from the mean number of peptides identified in the target samples. This parameter was termed peptide count difference. The mean number of proteins identifications of each protein in triplicate was taken and the difference was calculated. This parameter was termed presence difference and describes how consistently a given protein was found. Lastly, proteins are ranked intra-experimentally by their intensity and divided by the total number of identified proteins. This

results in a relative abundance value with each protein assigned a value from 0 (absent) to 1 (most abundant). The mean control abundance rank is then subtracted from the target aptamer abundance rank and this parameter compares different proteins within an experiment. This parameter was termed abundance rank difference and describes the change of relative abundance of a protein.

The list of proteins was reduced to remove proteins that cannot (logically) be the aptamer binding partner. If a protein met one of the following criteria, it was removed from the list of potential targets: present in less than 50% of aptamer replicates, a negative calculated presence difference, a negative calculated abundance rank difference, a negative calculated log2 fold-change or a negative peptide difference. Simply put, a negative score for the aforementioned suggested that the protein was more abundance or enriched in the control sample or in the case of being present in less than 50% of the aptamer sample replicates, is not a strong enough candidate. Thus, proteins that meet these criteria are very unlikely to be the aptamer binding target. This simplifies the ranking of potential protein targets and increases sensitivity.

The volcano plots in **Figure 4.5** reinforce the importance of the careful consideration of all five parameters. In some cases, a p-value and/or a $\log_2$fold-change cannot be calculated due to insufficient information, or if the information renders incomputable (for instance, log of a negative number or a zero in the denominator). Nevertheless, interesting information can be extracted. The nucleolar protein Nucleolin (NCL) is found to be negatively enriched (p-value = 0.0001) in the aptamer sample relative to the control samples in method A. NCL inherently binds nucleic acids traditionally in eukaryotic cells[142] thus, this is an expected result. Similarly, method B identified ras-related nuclear protein (RAN) as negatively enriched (p-value > 0.05) in the aptamer sample relative to the control sample in method B. RAN is GTP binding protein responsible for the translocation of RNA and protein[143] therefore, using the same rationale this is also an expected result. Despite NCL and RAN having statistically significant p-values, they were rejected from the potential binding partner proteins because of their negative enrichment, further enforcing the importance of a strategic approach.

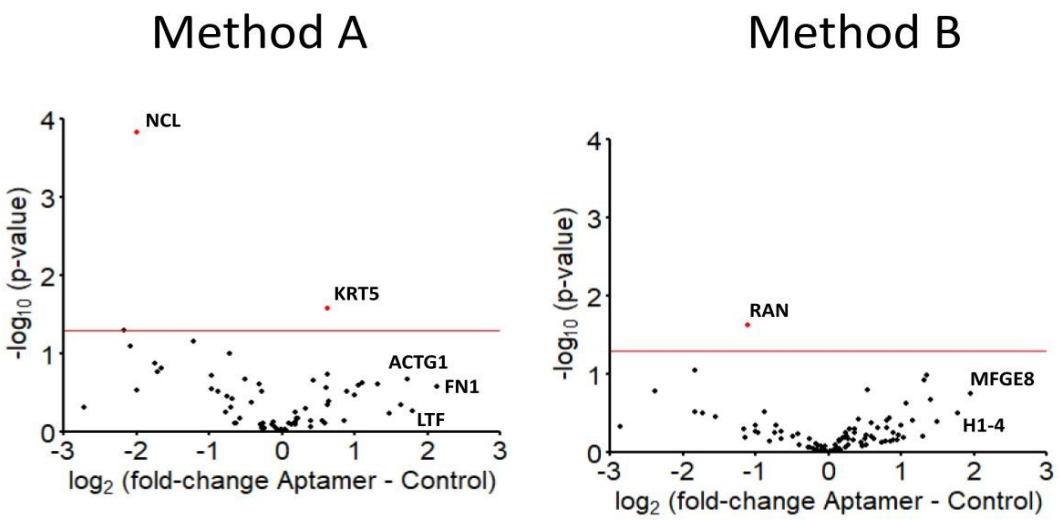

Figure 4.5. Method A vs. Method B: -log$_{10}$(p-value) against log$_2$fold-change. Method A identified 199 proteins, 68 proteins of which are qualified for the volcano plot. Method B identified 237 proteins, 101 qualified for the volcano plot. The red line indicated a p-value threshold of 0.05.

Additional information:
NCL= Nucleolin
RAS= Ras-related nuclear protein
ACTG1= Actin, cytoplasmic 2
FN1= Fibronectin 1
LTF= Lactotransferrin
MFGE8= Milk fat globule-EGF factor 8 protein (lactadherin)
H1-4= Histone H1.4
KRT5= Keratin 5

Some positively enriched identified proteins include Lactotransferrin (LTF), Milk fat globule-EGF factor 8 protein (MFGE8), Actin (ACTG1), Fibronectin 1 (FN1), Histone H1.4 (H1-4) and KRT5 (Keratin 5). LTF and MFGR8 are both breast cell specific proteins, where as ACTG1 and FN1 are serve a general housekeeping role. [144,145] In contrast, Kertain 5 (KRT5) is evidently a contaminant and Histone H1.4 (H1-4) is a DNA binding protein. Therefore, although the p-value and log2fold-change are commonly used parameters, they do not yield conclusive evidence alone. Thus, it is important to obtain a bigger picture by considering all five parameters in conjunction.

Prior to scoring proteins for their relative potential to be the binding target, the protein list is reduced by proteins that meet the criteria for evidently non-binding targets. The rationale for this approach is that proteins that were found more in abundant or enriched cannot and should not

be the potential aptamer binding target, therefore if they are removed, the list becomes simplified and the rank becomes more sensitive to each protein's individual score. All parameters should be considered during the reduction of the protein list, since as it was eluded to earlier, most proteins do not qualify for a score in every single parameter.

Figure 4.6 is a visual representation of the proteins that qualified for the scoring system. The assigned score for method A is shown on the X axis and the assigned score for method B is on the Y axis. The assigned score ranges from 0 to 1 and evenly accounts for all 5 parameters. It is possible that proteins that scored better in method A relative to method B may have been binding to the surface of EVs instead of intrinsically being a part of the EV membrane. This could be explained by method A involving 4 additional washing steps and therefore more readily washing away proteins that may be co-isolated with EVs. For instance, MFGE8 (Lactadherin) is a glycoprotein secreted into the extracellular matrix and binds phosphatidylserine enriched cell surface via a receptor dependent mechanism. We speculate that this protein was detected because it was bound to the surface of EVs, acknowledging that protein-protein interactions may play a role in the results we obtained.[146] Proteins that scored well in method 1 but low in method 2 perhaps were not able to retain good aptamer-protein affinity in the presence of the lysis buffer and thus experienced a disruption of interactions.

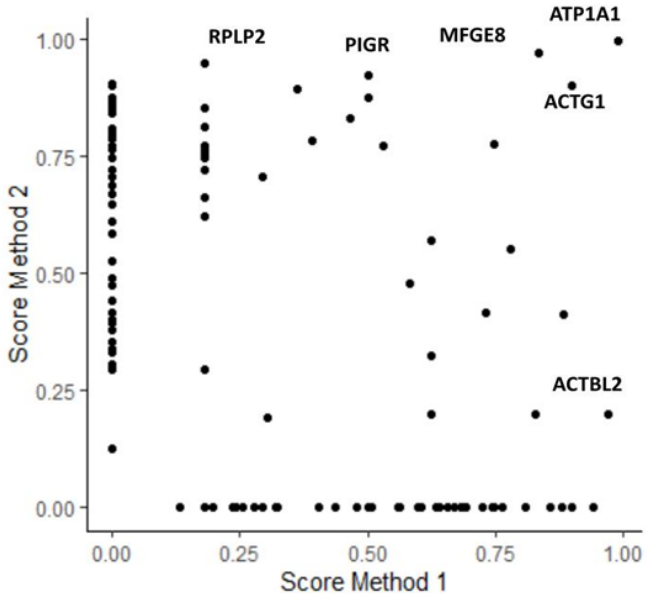

Figure 4.6. Protein Score: Method A vs. Method B. Protein score that is computed by five parameters: p-value, log2fold-change, peptide difference, presence difference and abundance rank difference**.** Score of proteins identified by method A are plotted against score of proteins identified in method B.

The mean score of method A and B is taken to make the finalized rank in determining which probable binding partner as summarized in **Table 4.2.**

Table 4.2 Top Scoring EV Protein Targets Obtained by Pull-Down

Protein Name	Gene	$\bar{x}$ Score	Functional Role
Sodium/potassium-transporting ATPase subunit alpha-1	ATP1A1	0.98	Osmotic regulation
Actin, cytoplasmic 2	ACTG1	0.89	Cell motility
Lactadherin	MFGE8	0.88	Angiogenesis, cell adhesion
Peroxiredoxin-1; Peroxiredoxin-2	PRDX1; PRDX2	0.78	Peroxidase activity
Polymeric immunoglobulin receptor; Secretory component	PIGR	0.72	Transport immune complexes
Elongation factor 1-gamma	EEF1G	0.70	-
Heat shock cognate 71 kDa protein	HSPA8	0.68	Molecular chaperone
L-lactate dehydrogenase B chain	LDHB	0.68	Carbohydrate metabolism
D-3-phosphoglycerate dehydrogenase	PHGDH	0.67	Catalyzes oxidation reaction
Cofilin-1; Cofilin-2	CFL1; CFL2	0.63	Regulates actin dynamics

It should be noted, however, that the nature of this study does not yield strong enough evidence to suggest that the after mentioned proteins are clinically relevant biomarkers. Instead, we aim to identify the protein with the highest chance of being the aptamer binding partner and assess for potential relationship to cancer. Sodium/potassium-transporting ATPase subunit alpha-1 (ATP1A1) was identified (**Figure 4.7**) chosen for further investigation.[147] It has been shown that the inhibition of ATP1A1 in intervertebral disc cells that resulted in a G2/M cell cycle block, triggering the cell to re-balance the osmolarity, ultimately having an anti-proliferative effect.[148] Furthermore, ATP1A1 has been reported to be upregulated on melanoma cells and furthermore proposed as a biomarker. [149]

Among the other top 9 proteins to likely be the aptamer binding target, elongation factor 1- gamma and lactadherin are particularly interesting for further investigation, since the others are not particularly relevant to cancer. Lactadherin has been shown to be highly expressed in breast cancer[150] promote tumour growth in a mouse model.[151] Further investigation could shed light on lactadherin's potential as a relevant breast cancer biomarker for more advanced and malignant breast cancer types. Elongation factor-1 gamma does not have a well-established role in the literature, however there is some evidence that it aids in the anchoring of other complexes.[152] Despite our lack in understanding of the functional role, mRNA transcript for elongation factor-1 gamma has been found over expressed in oreopharyngeal[153] pancreatic[154] and gastric[155] cancers, therefore we can speculate this proteins potential to serve as general cancer biomarker.

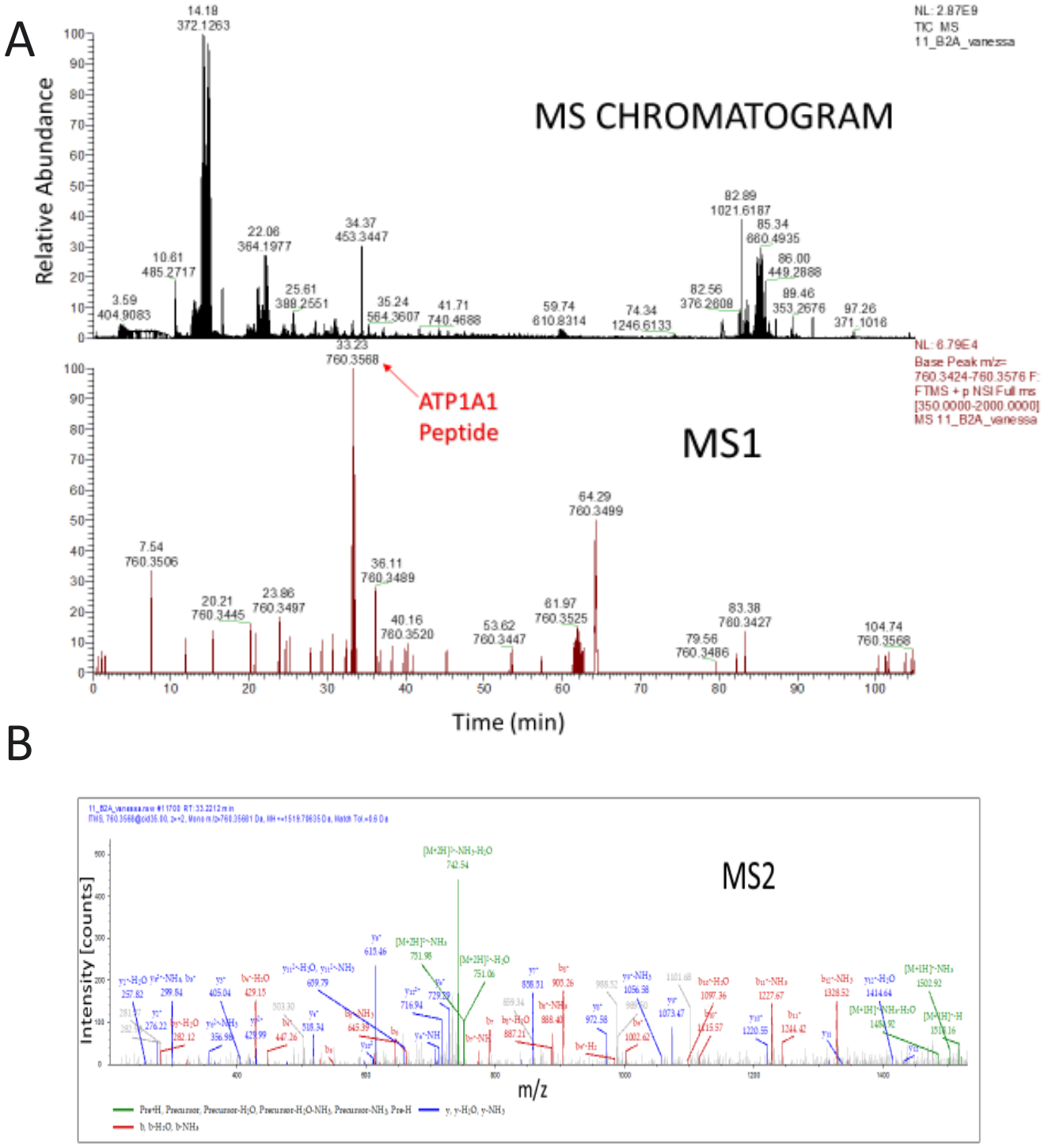

Figure 4.7. Chromatogram of aptamer-pull down sample by method B and fragmentation pattern of peptide of ATP1A1 protein with the best XCorr score identified by MS. (A) MS chromatogram and isolated precursor ion of monoisotopic peptide SPDFTNENPLETR, m/z = 760.35691 Da, MH+: 1519.70635 Da and rt: 33.22 min. (B) Fragmentation pattern of peptide: Identified with: Sequest HT (v1.17); XCorr:3.35.

VALIDATION OF ATP1A1 ON MDA-MB-231

Sodium/potassium-transporting ATPase subunit alpha-1 (ATP1A1) was chosen for further investigation. Five different concentrations of the ATP1A1 antibody were incubated with 100uL of isolated EVs from MDA-MB-231 cells. Separation index is commonly used to determine the appropriate concentration of antibody[139] for a new application. To the best of our knowledge, ATP1A1 has not been validated on EVs by flow cytometry, therefore determining the appropriate concentration of antibody is important to avoid false positive results. Separation index was calculated for each concentration by **Equation 4.5** and then plotted against the respective concentration.

$$Seperation\ Index = \frac{MedianSignal - MedianBackground}{84^{th}percentilemedianbackground - medianbackground)/0.995} \quad (4.5)$$

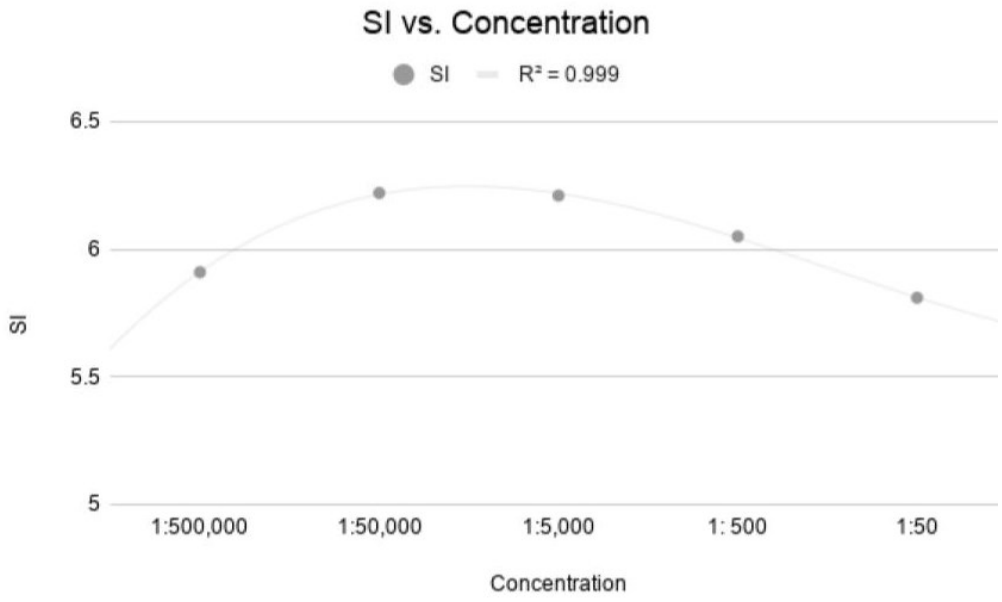

Figure 4.8. Titration of ATP1A1 antibody concentration for flow cytometry applications. 100uL of EVs were incubated with 5 different antibody concentrations for 20 minutes in the dark before running the samples on Beckman Coulter MoFlo Astrios EQ Cell Sorter. The data was analyzed Kaluza software. Separation index was calculated and plotted against varying concentrations. The maximum of the trendline was taken to be the optimal antibody concentration.

The optimal antibody concentration **(Figure 4.8)** was taken to be the maximum of the SI versus concentration curve. A 1:5000 dilution factor was used for the validation of the ATP1A1

protein on MDA-MB-231 EVs. When the optimal antibody concentration was added to a sample containing only EVs, (**Figure 4.9)** 93.91% of events were reported as negative for the antibody and the aptamer.

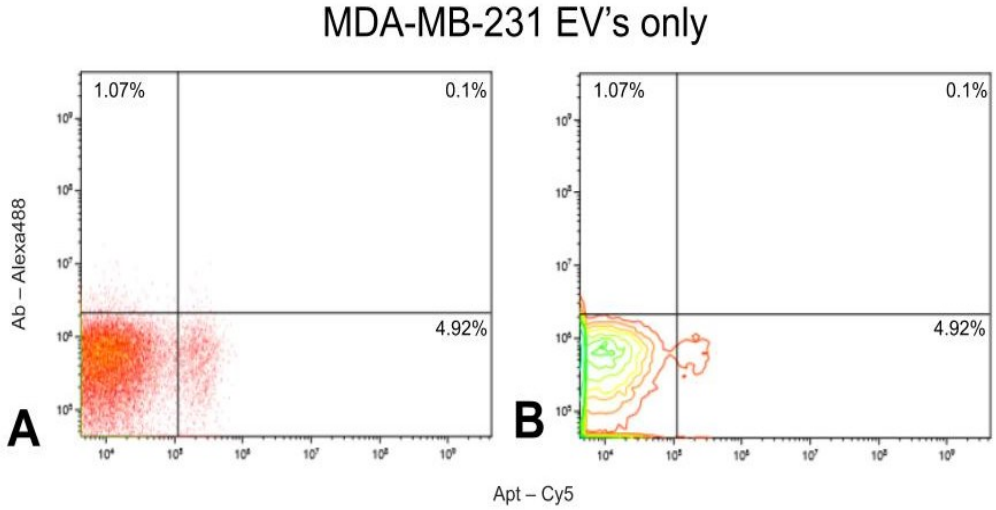

Figure 4.9. MDA-MB-231 EVs in PBS buffer shown as (A) density plot (B) contour plot. 100uL of EVs were isolated by density ultracentrifugation then resuspended in PBS. The data displays the events gated for singlets and non-aggregates.

After addition of VBS-1 aptamer, 45.05% of the events were detected as CY5 positive, demonstrating that most of the EVs are bound to the VBS-1 aptamer as shown in **Figure 4.10.**

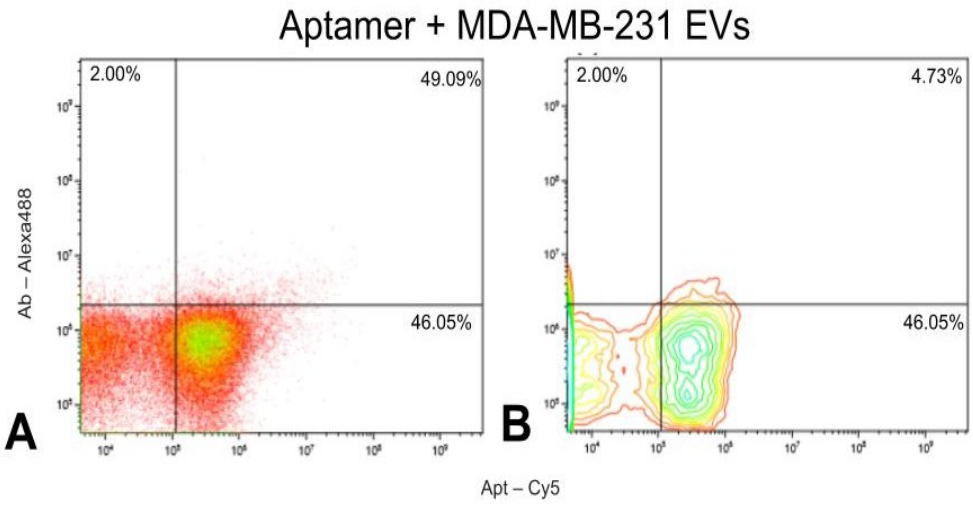

Figure 4.10. MDA-MB-231 EVs in PBS buffer with 1uM of VBS-1 aptamer shown as (A) density plot (B) contour plot. 100uL of EVs were isolated by density ultracentrifugation then resuspended in PBS. M1 aptamer was heated to 95°C (5 min) then cooled to 4°C (10 min) in PBS + Ca^{2+}/Mg^{2+} buffer. VBS-1 aptamer was added to EVs to give a final concentration of 1uM. EVs and aptamer was incubated at room temperature on a shaking plate for 30 min. The data displays the events gated for singlets and non-aggregates.

Moreover, after addition of ATP1A1 antibody, 49.09% of the events were detected as both CY5 positive and ATP1A1 positive, demonstrating that most of the EVs bound to the VBS-1 aptamer also bind to the ATP1A1 antibody as shown in **Figure 4.11.** This validates the presence of the ATP1A1 protein on MDA-MB-231 EVs.

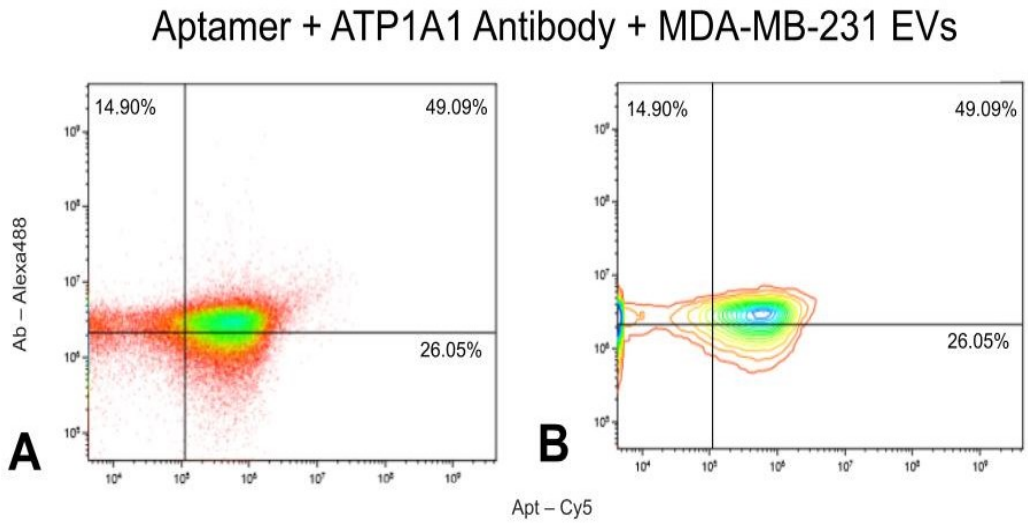

Figure 4.11. MDA-MB-231 EVs in PBS buffer with 1uM of VBS-1 aptamer and ATP1A1 Antibody shown as (A) density plot (B) contour plot. 100uL of EVs were isolated by density ultracentrifugation then resuspended in PBS. VBS-1 aptamer was heated to 95°C (5 min) then cooled to 4°C (10 min) in PBS + Ca^{2+}/Mg^{2+} buffer. VBS-1 aptamer was added to EVs to give a final concentration of 1uM. EVs and aptamer was incubated at room temperature on a shaking plate for 30 min. The data displays the events gated for singlets and non-aggregates.

The sodium/potassium-ATPase (Na+/K+-ATPase) is ubiquitously expressed transmembrane complex that facilitates the movement of 3 Na+ and 2 K+ ions down their electrochemical gradient, at the expense of hydrolysis of one ATP molecule. The oligomer is composed of α, β and γ subunits. The α subunit contains the binding site for ATP and cations; the β subunit assists in folding in positioning the α subunits within the membrane; and the γ subunit is non-essential to the function of the protein, it increases the affinity of the complex to ATP when present.[156] The α subunit was identified in the aptamer-based pull-down experiment. Protter (open source) was used to highlight the specific amino acids sequences involved in the binding of the aptamer and compared to the antibody to the ATP1A1 protein (UniProt accession: P05023). **Figure 4.12** shows amino acids highlighted in red are the peptide sequences identified by MS, whereas amino acids highlighted in blue show the epitope for the ATP1A1 antibody. It is

interesting to note the orientation of the protein relative to the binding regions of the aptamer and antibody – it seems as though the aptamer binds intracellularly if we were examining the protein as it would appear on a cell surface. However, the orientation of the protein on EVs is unconfirmed, it is possible that the transmembrane protein is flipped "inside-out" relative to how it would appear on cells. It would also be interesting to determine if the protein retains its function as we know it on EVs. To draw relevant conclusions on the functionality and orientation of Na+/K+-ATPase, additional studies should be carried out.

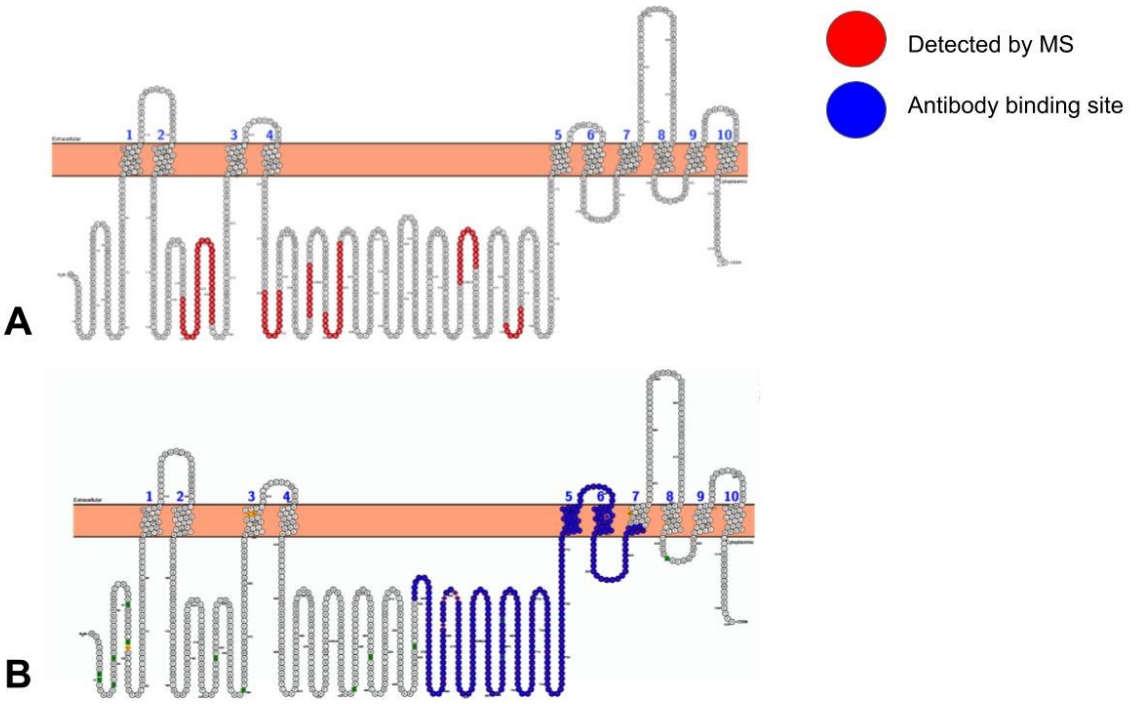

Figure 4.12. The sodium/potassium-ATPase α subunit: peptides identified by MS compared to immunogenic peptide. Amino acids detected by MS are shown in red. Amino acids bind to the ATP1A1 antibody are shown in blue.

4.5 Conclusion

An aptamer-target protein experiment was conducted using two slightly different approaches. Method A involved incubation of the aptamer plus intact EVs, whereas method be involved incubation of aptamer plus lysed EVs. In both cases, proteins were identified by LC-MC/MS. A ranking system was strategically designed by assigning equal weight to five relevant parameters: p-value, log2-fold change, peptide difference, presence difference and abundance rank difference. The list of potential aptamer-protein targets was reduced to increase the sensitivity of ranking order. The remaining proteins were ranked by the average of the best three scoring parameters, and the average score of the two methods were calculated. ATP1A1 returned a score of 0.97, the average highest score of both methods and therefore was chosen for validation by flow cytometry. Flow cytometry revealed most of the EVs bound to VBS-1 aptamer (48%), also displayed detected fluorescence for the ATP1A1 antibody (49%). We can conclude that the proposed method of aptamer-based pull-down method on EVs was successful. Further studies are needed to understand the function of ATP1A1 and draw further conclusions on the clinical significance of the target protein.

4.6 Acknowledgments

I would like to wholeheartedly acknowledge Nico Hüttmann for is indispensable role in this final portion of the project. He assisted in the experimental design, preparation of the samples and analysis of the data obtained. Thank you for taking time out of your day to answer all my naïve questions and being patient whilst I learned. I sincerely appreciate your hard work and dedication to this project, and for treating it like your own from the very beginning. I could not have achieved this part of the thesis without you. I would also like to acknowledge Dr. Zoran Minic for running the samples on MS, for running the facility in a diligent and goal-oriented manner, and for being a wonderful mentor to our group.

5. LIMITATIONS

TECHNICAL

There are fundamental challenges that come along with studying a nanosized particle of biological origin. There is no EV isolation method to date that can produce a pure EV sample, nor a validation technique that can confidently validate all subgroups of EVs. Here, it is assumed that the isolation protocol yields intact EVs and that the selection occurred directed to them and not to any co-precipitated biomolecules. Furthermore, reproducibility of EV flow cytometry data between research groups has been subpar, even with high resolution instruments.[157]

EVS

There are no known EV specific markers, therefore there may be other vesicles or aggregates in the samples that we are not accounting for, since traditional DC methods have been shown to co-precipitate proteins, lipoproteins, and other contaminants.[158] Additionally, the use of EV-depleted FBS likely causes cell stress and may alter the EV profile in a manner that is not well understood. Lastly, our understanding of the biological role of ATP1A1 on EVs is not well understood which limits the conclusions that may be drawn.

CANCER

Cancer is a complex disease that is technically composed of an infinite number of subtypes. Here, aptamers were only selected to one of these subtypes (triple-negative breast cancer), the MDA-MB-231 cell line as model system. Furthermore, the true breast cancer subtypes likely extend beyond our current knowledge and understanding of the disease pathology. It is possible that the aptamer also binds to EVs from other breast cancer subtypes or EVs from an entirely different origin.

APTAMERS AND SELECTION

A rudimentary limitation of aptamer is their tendency bind biomolecules in a nonspecific fashion, driven by their charge. It is a challenge to understand the exact influence this may have on the selection outcome. Furthermore, a negative or counter selection step was not incorporated into the selection strategy used due technical challenges. Finally, all aptamer binding assays were done by flow cytometry, including an alternative method to test aptamer binding would support the choice of promising aptamer candidate for further investigation.

6. FUTURE DIRECTIONS

The potential of the VBS-1 aptamer as a probe for cancer detection from clinical samples will be further investigated in the following manner. Firstly, the affinity of the aptamer to the identified protein target will be determined. Then, the aptamer could be modified to increase biological and structural stability and further enhance its binding affinity. Finally, the utility of the aptamer for its clinical potential will be evaluated.

APTAMER CHARACTERIZATION

Determining the affinity of an aptamer to its target is important for understanding its potential for downstream applications. Further characterization of the VBS aptamer will include K_D determination of the aptamer to the ATP1A1 recombinant protein and in the biological context of EVs.

APTAMER MODIFICATION

It is of high interest to further improve the binding affinity of an aptamer after its selection as well as to increase the biological and chemical stability for its use in biofluids.[159] A common strategy is the truncation of sequence regions non-essential for the binding to its target. Reduction of aptamer length contributes to better stability and a more economical synthesis. Another strategy to increase aptamer stability is chemical modification, like 3' capping, modification of the phosphodiester backbone or the sugar ring. Furthermore, improvement of the aptamer binding affinity may be achieved through nucleobase chemical modification.[160]

TRANSLATION TO CLINICAL DIAGNOSIS

VBS-1 aptamer will be tested on EVs isolated from patient blood samples to differentiate between those with and without triple-negative breast cancer. The developed aptamer can also be used to isolate ATP1A1 positive EV subpopulations in lieu or in combination with antibody-based methods. Additionally, the potential of ATP1A1 using the VBS-1 aptamer or alternative approach for its diagnostic potential could be examined in a "preclinical exploratory study". From there, a potential biomarker would need to pass 4 additional phases of clinical development.[161] A potential therapeutic application may be investigated if the binding of the aptamer to ATP1A1 blocks its function, however a better understanding of the biological significance is required.

Cancer EVs can be isolated from other biofluids such as saliva and urine to detect oropharyngeal or bladder cancer, respectively.[162,163] Successful translation of the EV-SELEX procedure following the rationale of AptaBiD motivates the application of the same experimental approaches to more diseases that can be detected by EVs in biofluids.

7. REFERENCES

(1) World Health Organization. *Ten threats to global health in 2019*, 2019.

(2) Petrelli, N. J.; Winer, E. P.; Brahmer, J.; Dubey, S.; Smith, S.; Thomas, C.; Vahdat, L. T.; Obel, J.; Vogelzang, N.; Markman, M.*; et al.* Clinical Cancer Advances 2009: major research advances in cancer treatment, prevention, and screening--a report from the American Society of Clinical Oncology. *Journal of clinical oncology : official journal of the American Society of Clinical Oncology* **2009**, *27*, 6052–6069.

(3) Hawkes, N. Cancer survival data emphasise importance of early diagnosis. *BMJ (Clinical research ed.)* **2019**, *364*, l408.

(4) World Health Organization. *Early cancer diagnosis saves lives, cuts treatment costs.*, 2017.

(5) Zhang, X.; Yuan, X.; Shi, H.; Wu, L.; Qian, H.; Xu, W. Exosomes in cancer: small particle, big player. *Journal of hematology & oncology* **2015**, *8*, 83.

(6) Simons, M.; Raposo, G. Exosomes--vesicular carriers for intercellular communication. *Current opinion in cell biology* **2009**, *21*, 575–581.

(7) Halvaei, S.; Daryani, S.; Eslami-S, Z.; Samadi, T.; Jafarbeik-Iravani, N.; Bakhshayesh, T. O.; Majidzadeh-A, K.; Esmaeili, R. Exosomes in Cancer Liquid Biopsy: A Focus on Breast Cancer. *Molecular Therapy. Nucleic Acids* **2018**, *10*, 131–141.

(8) Hanahan, D.; Weinberg, R. A. Hallmarks of cancer: the next generation. *Cell* **2011**, *144*, 646–674.

(9) Pitot, H. C. The molecular biology of carcinogenesis. *Cancer* **1993**, *72*, 962–970.

(10) Hanahan, D.; Weinberg, R. A. The Hallmarks of Cancer. *Cell* **2000**, *100*, 57–70.

(11) He, Z.; Yu, W. Stable feature selection for biomarker discovery. *Computational biology and chemistry* **2010**, *34*, 215–225.

(12) Strimbu, K.; Tavel, J. A. What are biomarkers? *Current opinion in HIV and AIDS* **2010**, *5*, 463–466.

(13) Hicks, C.; Asfour, R.; Pannuti, A.; Miele, L. An integrative genomics approach to biomarker discovery in breast cancer. *Cancer Informatics* **2011**, *10*, 185–204.

(14) Jin, C.; Qiu, L.; Li, J.; Fu, T.; Zhang, X.; Tan, W. Cancer biomarker discovery using DNA aptamers. *The Analyst* **2016**, *141*, 461–466.

(15) Salih, M.; Zietse, R.; Hoorn, E. J. Urinary extracellular vesicles and the kidney: biomarkers and beyond. *American journal of physiology. Renal physiology* **2014**, *306*, F1251-9.

(16) Harding, C.; Heuser, J.; Stahl, P. Receptor-mediated endocytosis of transferrin and recycling of the transferrin receptor in rat reticulocytes. *The Journal of Cell Biology* **1983**, *97*, 329–339.

(17) Pan, B.-T.; Johnstone, R. M. Fate of the transferrin receptor during maturation of sheep reticulocytes in vitro: Selective externalization of the receptor. *Cell* **1983**, *33*, 967–978.

(18) H Rashed, M.; Bayraktar, E.; K Helal, G.; Abd-Ellah, M. F.; Amero, P.; Chavez-Reyes, A.; Rodriguez-Aguayo, C. Exosomes: From Garbage Bins to Promising Therapeutic Targets. *International journal of molecular sciences* **2017**, *18*.

(19) Raposo, G.; Nijman, H. W.; Stoorvogel, W.; Liejendekker, R.; Harding, C. V.; Melief, C. J.; Geuze, H. J. B lymphocytes secrete antigen-presenting vesicles. *The Journal of Experimental Medicine* **1996**, *183*, 1161–1172.

(20) Admyre, C.; Johansson, S. M.; Qazi, K. R.; Filén, J.-J.; Lahesmaa, R.; Norman, M.; Neve, E. P. A.; Scheynius, A.; Gabrielsson, S. Exosomes with immune modulatory features are present in human breast milk. *Journal of immunology (Baltimore, Md. : 1950)* **2007**, *179*, 1969–1978.

(21) Gu, Y.; Li, M.; Wang, T.; Liang, Y.; Zhong, Z.; Wang, X.; Zhou, Q.; Chen, L.; Lang, Q.; He, Z.*; et al.* Lactation-related microRNA expression profiles of porcine breast milk exosomes. *PloS one* **2012**, *7*, e43691.

(22) Simhadri, V. R.; Reiners, K. S.; Hansen, H. P.; Topolar, D.; Simhadri, V. L.; Nohroudi, K.; Kufer, T. A.; Engert, A.; Pogge von Strandmann, E. Dendritic cells release HLA-B-associated transcript-3 positive exosomes to regulate natural killer function. *PloS one* **2008**, *3*, e3377.

(23) Margolis, L.; Sadovsky, Y. The biology of extracellular vesicles: The known unknowns. *PLoS biology* **2019**, *17*, e3000363.

(24) van Niel, G.; D'Angelo, G.; Raposo, G. Shedding light on the cell biology of extracellular vesicles. *Nature reviews. Molecular cell biology* **2018**, *19*, 213–228.

(25) Stahl, P. D.; Raposo, G. Extracellular Vesicles: Exosomes and Microvesicles, Integrators of Homeostasis. *Physiology (Bethesda, Md.)* **2019**, *34*, 169–177.

(26) Lötvall, J.; Hill, A. F.; Hochberg, F.; Buzás, E. I.; Di Vizio, D.; Gardiner, C.; Gho, Y. S.; Kurochkin, I. V.; Mathivanan, S.; Quesenberry, P.*; et al.* Minimal experimental requirements for definition of extracellular vesicles and their functions: a position statement from the International Society for Extracellular Vesicles. *Journal of Extracellular Vesicles* **2014**, *3*, 26913.

(27) Théry, C.; Witwer, K. W.; Aikawa, E.; Alcaraz, M. J.; Anderson, J. D.; Andriantsitohaina, R.; Antoniou, A.; Arab, T.; Archer, F.; Atkin-Smith, G. K.*; et al.* Minimal information for studies of extracellular vesicles 2018 (MISEV2018): a position statement of the International Society for Extracellular Vesicles and update of the MISEV2014 guidelines. *Journal of Extracellular Vesicles* **2018**, *7*, 1535750.

(28) Colombo, M.; Moita, C.; van Niel, G.; Kowal, J.; Vigneron, J.; Benaroch, P.; Manel, N.; Moita, L. F.; Théry, C.; Raposo, G. Analysis of ESCRT functions in exosome biogenesis, composition and secretion highlights the heterogeneity of extracellular vesicles. *Journal of cell science* **2013**, *126*, 5553–5565.

(29) Johnstone, R. M.; Adam, M.; Hammond, J. R.; Orr, L.; Turbide, C. Vesicle formation during reticulocyte maturation. Association of plasma membrane activities with released vesicles (exosomes). *The Journal of biological chemistry* **1987**, *262*, 9412–9420.

(30) Pasquet, J. M.; Dachary-Prigent, J.; Nurden, A. T. Calcium influx is a determining factor of calpain activation and microparticle formation in platelets. *European journal of biochemistry* **1996**, *239*, 647–654.

(31) Ihara, T.; Yamamoto, T.; Sugamata, M.; Okumura, H.; Ueno, Y. The process of ultrastructural changes from nuclei to apoptotic body. *Virchows Archiv : an international journal of pathology* **1998**, *433*, 443–447.

(32) Hessvik, N. P.; Llorente, A. Current knowledge on exosome biogenesis and release. *Cellular and Molecular Life Sciences* **2018**, *75*, 193–208.

(33) Ståhl, A.-L.; Johansson, K.; Mossberg, M.; Kahn, R.; Karpman, D. Exosomes and microvesicles in normal physiology, pathophysiology, and renal diseases. *Pediatric nephrology (Berlin, Germany)* **2019**, *34*, 11–30.

(34) Minciacchi, V. R.; Freeman, M. R.; Di Vizio, D. Extracellular vesicles in cancer: exosomes, microvesicles and the emerging role of large oncosomes. *Seminars in cell & developmental biology* **2015**, *40*, 41–51.

(35) Skog, J.; Würdinger, T.; van Rijn, S.; Meijer, D. H.; Gainche, L.; Sena-Esteves, M.; Curry, W. T.; Carter, B. S.; Krichevsky, A. M.; Breakefield, X. O. Glioblastoma microvesicles transport RNA and proteins that promote tumour growth and provide diagnostic biomarkers. *Nature cell biology* **2008**, *10*, 1470–1476.

(36) Webber, J. P.; Spary, L. K.; Sanders, A. J.; Chowdhury, R.; Jiang, W. G.; Steadman, R.; Wymant, J.; Jones, A. T.; Kynaston, H.; Mason, M. D.*; et al.* Differentiation of tumour-promoting stromal myofibroblasts by cancer exosomes. *Oncogene* **2015**, *34*, 290–302.
(37) Webber, J.; Steadman, R.; Mason, M. D.; Tabi, Z.; Clayton, A. Cancer exosomes trigger fibroblast to myofibroblast differentiation. *Cancer research* **2010**, *70*, 9621–9630.
(38) Lee, T. H.; Chennakrishnaiah, S.; Audemard, E.; Montermini, L.; Meehan, B.; Rak, J. Oncogenic ras-driven cancer cell vesiculation leads to emission of double-stranded DNA capable of interacting with target cells. *Biochemical and biophysical research communications* **2014**, *451*, 295–301.
(39) Syn, N. L.; Wang, L.; Chow, E. K.-H.; Lim, C. T.; Goh, B.-C. Exosomes in Cancer Nanomedicine and Immunotherapy: Prospects and Challenges. *Trends in biotechnology* **2017**, *35*, 665–676.
(40) Zomer, A.; van Rheenen, J. Implications of Extracellular Vesicle Transfer on Cellular Heterogeneity in Cancer: What Are the Potential Clinical Ramifications? *Cancer research* **2016**, *76*, 2071–2075.
(41) Simpson, R. J.; Lim, J. W.; Moritz, R. L.; Mathivanan, S. Exosomes: proteomic insights and diagnostic potential. *Expert review of proteomics* **2009**, *6*, 267–283.
(42) Taylor, D. D.; Gercel-Taylor, C. MicroRNA signatures of tumor-derived exosomes as diagnostic biomarkers of ovarian cancer. *Gynecologic oncology* **2008**, *110*, 13–21.
(43) Gallo, A.; Tandon, M.; Alevizos, I.; Illei, G. G. The majority of microRNAs detectable in serum and saliva is concentrated in exosomes. *PloS one* **2012**, *7*, e30679.
(44) Ruhen, O.; Meehan, K. Tumor-Derived Extracellular Vesicles as a Novel Source of Protein Biomarkers for Cancer Diagnosis and Monitoring. *Proteomics* **2019**, *19*, e1800155.
(45) Lane, R. E.; Korbie, D.; Hill, M. M.; Trau, M. Extracellular vesicles as circulating cancer biomarkers: opportunities and challenges. *Clinical and translational medicine* **2018**, *7*, 14.
(46) Rabinowits, G.; Gerçel-Taylor, C.; Day, J. M.; Taylor, D. D.; Kloecker, G. H. Exosomal microRNA: a diagnostic marker for lung cancer. *Clinical lung cancer* **2009**, *10*, 42–46.
(47) Soldevilla, B.; Rodríguez, M.; San Millán, C.; García, V.; Fernández-Periañez, R.; Gil-Calderón, B.; Martín, P.; García-Grande, A.; Silva, J.; Bonilla, F.*; et al.* Tumor-derived exosomes are enriched in ΔNp73, which promotes oncogenic potential in acceptor cells and correlates with patient survival. *Human molecular genetics* **2014**, *23*, 467–478.

(48) Kogure, T.; Yan, I. K.; Lin, W.-L.; Patel, T. Extracellular Vesicle-Mediated Transfer of a Novel Long Noncoding RNA TUC339: A Mechanism of Intercellular Signaling in Human Hepatocellular Cancer. *Genes & cancer* **2013**, *4*, 261–272.

(49) Chen, I.-H.; Xue, L.; Hsu, C.-C.; Paez, J. S. P.; Pan, L.; Andaluz, H.; Wendt, M. K.; Iliuk, A. B.; Zhu, J.-K.; Tao, W. A. Phosphoproteins in extracellular vesicles as candidate markers for breast cancer. *Proceedings of the National Academy of Sciences of the United States of America* **2017**, *114*, 3175–3180.

(50) Vykoukal, J.; Sun, N.; Aguilar-Bonavides, C.; Katayama, H.; Tanaka, I.; Fahrmann, J. F.; Capello, M.; Fujimoto, J.; Aguilar, M.; Wistuba, I. I.*; et al.* Plasma-derived extracellular vesicle proteins as a source of biomarkers for lung adenocarcinoma. *Oncotarget* **2017**, *8*, 95466–95480.

(51) Li, A.; Zhang, T.; Zheng, M.; Liu, Y.; Chen, Z. Exosomal proteins as potential markers of tumor diagnosis. *Journal of hematology & oncology* **2017**, *10*, 175.

(52) Atay, S.; Wilkey, D. W.; Milhem, M.; Merchant, M.; Godwin, A. K. Insights into the Proteome of Gastrointestinal Stromal Tumors-Derived Exosomes Reveals New Potential Diagnostic Biomarkers. *Mol Cell Proteomics* **2018**, *17*, 495–515.

(53) Sun, Y.; Huo, C.; Qiao, Z.; Shang, Z.; Uzzaman, A.; Liu, S.; Jiang, X.; Fan, L.-Y.; Ji, L.; Guan, X.*; et al.* Comparative Proteomic Analysis of Exosomes and Microvesicles in Human Saliva for Lung Cancer. *Journal of proteome research* **2018**, *17*, 1101–1107.

(54) Smalley, D. M.; Sheman, N. E.; Nelson, K.; Theodorescu, D. Isolation and identification of potential urinary microparticle biomarkers of bladder cancer. *Journal of proteome research* **2008**, *7*, 2088–2096.

(55) Raimondo, F.; Morosi, L.; Corbetta, S.; Chinello, C.; Brambilla, P.; Della Mina, P.; Villa, A.; Albo, G.; Battaglia, C.; Bosari, S.*; et al.* Differential protein profiling of renal cell carcinoma urinary exosomes. *Molecular bioSystems* **2013**, *9*, 1220–1233.

(56) Principe, S.; Jones, E. E.; Kim, Y.; Sinha, A.; Nyalwidhe, J. O.; Brooks, J.; Semmes, O. J.; Troyer, D. A.; Lance, R. S.; Kislinger, T.*; et al.* In-depth proteomic analyses of exosomes isolated from expressed prostatic secretions in urine. *Proteomics* **2013**, *13*, 1667–1671.

(57) Øverbye, A.; Skotland, T.; Koehler, C. J.; Thiede, B.; Seierstad, T.; Berge, V.; Sandvig, K.; Llorente, A. Identification of prostate cancer biomarkers in urinary exosomes. *Oncotarget* **2015**, *6*, 30357–30376.

(58) Sequeiros, T.; Rigau, M.; Chiva, C.; Montes, M.; Garcia-Grau, I.; Garcia, M.; Diaz, S.; Celma, A.; Bijnsdorp, I.; Campos, A.*; et al.* Targeted proteomics in urinary extracellular vesicles identifies biomarkers for diagnosis and prognosis of prostate cancer. *Oncotarget* **2017**, *8*, 4960–4976.

(59) Choi, D.-S.; Park, J. O.; Jang, S. C.; Yoon, Y. J.; Jung, J. W.; Choi, D.-Y.; Kim, J.-W.; Kang, J. S.; Park, J.; Hwang, D.*; et al.* Proteomic analysis of microvesicles derived from human colorectal cancer ascites. *Proteomics* **2011**, *11*, 2745–2751.

(60) Shender, V. O.; Pavlyukov, M. S.; Ziganshin, R. H.; Arapidi, G. P.; Kovalchuk, S. I.; Anikanov, N. A.; Altukhov, I. A.; Alexeev, D. G.; Butenko, I. O.; Shavarda, A. L.*; et al.* Proteome-metabolome profiling of ovarian cancer ascites reveals novel components involved in intercellular communication. *Mol Cell Proteomics* **2014**, *13*, 3558–3571.

(61) Wang, L.; Duan, W.; Yan, S.; Xie, Y.; Wang, C. Circulating long non-coding RNA colon cancer-associated transcript 2 protected by exosome as a potential biomarker for colorectal cancer. *Biomedicine & pharmacotherapy = Biomedecine & pharmacotherapie* **2019**, *113*, 108758.

(62) Moon, P.-G.; Lee, J.-E.; Cho, Y.-E.; Lee, S. J.; Jung, J. H.; Chae, Y. S.; Bae, H.-I.; Kim, Y.-B.; Kim, I.-S.; Park, H. Y.*; et al.* Identification of Developmental Endothelial Locus-1 on Circulating Extracellular Vesicles as a Novel Biomarker for Early Breast Cancer Detection. *Clinical cancer research : an official journal of the American Association for Cancer Research* **2016**, *22*, 1757–1766.

(63) Cufaro, M. C.; Pieragostino, D.; Lanuti, P.; Rossi, C.; Cicalini, I.; Federici, L.; Laurenzi, V. de; Del Boccio, P. Extracellular Vesicles and Their Potential Use in Monitoring Cancer Progression and Therapy: The Contribution of Proteomics. *Journal of oncology* **2019**, *2019*, 1639854.

(64) Rupp, A.-K.; Rupp, C.; Keller, S.; Brase, J. C.; Ehehalt, R.; Fogel, M.; Moldenhauer, G.; Marmé, F.; Sültmann, H.; Altevogt, P. Loss of EpCAM expression in breast cancer derived serum exosomes: role of proteolytic cleavage. *Gynecologic oncology* **2011**, *122*, 437–446.

(65) Moon, P.-G.; Lee, J.-E.; Cho, Y.-E.; Lee, S. J.; Chae, Y. S.; Jung, J. H.; Kim, I.-S.; Park, H. Y.; Baek, M.-C. Fibronectin on circulating extracellular vesicles as a liquid biopsy to detect breast cancer. *Oncotarget* **2016**, *7*, 40189–40199.

(66) Melo, S. A.; Luecke, L. B.; Kahlert, C.; Fernandez, A. F.; Gammon, S. T.; Kaye, J.; LeBleu, V. S.; Mittendorf, E. A.; Weitz, J.; Rahbari, N.*; et al.* Glypican-1 identifies cancer exosomes and detects early pancreatic cancer. *Nature* **2015**, *523*, 177–182.

(67) Hornick, N. I.; Huan, J.; Doron, B.; Goloviznina, N. A.; Lapidus, J.; Chang, B. H.; Kurre, P. Serum Exosome MicroRNA as a Minimally-Invasive Early Biomarker of AML. *Scientific Reports* **2015**, *5*, 11295.

(68) Verma, M.; Lam, T. K.; Hebert, E.; Divi, R. L. Extracellular vesicles: potential applications in cancer diagnosis, prognosis, and epidemiology. *BMC clinical pathology* **2015**, *15*, 6.

(69) McKiernan, J.; Donovan, M. J.; Margolis, E.; Partin, A.; Carter, B.; Brown, G.; Torkler, P.; Noerholm, M.; Skog, J.; Shore, N.*; et al.* A Prospective Adaptive Utility Trial to Validate Performance of a Novel Urine Exosome Gene Expression Assay to Predict High-grade Prostate Cancer in Patients with Prostate-specific Antigen 2-10ng/ml at Initial Biopsy. *European urology* **2018**, *74*, 731–738.

(70) Sullenger, B. A.; Gallardo, H. F.; Ungers, G. E.; Gilboa, E. Analysis of trans-acting response decoy RNA-mediated inhibition of human immunodeficiency virus type 1 transactivation. *Journal of Virology* **1991**, *65*, 6811–6816.

(71) Zhang, Y.; Lai, B. S.; Juhas, M. Recent Advances in Aptamer Discovery and Applications. *Molecules* **2019**, *24*.

(72) Prabhakar, P. S.; Sharma, P.; Mitra, A. *Pairing interactions between nucleobases and ligands in aptamer:ligand complexes of riboswitches: Crystal structure analysis, classification, optimal structures and accurate interaction energies*, 2019.

(73) Tuerk, C.; Gold, L. Systematic evolution of ligands by exponential enrichment: RNA ligands to bacteriophage T4 DNA polymerase. *Science (New York, N.Y.)* **1990**, *249*, 505–510.

(74) Raddatz, M.-S. L.; Dolf, A.; Endl, E.; Knolle, P.; Famulok, M.; Mayer, G. Enrichment of cell-targeting and population-specific aptamers by fluorescence-activated cell sorting. *Angewandte Chemie (International ed. in English)* **2008**, *47*, 5190–5193.

(75) Rahimizadeh, K.; AlShamaileh, H.; Fratini, M.; Chakravarthy, M.; Stephen, M.; Shigdar, S.; Veedu, R. N. Development of Cell-Specific Aptamers: Recent Advances and Insight into the Selection Procedures. *Molecules (Basel, Switzerland)* **2017**, *22*.

(76) Lauridsen, L. H.; Doessing, H. B.; Long, K. S.; Nielsen, A. T. A Capture-SELEX Strategy for Multiplexed Selection of RNA Aptamers Against Small Molecules. *Methods in molecular biology (Clifton, N.J.)* **2018**, *1671*, 291–306.

(77) Zykovich, A.; Korf, I.; Segal, D. J. Bind-n-Seq: high-throughput analysis of in vitro protein-DNA interactions using massively parallel sequencing. *Nucleic Acids Research* **2009**, *37*, e151.

(78) Berezovski, M.; Musheev, M.; Drabovich, A.; Krylov, S. N. Non-SELEX selection of aptamers. *Journal of the American Chemical Society* **2006**, *128*, 1410–1411.

(79) Xu, H.; Liao, C.; Zuo, P.; Liu, Z.; Ye, B.-C. Magnetic-Based Microfluidic Device for On-Chip Isolation and Detection of Tumor-Derived Exosomes. *Analytical chemistry* **2018**, *90*, 13451–13458.

(80) Jin, D.; Yang, F.; Zhang, Y.; Liu, L.; Zhou, Y.; Wang, F.; Zhang, G.-J. ExoAPP: Exosome-Oriented, Aptamer Nanoprobe-Enabled Surface Proteins Profiling and Detection. *Analytical chemistry* **2018**, *90*, 14402–14411.

(81) Zhao, L.; Huang, Y.; Dong, Y.; Han, X.; Wang, S.; Liang, X. Aptamers and Aptasensors for Highly Specific Recognition and Sensitive Detection of Marine Biotoxins: Recent Advances and Perspectives. *Toxins* **2018**, *10*.

(82) Gobbo, J.; Marcion, G.; Cordonnier, M.; Dias, A. M. M.; Pernet, N.; Hammann, A.; Richaud, S.; Mjahed, H.; Isambert, N.; Clausse, V.*; et al.* Restoring Anticancer Immune Response by Targeting Tumor-Derived Exosomes With a HSP70 Peptide Aptamer. *Journal of the National Cancer Institute* **2016**, *108*.

(83) Rérole, A.-L.; Gobbo, J.; Thonel, A. de; Schmitt, E.; Pais de Barros, J. P.; Hammann, A.; Lanneau, D.; Fourmaux, E.; Demidov, O. N.; Deminov, O.*; et al.* Peptides and aptamers targeting HSP70: a novel approach for anticancer chemotherapy. *Cancer research* **2011**, *71*, 484–495.

(84) Berezovski, M. V.; Lechmann, M.; Musheev, M. U.; Mak, T. W.; Krylov, S. N. Aptamer-facilitated biomarker discovery (AptaBiD). *Journal of the American Chemical Society* **2008**, *130*, 9137–9143.

(85) Wilson, I. D.; Adlard, E. R.; Cooke, M.; Poole, C. F. *Encyclopedia of separation science*; Academic: San Diego, Calif., London, 2000.

(86) ThermoScientific. *Convert between times gravity (xg) and centrifuge rotor speed (RPM)*. Tech Tip #40, 2009.
(87) Jeppesen, D. K.; Hvam, M. L.; Primdahl-Bengtson, B.; Boysen, A. T.; Whitehead, B.; Dyrskjøt, L.; Orntoft, T. F.; Howard, K. A.; Ostenfeld, M. S. Comparative analysis of discrete exosome fractions obtained by differential centrifugation. *Journal of Extracellular Vesicles* **2014**, *3*, 25011.
(88) Iwai, K.; Minamisawa, T.; Suga, K.; Yajima, Y.; Shiba, K. Isolation of human salivary extracellular vesicles by iodixanol density gradient ultracentrifugation and their characterizations. *Journal of Extracellular Vesicles* **2016**, *5*, 30829.
(89) van Deun, J.; Mestdagh, P.; Sormunen, R.; Cocquyt, V.; Vermaelen, K.; Vandesompele, J.; Bracke, M.; Wever, O. de; an Hendrix. The impact of disparate isolation methods for extracellular vesicles on downstream RNA profiling. *Journal of Extracellular Vesicles* **2014**, *3*.
(90) Yu, L.-L.; Zhu, J.; Liu, J.-X.; Jiang, F.; Ni, W.-K.; Qu, L.-S.; Ni, R.-Z.; Lu, C.-H.; Xiao, M.-B. A Comparison of Traditional and Novel Methods for the Separation of Exosomes from Human Samples. *BioMed research international* **2018**, *2018*, 3634563.
(91) Giebel, B.; Helmbrecht, C. Methods to Analyze EVs. *Methods in molecular biology (Clifton, N.J.)* **2017**, *1545*, 1–20.
(92) Dragovic, R. A.; Gardiner, C.; Brooks, A. S.; Tannetta, D. S.; Ferguson, D. J. P.; Hole, P.; Carr, B.; Redman, C. W. G.; Harris, A. L.; Dobson, P. J.*; et al.* Sizing and phenotyping of cellular vesicles using Nanoparticle Tracking Analysis. *Nanomedicine : nanotechnology, biology, and medicine* **2011**, *7*, 780–788.
(93) Miller, C. The Stokes-Einstein Law for Diffusion in Solution.: Preeceedings of the Royal Society of London. Series A, Containing Papers of a Mathematical and Physical Character. **1924**, *106*, 746–749.
(94) van der Pol, E.; Coumans, F. A. W.; Grootemaat, A. E.; Gardiner, C.; Sargent, I. L.; Harrison, P.; Sturk, A.; van Leeuwen, T. G.; Nieuwland, R. Particle size distribution of exosomes and microvesicles determined by transmission electron microscopy, flow cytometry, nanoparticle tracking analysis, and resistive pulse sensing. *Journal of thrombosis and haemostasis : JTH* **2014**, *12*, 1182–1192.
(95) Zhang, H.; Freitas, D.; Kim, H. S.; Fabijanic, K.; Li, Z.; Chen, H.; Mark, M. T.; Molina, H.; Martin, A. B.; Bojmar, L.*; et al.* Identification of distinct nanoparticles and subsets of

extracellular vesicles by asymmetric flow field-flow fractionation. *Nature cell biology* **2018**, *20*, 332–343.

(96) Filipe, V.; Hawe, A.; Jiskoot, W. Critical evaluation of Nanoparticle Tracking Analysis (NTA) by NanoSight for the measurement of nanoparticles and protein aggregates. *Pharmaceutical research* **2010**, *27*, 796–810.

(97) Zabeo, D.; Cvjetkovic, A.; Lässer, C.; Schorb, M.; Lötvall, J.; Höög, J. L. Exosomes purified from a single cell type have diverse morphology. *Journal of Extracellular Vesicles* **2017**, *6*, 1329476.

(98) Tian, Y.; Ma, L.; Gong, M.; Su, G.; Zhu, S.; Zhang, W.; Wang, S.; Li, Z.; Chen, C.; Li, L.*; et al.* Protein Profiling and Sizing of Extracellular Vesicles from Colorectal Cancer Patients via Flow Cytometry. *ACS nano* **2018**, *12*, 671–680.

(99) Morales-Kastresana, A.; Jones, J. C. Flow Cytometric Analysis of Extracellular Vesicles. *Methods in molecular biology (Clifton, N.J.)* **2017**, *1545*, 215–225.

(100) van der Pol, E.; van Gemert, M. J. C.; Sturk, A.; Nieuwland, R.; van Leeuwen, T. G. Single vs. swarm detection of microparticles and exosomes by flow cytometry. *Journal of thrombosis and haemostasis : JTH* **2012**, *10*, 919–930.

(101) Gardiner, C.; Shaw, M.; Hole, P.; Smith, J.; Tannetta, D.; Redman, C. W.; Sargent, I. L. Measurement of refractive index by nanoparticle tracking analysis reveals heterogeneity in extracellular vesicles. *Journal of Extracellular Vesicles* **2014**, *3*, 25361.

(102) Rikkert, L. G.; Nieuwland, R.; Terstappen, L. W. M. M.; Coumans, F. A. W. Quality of extracellular vesicle images by transmission electron microscopy is operator and protocol dependent. *Journal of Extracellular Vesicles* **2019**, *8*, 1555419.

(103) Coumans, F. A. W.; Brisson, A. R.; Buzas, E. I.; Dignat-George, F.; Drees, E. E. E.; El-Andaloussi, S.; Emanueli, C.; Gasecka, A.; an Hendrix; Hill, A. F.*; et al.* Methodological Guidelines to Study Extracellular Vesicles. *Circulation research* **2017**, *120*, 1632–1648.

(104) van Deun, J.; Mestdagh, P.; Agostinis, P.; Akay, Ö.; Anand, S.; Anckaert, J.; Martinez, Z. A.; Baetens, T.; Beghein, E.; Bertier, L.*; et al.* EV-TRACK: transparent reporting and centralizing knowledge in extracellular vesicle research. *Nature methods* **2017**, *14*, 228–232.

(105) Leslie, S. R.; Fields, A. P.; Cohen, A. E. Convex lens-induced confinement for imaging single molecules. *Analytical chemistry* **2010**, *82*, 6224–6229.

(106) Scott, S.; Xu, Z. M.; Kouzine, F.; Berard, D. J.; Shaheen, C.; Gravel, B.; Saunders, L.; Hofkirchner, A.; Leroux, C.; Laurin, J.*; et al. Visualizing structure-mediated interactions in supercoiled DNA molecules* 86, 2018.

(107) Leslie, S. R.; Kamanzi, A.; Berard, D.; Shayegan, M.; Henkin, G.; Leith, J.; Scott, S.; Stabile, F. BIOLOGICAL CONFINEMENT PHYSICS: SQUEEZING NEW INFORMATION OUT OF COMPLEX MACROMOLECULES: Biological Confinement Physics. *LA PHYSIQUE AU CANADA*.

(108) Shayegan, M.; Tahvildari, R.; Metera, K.; Kisley, L.; Michnick, S. W.; Leslie, S. R. Probing Inhomogeneous Diffusion in the Microenvironments of Phase-Separated Polymers under Confinement. *Journal of the American Chemical Society* **2019**, *141*, 7751–7757.

(109) Thiombane, N. K.; Coutin, N.; Berard, D.; Tahvildari, R.; Leslie, S.; Nislow, C. Single-cell analysis for drug development using convex lens-induced confinement imaging. *BioTechniques* **2019**, *67*, 210–217.

(110) Lobb, R. J.; Becker, M.; Wen, S. W.; Wong, C. S. F.; Wiegmans, A. P.; Leimgruber, A.; Möller, A. Optimized exosome isolation protocol for cell culture supernatant and human plasma. *Journal of Extracellular Vesicles* **2015**, *4*, 27031.

(111) Sun, Y.; Xia, Z.; Shang, Z.; Sun, K.; Niu, X.; Qian, L.; Fan, L.-Y.; Cao, C.-X.; Xiao, H. Facile preparation of salivary extracellular vesicles for cancer proteomics. *Scientific Reports* **2016**, *6*, 24669.

(112) Bachurski, D.; Schuldner, M.; Nguyen, P.-H.; Malz, A.; Reiners, K. S.; Grenzi, P. C.; Babatz, F.; Schauss, A. C.; Hansen, H. P.; Hallek, M.*; et al.* Extracellular vesicle measurements with nanoparticle tracking analysis - An accuracy and repeatability comparison between NanoSight NS300 and ZetaView. *Journal of Extracellular Vesicles* **2019**, *8*, 1596016.

(113) Schneider, C. A.; Rasband, W. S.; Eliceiri, K. W. NIH Image to ImageJ: 25 years of image analysis. *Nature methods* **2012**, *9*, 671–675.

(114) Lässer, C.; Jang, S. C.; Lötvall, J. Subpopulations of extracellular vesicles and their therapeutic potential. *Molecular aspects of medicine* **2018**, *60*, 1–14.

(115) Onódi, Z.; Pelyhe, C.; Terézia Nagy, C.; Brenner, G. B.; Almási, L.; Kittel, Á.; Manček-Keber, M.; Ferdinandy, P.; Buzás, E. I.; Giricz, Z. Isolation of High-Purity Extracellular Vesicles by the Combination of Iodixanol Density Gradient Ultracentrifugation and Bind-Elute Chromatography From Blood Plasma. *Frontiers in physiology* **2018**, *9*, 1479.

(116) Momen-Heravi, F. Isolation of Extracellular Vesicles by Ultracentrifugation. *Methods in molecular biology (Clifton, N.J.)* **2017**, *1660*, 25–32.
(117) Buschmann, D.; Kirchner, B.; Hermann, S.; Märte, M.; Wurmser, C.; Brandes, F.; Kotschote, S.; Bonin, M.; Steinlein, O. K.; Pfaffl, M. W.*; et al.* Evaluation of serum extracellular vesicle isolation methods for profiling miRNAs by next-generation sequencing. *Journal of Extracellular Vesicles* **2018**, *7*, 1481321.
(118) Tian, Y.; Gong, M.; Hu, Y.; Liu, H.; Zhang, W.; Zhang, M.; Hu, X.; Aubert, D.; Zhu, S.; Wu, L.*; et al.* Quality and efficiency assessment of six extracellular vesicle isolation methods by nano-flow cytometry. *Journal of Extracellular Vesicles* **2020**, *9*, 1697028.
(119) Boyd, R.; Pichaimuthu, S.; Cuenat, A. New approach to inter-technique comparisons for nanoparticle size measurements: using atomic force microscopy, nanoparticle tracking analysis and dynamic light scattering: Colloids Surf A Physicochem Eng Asp, *387*, 35–42.
(120) Doyle, L. M.; Wang, M. Z. Overview of Extracellular Vesicles, Their Origin, Composition, Purpose, and Methods for Exosome Isolation and Analysis. *Cells* **2019**, *8*.
(121) Pospichalova, V.; Svoboda, J.; Dave, Z.; Kotrbova, A.; Kaiser, K.; Klemova, D.; Ilkovics, L.; Hampl, A.; Crha, I.; Jandakova, E.*; et al.* Simplified protocol for flow cytometry analysis of fluorescently labeled exosomes and microvesicles using dedicated flow cytometer. *Journal of Extracellular Vesicles* **2015**, *4*, 25530.
(122) Ter-Ovanesyan, D.; Kowal, E. J. K.; Regev, A.; Church, G. M.; Cocucci, E. Imaging of Isolated Extracellular Vesicles Using Fluorescence Microscopy. *Methods in molecular biology (Clifton, N.J.)* **2017**, *1660*, 233–241.
(123) Deregibus, M. C.; Figliolini, F.; D'Antico, S.; Manzini, P. M.; Pasquino, C.; Lena, M. de; Tetta, C.; Brizzi, M. F.; Camussi, G. Charge-based precipitation of extracellular vesicles. *International journal of molecular medicine* **2016**, *38*, 1359–1366.
(124) Zhu, Q.; Liu, G.; Kai, M. DNA Aptamers in the Diagnosis and Treatment of Human Diseases. *Molecules (Basel, Switzerland)* **2015**, *20*, 20979–20997.
(125) Orava, E. W.; Cicmil, N.; Gariépy, J. Delivering cargoes into cancer cells using DNA aptamers targeting internalized surface portals. *Biochimica et biophysica acta* **2010**, *1798*, 2190–2200.
(126) Reuter, J. S.; Mathews, D. H. RNAstructure: software for RNA secondary structure prediction and analysis. *BMC bioinformatics* **2010**, *11*, 129.

(127) Vidic, M.; Smuc, T.; Janez, N.; Blank, M.; Accetto, T.; Mavri, J.; Nascimento, I. C.; Nery, A. A.; Ulrich, H.; Lah, T. T. In Silico Selection Approach to Develop DNA Aptamers for a Stem-like Cell Subpopulation of Non-small Lung Cancer Adenocarcinoma Cell Line A549. *Radiology and oncology* **2018**, *52*, 152–159.
(128) Beier, R.; Boschke, E.; Labudde, D. New strategies for evaluation and analysis of SELEX experiments. *BioMed research international* **2014**, *2014*, 849743.
(129) Hoinka, J.; Berezhnoy, A.; Sauna, Z. E.; Gilboa, E.; Przytycka, T. M. AptaCluster - A Method to Cluster HT-SELEX Aptamer Pools and Lessons from its Application. *Research in computational molecular biology : ... Annual International Conference, RECOMB ... : proceedings. RECOMB (Conference : 2005-)* **2014**, *8394*, 115–128.
(130) Laganowsky, A.; Reading, E.; Hopper, J. T. S.; Robinson, C. V. Mass spectrometry of intact membrane protein complexes. *Nature protocols* **2013**, *8*, 639–651.
(131) León, I. R.; Schwämmle, V.; Jensen, O. N.; Sprenger, R. R. Quantitative assessment of in-solution digestion efficiency identifies optimal protocols for unbiased protein analysis. *Mol Cell Proteomics* **2013**, *12*, 2992–3005.
(132) Loo, R. R.; Dales, N.; Andrews, P. C. Surfactant effects on protein structure examined by electrospray ionization mass spectrometry. *Protein science : a publication of the Protein Society* **1994**, *3*, 1975–1983.
(133) Zhang, N.; Li, L. Effects of common surfactants on protein digestion and matrix-assisted laser desorption/ionization mass spectrometric analysis of the digested peptides using two-layer sample preparation. *Rapid communications in mass spectrometry : RCM* **2004**, *18*, 889–896.
(134) Wiśniewski, J. R.; Zougman, A.; Nagaraj, N.; Mann, M. Universal sample preparation method for proteome analysis. *Nature methods* **2009**, *6*, 359–362.
(135) Cox, J.; Mann, M. MaxQuant enables high peptide identification rates, individualized p.p.b.-range mass accuracies and proteome-wide protein quantification. *Nature biotechnology* **2008**, *26*, 1367–1372.
(136) Cox, J.; Neuhauser, N.; Michalski, A.; Scheltema, R. A.; Olsen, J. V.; Mann, M. Andromeda: a peptide search engine integrated into the MaxQuant environment. *Journal of proteome research* **2011**, *10*, 1794–1805.
(137) Nagaraj, N.; Kulak, N. A.; Cox, J.; Neuhauser, N.; Mayr, K.; Hoerning, O.; Vorm, O.; Mann, M. System-wide perturbation analysis with nearly complete coverage of the yeast

proteome by single-shot ultra HPLC runs on a bench top Orbitrap. *Mol Cell Proteomics* **2012**, *11*, M111.013722.

(138) Cox, J.; Hein, M. Y.; Luber, C. A.; Paron, I.; Nagaraj, N.; Mann, M. Accurate proteome-wide label-free quantification by delayed normalization and maximal peptide ratio extraction, termed MaxLFQ. *Mol Cell Proteomics* **2014**, *13*, 2513–2526.

(139) UWCC Flow Cytometry Laboratory. Titrating Antibodies for Flow Cytometry. https://cancer.wisc.edu/research/wp-content/uploads/2017/03/Flow_TechNotes_Antibody-Titrations_20170918.pdf.

(140) Oberg, A. L.; Mahoney, D. W. Statistical methods for quantitative mass spectrometry proteomic experiments with labeling. *BMC bioinformatics* **2012**, *13 Suppl 16*, S7.

(141) Waters. Non-Linear Dynamics: A Waters Company. http://www.nonlinear.com/progenesis/qi-for-proteomics/v1.0/faq/pq-values.aspx.

(142) Carninci, P.; Kasukawa, T.; Katayama, S.; Gough, J.; Frith, M. C.; Maeda, N.; Oyama, R.; Ravasi, T.; Lenhard, B.; Wells, C.*; et al.* The transcriptional landscape of the mammalian genome. *Science (New York, N.Y.)* **2005**, *309*, 1559–1563.

(143) Ren, M.; Drivas, G.; D'Eustachio, P.; Rush, M. G. Ran/TC4: a small nuclear GTP-binding protein that regulates DNA synthesis. *The Journal of Cell Biology* **1993**, *120*, 313–323.

(144) To, W. S.; Midwood, K. S. Plasma and cellular fibronectin: distinct and independent functions during tissue repair. *Fibrogenesis & tissue repair* **2011**, *4*, 21.

(145) Renaud, L. P.; Kelly, J. S. Proceedings: Response of identified ventromedial hypothalamic nucleus neurons to putative neurotransmitters applied by microiontophoresis. *British journal of pharmacology* **1975**, *55*, 277P-278P.

(146) Raijmakers, R.; Noordman, Y. E.; van Venrooij, W. J.; Pruijn, G. J. M. Protein-protein interactions of hCsl4p with other human exosome subunits. *Journal of molecular biology* **2002**, *315*, 809–818.

(147) Mavrogonatou, E.; Kletsas, D. High osmolality activates the G1 and G2 cell cycle checkpoints and affects the DNA integrity of nucleus pulposus intervertebral disc cells triggering an enhanced DNA repair response. *DNA repair* **2009**, *8*, 930–943.

(148) Mavrogonatou, E.; Papadimitriou, K.; Urban, J. P.; Papadopoulos, V.; Kletsas, D. Deficiency in the α1 subunit of Na+/K+-ATPase enhances the anti-proliferative effect of high

osmolality in nucleus pulposus intervertebral disc cells. *Journal of cellular physiology* **2015**, *230*, 3037–3048.

(149) Mathieu, V.; Pirker, C.; Martin de Lassalle, E.; Vernier, M.; Mijatovic, T.; DeNeve, N.; Gaussin, J.-F.; Dehoux, M.; Lefranc, F.; Berger, W.*; et al.* The sodium pump alpha1 sub-unit: a disease progression-related target for metastatic melanoma treatment. *Journal of cellular and molecular medicine* **2009**, *13*, 3960–3972.

(150) Carrascosa, C.; Obula, R. G.; Missiaglia, E.; Lehr, H.-A.; Delorenzi, M.; Frattini, M.; Rüegg, C.; Mariotti, A. MFG-E8/lactadherin regulates cyclins D1/D3 expression and enhances the tumorigenic potential of mammary epithelial cells. *Oncogene* **2012**, *31*, 1521–1532.

(151) Neutzner, M.; Lopez, T.; Feng, X.; Bergmann-Leitner, E. S.; Leitner, W. W.; Udey, M. C. MFG-E8/lactadherin promotes tumor growth in an angiogenesis-dependent transgenic mouse model of multistage carcinogenesis. *Cancer research* **2007**, *67*, 6777–6785.

(152) Guo, Z.; Neilson, L. J.; Zhong, H.; Murray, P. S.; Zanivan, S.; Zaidel-Bar, R. E-cadherin interactome complexity and robustness resolved by quantitative proteomics. *Science signaling* **2014**, *7*, rs7.

(153) Mimori, K.; Mori, M.; Inoue, H.; Ueo, H.; Mafune, K.; Akiyoshi, T.; Sugimachi, K. Elongation factor 1 gamma mRNA expression in oesophageal carcinoma. *Gut* **1996**, *38*, 66–70.

(154) Lew, Y.; Jones, D. V.; Mars, W. M.; Evans, D.; Byrd, D.; Frazier, M. L. Expression of elongation factor-1 gamma-related sequence in human pancreatic cancer. *Pancreas* **1992**, *7*, 144–152.

(155) Mimori, K.; Mori, M.; Tanaka, S.; Akiyoshi, T.; Sugimachi, K. The Overexpression of Elongation Factor 1 Gamma mRNA in Gastric Carcinoma **1995**, *75*, 1446–1449.

(156) Santa Cruz Biotechnology, I. *Datasheet: Datasheet: Na+/K+-ATPase α (H-3): sc-48345*. https://datasheets.scbt.com/sc-48345.pdf.

(157) Welsh, J. A.; Holloway, J. A.; Wilkinson, J. S.; Englyst, N. A. Extracellular Vesicle Flow Cytometry Analysis and Standardization. *Frontiers in cell and developmental biology* **2017**, *5*, 78.

(158) Gardiner, C.; Di Vizio, D.; Sahoo, S.; Théry, C.; Witwer, K. W.; Wauben, M.; Hill, A. F. Techniques used for the isolation and characterization of extracellular vesicles: results of a worldwide survey. *Journal of Extracellular Vesicles* **2016**, *5*, 32945.

(159) Kratschmer, C.; Levy, M. Effect of Chemical Modifications on Aptamer Stability in Serum. *Nucleic acid therapeutics* **2017**, *27*, 335–344.
(160) Ni, S.; Yao, H.; Wang, L.; Lu, J.; Jiang, F.; Lu, A.; Zhang, G. Chemical Modifications of Nucleic Acid Aptamers for Therapeutic Purposes. *International journal of molecular sciences* **2017**, *18*.
(161) Pepe, M. S.; Etzioni, R.; Feng, Z.; Potter, J. D.; Thompson, M. L.; Thornquist, M.; Winget, M.; Yasui, Y. Phases of biomarker development for early detection of cancer. *Journal of the National Cancer Institute* **2001**, *93*, 1054–1061.
(162) Liu, Y.-R.; Ortiz-Bonilla, C. J.; Lee, Y.-F. Extracellular Vesicles in Bladder Cancer: Biomarkers and Beyond. *International journal of molecular sciences* **2018**, *19*.
(163) Xie, C.; Ji, N.; Tang, Z.; Li, J.; Chen, Q. The role of extracellular vesicles from different origin in the microenvironment of head and neck cancers. *Molecular cancer* **2019**, *18*, 83.